

Kinetic and mechanistic features of nitroxide mediated (co)polymerization

*Dissertation presented in partial fulfilment of the requirements for the degree of PhD in Polymer
Science at the University of Stellenbosch*

by



Supervisor: Prof Bert Klumperman

University of Stellenbosch – Faculty of Science

Department of Chemistry and Polymer Science

March 2011

DECLARATION

By Submitting this dissertation electronically, I declare that the entirety of the work contained therein is my own, original work, that I am the sole author thereof (save to the extent explicitly otherwise stated), that reproduction and publication thereof by Stellenbosch University will not infringe any third party rights and that I have not previously in its entirety or in part submitted it for obtaining any qualification.

Lebohang Hlalele

Stellenbosch, February 2011

Copyright© 2011 University of Stellenbosch

All rights reserved

Abstract

In this dissertation, the primary aim was to investigate the kinetic and mechanistic features of homo- and copolymerization of styrene and *n*-butyl acrylate via *in situ* ^1H and ^{31}P NMR, with persistent radical species (in the form of the nitroxide DEPN) mediating the processes. Homopolymerization of styrene and *n*-butyl acrylate using the alkoxyamine MAMA-DEPN have been studied via *in situ* ^1H NMR. The kinetic and mechanistic features of the high temperature nitroxide mediated homopolymerization of *n*-butyl acrylate are dealt with. The rate of polymerization of *n*-butyl acrylate was observed to be independent of the initial concentration of the alkoxyamine initiator. The co-existence of secondary propagating radicals and mid-chain radicals, and thermal auto-initiation of *n*-butyl acrylate are dealt with in explaining the observed phenomenon of rate independence. The rate coefficient for thermal auto-initiation of *n*-butyl acrylate was determined as $3.54 \times 10^{-7} \text{ L mol}^{-1} \text{ s}^{-1}$ via *in situ* ^1H NMR experiments. Among reactions the mid-chain radicals can undergo, the β -fragmentation results in the formation of a secondary propagating radical and a chain bearing a 1,1-disubstituted alkene end group. The evolution of the chains bearing the 1,1-disubstituted alkene end groups showed a first order dependence on time, indicating that the incorporation of such species in the growing chains was negligible. With the aid of simulations carried out using the Predici software package, it has been demonstrated in conjunction with experimental data that the thermal auto-initiation can be ascribed to the observed phenomenon of rate independence.

The reactivity ratios for the styrene/*n*-butyl acrylate copolymerization system mediated by DEPN were determined as $r_s = 0.74$ and $r_B = 0.23$. The terminal monomer unit of dormant chains was tracked via *in situ* ^{31}P NMR. Simulations of the copolymerization process assuming the penultimate unit model resulted in good agreement between the copolymerization data extracted from both *in situ* ^1H and ^{31}P NMR. The parameter estimation tool of the Predici software package was used to estimate the rate coefficients governing the NMP equilibrium of polymeric radicals with the *n*-butyl acrylate as the terminal unit. The equilibrium coefficient obtained from homopolymerization of *n*-butyl acrylate is a composite of two equilibria, one involving the secondary propagating radical and the other the mid-chain radical. This equilibrium constant from *n*-butyl acrylate homopolymerization experiments cannot be directly adapted into the

copolymerization, as the effect of mid-chain radicals is non-existent in a copolymerization process.

Uittreksel

Die primêre doel van hierdie proefskrif was om die kinetiese en meganiese eienskappe van homo- en ko-polimerisasie van stireen en *n*-butielakrilaat te ondersoek deur *in situ* ^1H en ^{31}P KMR, met volgehoue radikale spesies (in die vorm van die nitroksied DEPN) wat optree as tussenganger in die prosesse. Homopolimerisasie van stireen en *n*-butielakrilaat met behulp van die alkoksiamien MAMA-DEPN is bestudeer deur *in situ* ^1H KMR. Die kinetiese en meganiese eienskappe van die hoë temperatuur nitroksied-beheerde homopolimerisasie van *n*-butielakrilaat is ook bestudeer. Daar is waargeneem dat die tempo van polimerisasie van *n*-butielakrilaat onafhanklik is van die aanvanklike konsentrasie van die alkoksiamieninisiëerder. Die mede-bestaan van sekondêre voortplantingsradikale, mid-kettingradikale en termiese outo-inisiasie van *n*-butielakrilaat word verduidelik deur die verklaring van die waargenome verskynsel van tempo onafhanklikheid. Die tempo koëffisiënt vir termiese outo-inisiasie van *n*-butielakrilaat is $3,54 \times 10^{-7} \text{ L mol}^{-1} \text{ s}^{-1}$ via *in situ* ^1H KMR eksperimente. Die mid-kettingradikaal kan onder andere β -fragmentasie ondergaan wat lei tot die vorming van 'n sekondêre voortplantingsradikaal en 'n ketting met 'n 1,1-digesubstitueerde alkeeneindgroep. Die ontwikkeling van die kettings met die 1,1-digesubstitueerde alkeeneindgroepe het 'n eerste orde afhanklikheid van tyd, wat aandui dat die invoeging van die spesies geen invloed op die groeiende ketting het nie. Simulasies met die Predici sagtewarepakket in samewerking met eksperimentele data het gedemonstreer dat die termiese outo-inisiasie toegeskryf kan word aan die tempo onafhanklikheid.

Die reaktiwiteitsverhoudings vir die stireen/*n*-butielakrilaat kopolimerisasie stelsel beheer deur DEPN is onderskeidelik bepaal as $r_S = 0.74$ en $r_B = 0.23$. Die terminale monomeereenheid van die onaktiewe kettings is gevolg deur *in situ* ^{31}P KMR. Simulasies van die kopolimerisasieproses met die aanvaarding van die voorlaaste eenheidsmodel het goed vergelyk met die kopolimerisasie data verkry van beide die *in situ* ^1H en ^{31}P KMR. Die parameter beraming van die Predici sagtewarepakket is gebruik om die tempo koëffisiënt vir die NMP ewewig van polimerisasieradikale met *n*-butielakrilaat as terminale eenheid te bepaal. Die ewewig koëffisiënt van die homopolimerisasie van *n*-butielakrilaat is 'n samestelling van twee ewewigte, een van die sekondêre voortplantingsradikaal en die ander van die mid-kettingradikaal. Hierdie

ewewigskonstante van *n*-butielakrylaat homopolimerisasie eksperimente kan nie direk aangepas word in die kopolimerisasie nie omdat die effek van die mid-kettingradikale nie bestaan in die kopolimerisasie proses nie.

Table of Contents

Abstract.....	v
Uittreksel.....	vii
Table of Contents.....	ix
List of Figures.....	xiii
List of Schemes.....	xx
List of Tables.....	xxii
List of Acronyms.....	xxiii
List of Symbols.....	xxv
Chapter I: Introduction.....	1
1.1 Free Radical Polymerization.....	2
1.2 Controlled/Living Radical Polymerization (CRP).....	3
1.2.1 RAFT mediated polymerization.....	4
1.2.2 ATRP.....	4
1.2.3 NMP.....	5
1.3 <i>In situ</i> NMR Spectroscopy.....	5
1.4 Objectives of this work.....	5
1.5 Outline.....	6
References.....	8
Chapter II: Controlled/Living Radical Polymerization Kinetics-An Overview.....	9
2.1 Living Radical Polymerization; Concepts.....	10
2.2 Nitroxide Mediated Polymerization (NMP).....	11
2.2.1 Basic Mechanism.....	11
2.2.2 Bimolecular vs Unimolecular NMP Processes.....	12
2.2.3 Nitroxides Development: Review.....	14
2.2.4 Alkoxyamine Synthetic Approaches.....	15
2.2.5 Kinetic Aspects of NMP.....	17
2.2.6 The NMP Equilibrium Constant (K).....	22
2.2.7 Rate Constants of Activation.....	23
2.2.8 Rate enhancement in NMP with the aid of additives.....	25

2.2.9 The potential of NMP, advantages over other living systems and the drawbacks of the technique	26
References.....	27
Chapter III: Nitroxide Mediated Homopolymerization of Styrene and <i>n</i> -Butyl Acrylate.....	31
3.1 Introduction.....	32
3.1.1 Propagation and termination rate coefficients	32
3.1.2 Determination of the equilibrium constant	36
3.2 <i>In situ</i> ¹ H NMR spectroscopy: Analysis	38
3.3 Synthesis of the alkoxyamine 2-methyl-2[N-tert-butyl-N-(1-diethoxyphosphoryl-2,2-dimethoxypropyl)aminoxy]propionic acid (MAMA-DEPN)	40
3.3.1 Experimental	40
3.4 Homopolymerization of styrene and <i>n</i> -butyl acrylate	44
3.4.1 Experimental	44
3.4.2 Results and discussion	45
3.4.3 Conclusion	47
3.5 The Persistent Radical Effect (PRE) Theory: Experimental validity	47
3.5.1 Experimental	47
3.5.2 Results and discussion	50
3.5.3 Conclusion	51
3.6 Systematic study of the effect of varying the alkoxyamine concentration in styrene and <i>n</i> -butyl acrylate homopolymerization reactions.....	52
3.6.1 Experimental	53
3.6.2 Results and Discussion	53
3.6.3 Conclusion	67
3.7 Summary	67
References.....	69
Chapter IV: Secondary Reactions in <i>n</i> -Butyl Acrylate Polymerization and Theoretical Considerations.....	73
4.1 Introduction.....	74
4.2 Investigating the NMP equilibrium involving the MCR	79
4.2.1 Experimental	80

4.2.2 Results and discussion	81
4.2.4 Conclusion	83
4.3 Kinetic model for <i>n</i> -butyl acrylate polymerization mediated by persistent radical species	84
4.3.1 Methodology	86
4.3.2 Results and discussion	86
4.3.3 Conclusion	97
4.4 Summary	97
References.....	99
Chapter V: Nitroxide mediated copolymerization of styrene and <i>n</i> -butyl acrylate.....	101
<i>Synopsis</i>	101
5.1 Introduction.....	102
5.1.1 Copolymerization models	102
5.1.2 Reactivity ratios in the copolymerization of styrene and <i>n</i> -butyl acrylate	105
5.2 Experimental	108
5.2.1 Chemicals.....	108
5.2.2 Procedure for the <i>in situ</i> ¹ H NMR copolymerization of styrene and <i>n</i> -butyl acrylate	108
5.2.3 Procedure for the <i>in situ</i> ³¹ P NMR copolymerization of styrene and <i>n</i> -butyl acrylate	108
5.3 Results and discussion	109
5.3.1 Quantitative monitoring of monomer consumption via <i>in situ</i> ¹ H NMR	109
5.3.2 Assessment of the reactivity ratios	110
5.3.3 Instantaneous comonomer and copolymer composition.....	111
5.3.4 Conversion index plots	115
5.3.5 Monitoring the terminal unit.....	118
5.4 Conclusion	131
References.....	132
Chapter VI: Epilogue	134
6.1 Homopolymerization of <i>n</i> -butyl acrylate.....	134
6.2 Copolymerization of styrene and <i>n</i> -butyl acrylate.....	136
6.3 Simulation of the homopolymerization and copolymerization via Predici	136

6.4 Recommendations.....	137
References.....	139
Acknowledgements.....	140

List of Figures

Figure 3-1: The ^1H NMR spectra (δ in the range 1 ppm to 8.5 ppm) at different times during the polymerization of *n*-butyl acrylate at 120 °C initiated by MAMA-DEPN in DMSO- d_6 . In the region labelled “B” are peaks due to the vinyl protons of *n*-butyl acrylate monomer and the peak labelled “A” is due to the –CHO proton of the reference (DMF).

Figure 3-2: The enlarged region of the part labelled “B” in Figure 3-1 showing the spectral region of the vinyl protons of the *n*-butyl acrylate monomer, during the polymerization at 120 °C initiated by MAMA-DEPN in DMSO- d_6

Figure 3-3: ^1H NMR spectrum of MAMA-DEPN

Figure 3-4: Mass spectrum of MAMA-DEPN

Figure 3-5: Evolution of $\ln(1/(1-\xi))$ as a function of time for the homopolymerization of *n*-butyl acrylate in DMSO- d_6 at 120 °C with MAMA-DEPN as the initiator/mediator agent.

Figure 3-6: Evolution of $\ln(1/(1-\xi))$ as a function of time for the homopolymerization of styrene in DMSO- d_6 at 120 °C with MAMA-DEPN as the initiator/mediator agent.

Figure 3-7: The Size Exclusion Chromatogram (SEC) of the DEPN end capped polystyrene macro-alkoxyamine (PS-DEPN).

Figure 3-8: The ^1H NMR spectrum of the DEPN end capped polystyrene (PS-DEPN) with the insert showing the doublet signal of the proton attached to the α -carbon of the end group DEPN.

Figure 3-9: Evolution of $\ln([M]_0/[M])$ as a function of time for the homopolymerization of styrene in DMSO- d_6 initiated by PS-DEPN at 120 °C.

Figure 3-10: Evolution of $\ln([M]_0/[M])$ as a function of $t^{2/3}$ for the homopolymerization of styrene in DMSO- d_6 initiated by PS-DEPN at 120 °C.

Figure 3-11: The evolution of conversion (ξ [-]) as function of the initial concentration of the alkoxyamine for the polymerization of styrene in DMSO- d_6 at 120°C.

Figure 3-12: Semi-logarithmic plot for *n*-butyl acrylate polymerization initiated with different initial alkoxyamine concentrations in DMSO-d₆ at 120 °C.

Figure 3-13: Conversion versus time plots for *n*-butyl acrylate polymerization initiated with different initial alkoxyamine concentrations in DMSO-d₆ at 100 °C.

Figure 3-14: The evolution of *n*-butyl acrylate concentration with time for thermally initiated polymerization in DMSO-d₆ in the presence of 4.52×10^{-02} mol L⁻¹ free DEPN at 120 °C.

Figure 3-15: The evolution of *n*-butyl acrylate conversion with time for thermally initiated polymerization in DMSO-d₆ in the presence of 5.30×10^{-02} mol L⁻¹ free DEPN at 120 °C.

Figure 3-16: The plot of the negative inverse monomer consumption with time (■) in the linear range with the solid line as the linear fit to the data with a slope = $3.54 \text{ E-}07 \text{ L mol}^{-1} \text{ s}^{-1}$ and adjusted $R^2 = 0.87$. [*n*-butyl acrylate] = 3.12 mol L⁻¹ and [DEPN] = 0.0452 mol L⁻¹ at 120 °C with DMSO-d₆ as the solvent.

Figure 3-17: ¹H NMR spectra at different reaction times illustrating the increasing intensity of the peak at around $\delta \sim 5.5$ ppm that is due to an increasing concentration of 1,1-disubstituted alkene end groups as a result of β -fragmentation of the MCRs in the polymerization of *n*-butyl acrylate at 120 °C with [MAMA-DEPN]₀ = 0.156 M, [*n*-butyl acrylate]₀ = 3.0 M and DMSO-d₆ = 65 % v/v.

Figure 3-18: The ¹H NMR spectrum taken after 2 hours of polymerization of *n*-butyl acrylate at 110 °C with [MAMA-DEPN]₀ = 0.1494 M, [*n*-butyl acrylate]₀ = 3.0 M and DMSO-d₆ = 65 % v/v. The insert shows the expanded region in the range $6.0 > \delta \text{ (ppm)} > 5.0$ with the marked peak, labelled A, assigned to one of the protons of the 1,1-disubstituted alkene end group resulting from the β -fragmentation of the MCRs.

Figure 3-19: The evolution of concentration of 1,1-disubstituted alkene end group vs. polymerization time during *n*-butyl acrylate polymerization at 120 °C with [MAMA-DEPN]₀ = 0.156 M, [*n*-butyl acrylate]₀ = 3.0 M and DMSO-d₆ = 65 % v/v.

Figure 3-20: The evolution of relative concentration of 1,1-disubstituted alkene end group vs. monomer conversion during *n*-butyl acrylate polymerization at 120 °C for different initial concentrations of the alkoxyamine MAMA-DEPN. $[n\text{-butyl acrylate}]_0 = 3.0 \text{ M}$ and $\text{DMSO-d}_6 = 65 \text{ \% v/v}$.

Figure 4-1: ^1H NMR spectrum of poly(*n*-butyl acrylate) in the region 4.7 – 2.8 ppm with the peaks labelled A, B and C assigned to signals of the protons labelled in Scheme 4-2.

Figure 4-2: ^1H NMR spectrum of styrene/*n*-butyl acrylate copolymerization mixture in the region 5.0 – 3.0 ppm with the peaks labelled A and C assigned to signals of the protons labelled in Scheme 4-2. ($f_s = 0.1$)

Figure 4-3: ^1H NMR spectrum of styrene/*n*-butyl acrylate copolymerization mixture in the region 5.0 – 3.0 ppm with the peaks labelled A and C assigned to signals of the protons labelled in Scheme 4-2. ($f_s = 0.4$)

Figure 4-4: The experimental evolution of *n*-butyl acrylate concentration with time compared with simulation data according to Scheme 4-3 for which $k'_c = 1.0 \times 10^6 \text{ L mol}^{-1} \text{ s}^{-1}$ and $k'_d = 5.32 \times 10^{-2} \text{ s}^{-1}$ and all other parameters are as listed in Table 4-1.

Figure 4-5: The experimental evolution of the concentration of 1,1-disubstituted alkene species with time compared with simulation data according to Scheme 4-3 for which $k'_c = 1.0 \times 10^6 \text{ L mol}^{-1} \text{ s}^{-1}$ and $k'_d = 5.32 \times 10^{-2} \text{ s}^{-1}$ and all other parameters are as listed in Table 4-1.

Figure 4-6: Simulated conversion index plots of *n*-butyl acrylate polymerization at different indicated initial concentration of the alkoxyamine (MAMA-DEPN) vs. experimental data for which $[\text{MAMA-DEPN}]_0$ for Experiments 1 (Exp. 1), 2 (Exp. 2) and 3 (Exp. 3) are 0.2, 0.15 and 0.10 mol L⁻¹, respectively.

Figure 4-7: The evolution of the concentration of species bearing 1,1-disubstituted alkene end group as a function of the initial concentration of MAMA-DEPN for *n*-butyl acrylate

polymerization conducted at 120 °C with all profiles simulated except for the labelled experimental data points (\circ), for which $[\text{MAMA-DEPN}]_0 = 0.016 \text{ mol L}^{-1}$.

Figure 4-8: The evolution of the concentration of *n*-butyl acrylate as a function the initial concentration of MAMA-DEPN for the polymerization conducted at 120 °C with all data simulated except for the labelled experimental data points (\circ), for which $[\text{MAMA-DEPN}]_0 = 0.016 \text{ mol L}^{-1}$.

Figure 4-9: Simulated fraction of MCR in *n*-butyl acrylate polymerization at 120 °C, as function of the initial concentration of the alkoxyamine.

Figure 4-10: Comparison of simulated conversion index plots of *n*-butyl acrylate polymerization model including (red lines) and excluding (blue lines) the equilibrium involving the MCR as a function of initial concentration of the alkoxyamine. Experimental conversion index plots is included for which the employed $[\text{MAMA-DEPN}]_0 = 0.15 \text{ mol L}^{-1}$.

Figure 4-11: Simulated evolution of 1,1-disubstituted alkene bearing species without thermal auto-initiation as a function of the initial concentration of the alkoxyamine. Experimental data for the evolution of the species is included for which the employed $[\text{MAMA-DEPN}]_0 = 0.15 \text{ mol L}^{-1}$.

Figure 4-12: Simulated conversion index plots of *n*-butyl acrylate without thermal auto-initiation as a function of the initial concentration of the alkoxyamine. Experimental data for the evolution of the species is included for which the employed $[\text{MAMA-DEPN}]_0 = 0.15 \text{ mol L}^{-1}$.

Figure 4-13: Simulated conversion index plots for *n*-butyl acrylate polymerization in the presence of 1 mol % free DEPN relative to MAMA-DEPN added with the thermal auto-initiation step taken into account, for different initial concentration of MAMA-DEPN.

Figure 4-14: Simulated conversion index plots for *n*-butyl acrylate polymerization in the presence of 1 mol % free DEPN relative to MAMA-DEPN added with the thermal auto-initiation step excluded, for different initial concentration of MAMA-DEPN.

Figure 4-15: Simulated conversion index plots for *n*-butyl acrylate polymerization in the presence of 2 mol % free DEPN relative to MAMA-DEPN added with the thermal auto-initiation step excluded, for different initial concentration of MAMA-DEPN.

Figure 4-16: Simulated and experimental evolution of monomer conversion in thermally initiated *n*-butyl acrylate polymerization in the presence of free DEPN. $[n\text{-butyl acrylate}]_0 = 3.09 \text{ mol L}^{-1}$ and $[\text{DEPN}]_0 = 0.053 \text{ mol L}^{-1}$

Figure 5-1: *In situ* ^1H NMR spectrum array for the copolymerization of styrene and *n*-butyl acrylate in DMSO-d_6 at $120 \text{ }^\circ\text{C}$.

Figure 5-2: The concentration profiles of styrene and *n*-butyl acrylate relative to the DMF internal reference for the copolymerization conducted in DMSO-d_6 at $120 \text{ }^\circ\text{C}$ ($f_s^0 = 0.4$).

Figure 5-3: Relative concentration of styrene [S] versus the ratio [B] / [S] from the *in situ* ^1H NMR analysis of the copolymerization of styrene and *n*-butyl acrylate with initial feed composition of $f_s^0 = 0.6$ ($r_s = 0.74, r_b = 0.23$).

Figure 5-4: The effect of overall conversion on the instantaneous comonomer composition at different initial feed composition.

Figure 5-5: The effect of feed composition on both the instantaneous comonomer composition and the instantaneous copolymer composition for $f_s^0 = 0.4 \ll f_{\text{azeotrope}}$.

Figure 5-6: Evolution of the cumulative fraction of styrene in the copolymer as a function of overall monomer conversion for $f_s^0 = 0.1$ (\circ), $f_s^0 = 0.4$ (\square), $f_s^0 = 0.6$ (\blacksquare) and $f_s^0 = 0.71$ (\bullet) with the solid lines representing the respective calculated cumulative fractions of styrene using $r_s = 0.74$ and $r_b = 0.23$.

Figure 5-7: The copolymer composition curve (\circ) for the copolymerization of styrene and *n*-butyl acrylate with the solid line indicating the theoretical copolymer composition calculated according to Equation 5-10 using $r_s = 0.74$ and $r_b = 0.23$.

Figure 5-8: The evolution of instantaneous comonomer composition with overall conversion for $f_s^0 = 0.1$.

Figure 5-9: Conversion index plot for the copolymerization of styrene and *n*-butyl acrylate at 120°C in DMSO- d_6 with 0.6 mole fraction styrene in the initial feed composition, using MAMA-DEPN as a unimolecular initiator.

Figure 5-10: Conversion index plot for the copolymerization of styrene and *n*-butyl acrylate at 120°C in DMSO- d_6 with 0.8 mole fraction styrene in the initial feed composition, using MAMA-DEPN as a unimolecular initiator.

Figure 5-11: Conversion index plots for the fractional conversion of styrene at different initial feed compositions for the styrene/*n*-butyl acrylate copolymerization at 120°C using MAMA-DEPN in DMSO- d_6 .

Figure 5-12: The overall conversion index plot for the copolymerization of styrene and *n*-butyl acrylate at 120°C using MAMA-DEPN in DMSO- d_6 at different initial feed compositions.

Figure 5-13: *In situ* ^{31}P NMR spectrum acquired 256 s into the copolymerization of styrene and *n*-butyl acrylate in DMSO- d_6 at 120 °C with the alkoxyamine MAMA-DEPN, at initial feed composition corresponding to $f_s^0 = 0.3$.

Figure 5-14: ^{31}P NMR spectra of the styrene/*n*-butyl acrylate copolymerization system at three initial feed compositions indicating signals due to dormant chains with styrene and *n*-butyl acrylate as terminal units.

Figure 5-15: ^{31}P NMR spectra of the styrene (B) and *n*-butyl acrylate (A) homopolymerization indicating the regions in which signals due to dormant chains with styrene and *n*-butyl acrylate terminal units are observed.

Figure 5-16: The evolution of the fraction of dormant chains with styrene and *n*-butyl acrylate as the terminal unit for $f_s^0 = 0.3$.

Figure 5-17: The evolution of the fraction of dormant chains with *n*-butyl acrylate as the terminal unit for $f_s^0 = 0.3$ and $f_s^0 = 0.58$.

Figure 5-18: The evolution of the fraction of dormant chains with *n*-butyl acrylate as the terminal unit as a function of both overall monomer conversion and instantaneous feed composition for the copolymerization of styrene and *n*-butyl acrylate with $f_s^0 = 0.3$.

Figure 5-19: Theoretical vs. experimental evolution of styrene concentration with time for $f_s^0 = 0.3$. k_c^B and k_d^B values used in the simulation are in Table 5-1.

Figure 5-20: Theoretical vs. experimental evolution of *n*-butyl acrylate concentration with time for $f_s^0 = 0.3$. k_c^B and k_d^B values used in the simulation are in Table 5-1.

Figure 5-21: Theoretical vs. experimental evolution of styrene concentration with time for $f_s^0 = 0.3$. k_c^B and k_d^B values used are $9.99 \times 10^5 \text{ L mol}^{-1} \text{ s}^{-1}$ and $9.66 \times 10^{-4} \text{ s}^{-1}$, respectively.

Figure 5-22: Theoretical vs. experimental evolution of *n*-butyl acrylate concentration with time for $f_s^0 = 0.3$. k_c^B and k_d^B values used are $9.99 \times 10^5 \text{ L mol}^{-1} \text{ s}^{-1}$ and $9.66 \times 10^{-4} \text{ s}^{-1}$, respectively.

Figure 5-23: Theoretical vs. experimental evolution of styrene concentration with time for $f_s^0 = 0.8$. k_c^B and k_d^B values used are $9.99 \times 10^5 \text{ L mol}^{-1} \text{ s}^{-1}$ and $9.66 \times 10^{-4} \text{ s}^{-1}$, respectively.

Figure 5-24: Theoretical vs. experimental evolution of *n*-butyl acrylate concentration with time for $f_s^0 = 0.8$. k_c^B and k_d^B values used are $9.99 \times 10^5 \text{ L mol}^{-1} \text{ s}^{-1}$ and $9.66 \times 10^{-4} \text{ s}^{-1}$, respectively.

Figure 5-25: Experimental and simulated fraction of dormant chains with *n*-butyl acrylate as the terminal unit in the copolymerization of styrene and *n*-butyl acrylate with $f_s^0 = 0.29$.

Figure 5-26: Experimental and simulated fraction of dormant chains with *n*-butyl acrylate as the terminal unit in the copolymerization of styrene and *n*-butyl acrylate with $f_s^0 = 0.58$.

List of Schemes

Scheme 1-1: Mechanism for conventional free radical polymerization

Scheme 1-2: Degenerative chain transfer equilibrium

Scheme 1-3: ATRP equilibrium

Scheme 1-4: NMP equilibrium

Scheme 2-1: Initiation and mediating steps in nitroxide mediated polymerization using MAMA-DEPN alkoxyamine.

Scheme 2-2: A bimolecular NMP system

Scheme 2-3: Examples of first generation nitroxides (TEMPO and its derivatives).

Scheme 2-4: Examples of second generation nitroxides

Scheme 2-5: Preparation of the alkoxyamine Styryl-TEMPO

Scheme 2-6: Preparation of the alkoxyamine MAMA-DEPN via ATRA technique

Scheme 2-7: The NMP equilibrium and the termination step.

Scheme 3-1: The log-log plot of the chain length dependent termination rate coefficient ($k_t^{i,j}$) as a function of chain length (i), illustrating the generalized composite model for the termination process. The schematic also shows the chain length dependent exponents (α_i) and the crossover chain lengths (i_{SL} and i_{gel}). The corresponding value of the termination between two monomeric radicals ($k_t^{1,1}$) is also depicted.

Scheme 3-2: Schematic representation of thermally initiated *n*-butyl acrylate (M) polymerization in the presence of a free nitroxide (Y).

Scheme 3-3: The intramolecular chain transfer to polymer via the 1,5-hydrogen shift from the antepenultimate unit resulting in the transformation of a secondary propagating radical (SPR) into the mid-chain radical (MCR) at a rate determined by the rate coefficient of backbiting (k_{bb}).

Scheme 3-4: Formation of mid-chain radicals (MCRs) from secondary propagating radicals (SPRs) via backbiting and the subsequent transformation of the MCR to SPR via β -fragmentation and monomer addition.

Scheme 4-1: Model for nitroxide mediated polymerization of *n*-butyl acrylate with the inclusion of intra-molecular chain transfer to polymer and the reversible deactivation-activation reaction between the MCR and the nitroxide. P and Q symbolise the SPR and MCR, respectively.

Scheme 4-2: The possible dormant structures of poly(*n*-butyl acrylate) illustrating the adducts of the SPR and the MCR with the nitroxide DEPN.

Scheme 4-3: Nitroxide mediated *n*-butyl acrylate polymerization model implemented into Predici

Scheme 4-4: General structures of an adduct of SPR and a nitroxide (Structure A) and MCR and a nitroxide (Structure B)

Scheme 5-1: Terminal unit model (TUM) reaction scheme for the copolymerization of styrene and *n*-butyl acrylate showing initiation, propagation and NMP equilibria reactions.

Scheme 5-2: Penultimate unit model (PUM) propagation scheme for the copolymerization of styrene and *n*-butyl acrylate.

Scheme 5-3: Chemical structures of styrene and *n*-butyl acrylate indicating the vinylic protons that were monitored for concentration profiles.

Scheme 5-4: Structures of dormant chains with styrene (A) and *n*-butyl acrylate (B) as the terminal unit.

Scheme 5-5: The implicit penultimate unit model (IPUM) for the copolymerization of styrene and *n*-butyl acrylate implemented into the Predici software package.

List of Tables

Table 3-1: Literature homopropagation rate coefficients of *n*-butyl acrylate at different temperatures

Table 3-2: Literature homopropagation rate coefficients of styrene at different temperatures

Table 4-1: Rate coefficients used in the kinetic modelling of *n*-butyl acrylate using the Predici simulation package.

Table 5-1: Rate parameters used in the simulation of the nitroxide mediated copolymerization of styrene and *n*-butyl acrylate as depicted in Scheme 5-5.

List of Acronyms

AIBN	2,2'-Azobis(isobutyronitrile)
ATRA	atom transfer radical addition
ATRP	atom transfer radical polymerization
B/BA	<i>n</i> -butyl acrylate
BIPNO	2,2,5-trimethyl-4-(isopropyl)-3-azahexane-3-oxyle
BPO	benzoyl peroxide
CRP	controlled/living radical polymerization
DEPN	<i>N</i> - <i>tert</i> -butyl- <i>N</i> -[1-diethylphosphono-(2,2-dimethylpropyl)] nitroxide
DFT	density functional theory
DMF	dimethyl formamide
DMSO- <i>d</i> ₆	deuterated dimethyl sulphoxide
ESI	electrospray ionization
ESR	electron spin resonance
FRP	free radical polymerization
HAc	acetic acid
HPLC	high performance liquid chromatography
IPUM	implicit penultimate unit model
MAMA-DEPN	2-methyl-2[N- <i>tert</i> -butyl- <i>N</i> -(1-diethoxyphosphoryl)-2,2-dimethoxypropyl]aminoxylpropionic acid
MCR	mid-chain radical
NMP	nitroxide mediated polymerization
NMR	nuclear magnetic resonance
PAA	peroxyacetic acid
PDI	polydispersity index

PhEt-BIPNO	<i>N-tert-butyl-N-(1-isopropyl-2-methyl-propyl)-O-(1-phenyl-ethyl)-hydroxylamine</i>
PhEt-TIPNO	<i>N-tert-butyl-N-(2-methyl-1-phenyl-propyl)-O-(1-phenyl-ethyl)-hydroxylamine</i>
PLP	pulsed laser polymerization
PMDETA	N,N,N',N'',N'''-pentamethyldiethylenetriamine
PRE	persistent radical effect
PUM	penultimate unit model
RAFT	reversible addition-fragmentation chain transfer
RAFT-CLD-T	reversible addition-fragmentation chain transfer – chain length dependent - termination
RAFT-SP-PLP	reversible addition-fragmentation chain transfer – single pulse – pulsed laser polymerization
RLPAC	run length per activation cycle
S	styrene
SEC	size exclusion chromatography
SP-PLP-ESR	single pulse – pulsed laser polymerization – electron spin resonance
SPR	secondary propagating radical
TEMPO	2,2,6,6-tetramethylpiperidine-1-oxyl
TIPNO	2,2,5-trimethyl-4-phenyl-3-azahexane-3-oxyl
TUM	terminal unit model
UHP	ultra high purity

List of Symbols

D_i	diffusion coefficient
f_i	fraction of monomer i in feed composition
F_i	fraction of monomer i in copolymer composition
i	chain length
K	equilibrium constant
k_{bb}	rate coefficient of backbiting
k_c	rate coefficient of combination
k_d	rate coefficient of dissociation
k_p	rate coefficient of propagation
k_t	rate coefficient of termination
k_{thrm}	rate coefficient of thermal auto-initiation
k_β	rate coefficient of β -fragmentation
k_p^{av}	average rate coefficient of propagation
k_p^B	rate coefficient of propagation of n -butyl acrylate
k_{add}^B / k_i^B	rate coefficient of first n -butyl acrylate addition to initiator radical
k_p^S	rate coefficient of propagation of styrene
k_{add}^S / k_i^S	rate coefficient of first styrene addition to initiator radical
k_p^t	rate coefficient of propagation of mid-chain radicals
k_c^t	rate coefficient of combination involving mid-chain radicals
k_d^t	rate coefficient of dissociation involving mid-chain radicals
k_t^t	rate coefficient of termination between secondary propagating radical and mid-chain radical
$k_t^{i,j}$	rate coefficient of termination of radicals with chain lengths of i and j
k_t^{tt}	rate coefficient of termination between two mid-chain radicals

N_A	Avagadro's constant
p	spin multiplicity factor
r	monomer reactivity ratio
R	universal gas constant
R_i	rate of initiation
R_{deact}	rate of deactivation
R_p	rate of polymerization
s	radical reactivity ratio
t	time
T	temperature
w_p	weight fraction of polymer
α_i	chain length dependent exponent
δ	chemical shift
Δ	heat
ξ	conversion
σ	capture radius of termination
θ	fraction of mid-chain radicals

Chapter I: Introduction

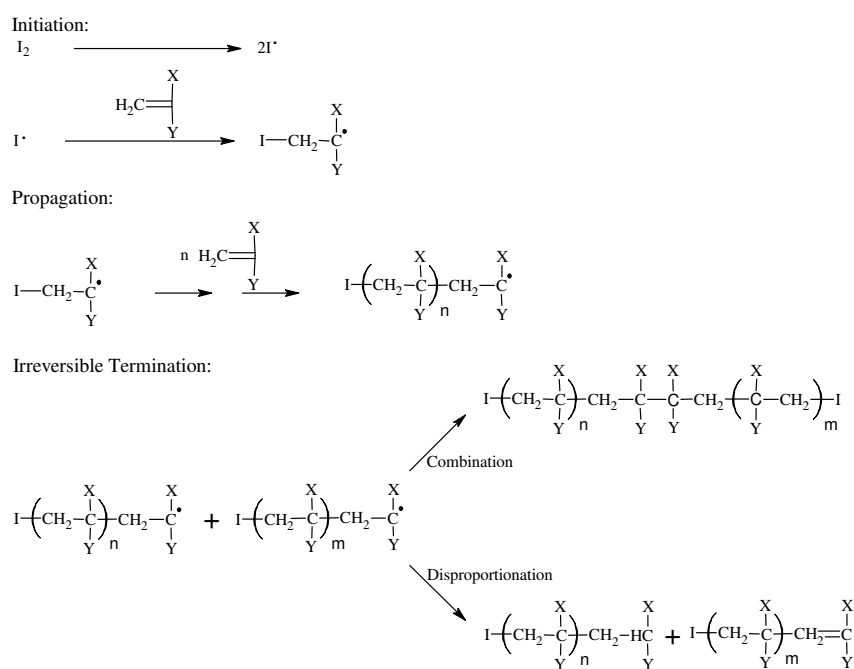
Synopsis

In this chapter a general introduction on conventional free radical polymerization is provided and a brief discussion of living/controlled free radical polymerization is given. An overview of the respective living/controlled free radical polymerization techniques, namely RAFT, ATRP and NMP is also given. This chapter concludes with the objectives of this work, together with a detailed outline of this dissertation.

1.1 Free Radical Polymerization

Natural polymeric materials have existed on earth for much longer than their synthetic counterparts. In their quest to understanding nature, mimicking some of nature's complex processes has become an ideal subject for some synthetic polymer chemists as far as polymeric materials are concerned. Synthetic polymeric materials find applications in numerous fields, with properties being improved continuously with research. A large fraction of the synthetic polymeric materials are produced via free radical polymerization (FRP), as they allow production of a wide variety of polymeric materials.

FRP comprises of three distinct steps, namely initiation, propagation and termination and these steps are as illustrated in Scheme 1-1. FRP is largely employed in industry in the production of a variety of polymers due to several advantages associated with it, which include a wide range of monomers that can be (co)polymerized and its tolerance to impurities. Due to its versatility, a wide range of homopolymers, copolymers and terpolymers can be produced with relative ease under industrial conditions.



Scheme 1-1: Mechanism for conventional free radical polymerization.

Irrespective of the advantages associated with FRP, the major drawback of the method lies in the difficulty to control the process. The lack of control is mainly due to continuous initiation and termination of radicals coupled with the high reactivity of radicals in the reaction medium which results in irreversible reaction of radicals with one another through either a coupling or disproportionation reaction. This results in the formation of termination products throughout the reaction, thus in conventional FRP, termination cannot be eliminated. The second drawback which is a direct consequence of the first one is poor control over molecular weight and molecular weight distribution. The high demand of advanced polymeric materials which require utmost control over the polymerization process, necessitated modification and improvement to conventional FRP in order to gain access to these materials. To address the limitations of conventional FRP, much attention has been paid to controlled/living radical polymerization over the past 15 years.

1.2 Controlled/Living Radical Polymerization (CRP)

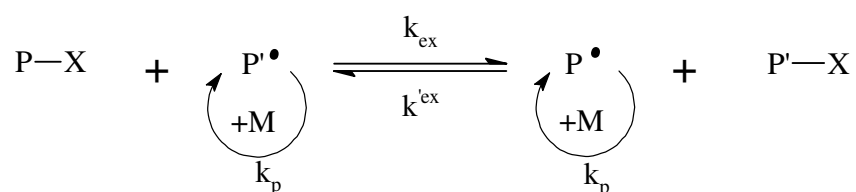
The concept of living polymerization was first discovered by Szwarc,¹ realizing that during styrene anionic polymerization all polymer chains grew until total consumption of the monomer and continued growing upon addition of more monomer. Upon addition of a suitable second monomer, a block copolymer was formed, and this behavior is attributed to the living character of the system. The molecular weight of the polymer formed could also be predicted based on the ratio of monomer to initiator and the resultant polydispersity indices were low, indicating control over the polymerization system.

Developments in CRP brought about new radical polymerization methods involving reversible activation–deactivation and degenerative exchange processes. In an ideal CRP, the degree of polymerization is observed to increase linearly with conversion and the polydispersity index decreases with conversion and often approaches unity. The key to CRP systems lies in the existence of a dynamic equilibrium between the propagating radicals and the dormant chains.² Radical trapping by a reversible activation–deactivation process relies on the persistent radical effect (PRE), as observed in both atom transfer radical polymerization (ATRP) and nitroxide mediated polymerization (NMP). On the other hand, systems dependent on degenerative transfer

are not based on PRE, as in the case of the reversible addition – fragmentation chain transfer (RAFT) mediated polymerization.

1.2.1 RAFT mediated polymerization

In a RAFT mediated polymerization system, chain transfer agents are added to provide a controlled and living character to the system, resulting in controlled molecular weight and molecular weight distribution, together with control of the chain end functionalities of the polymer.³

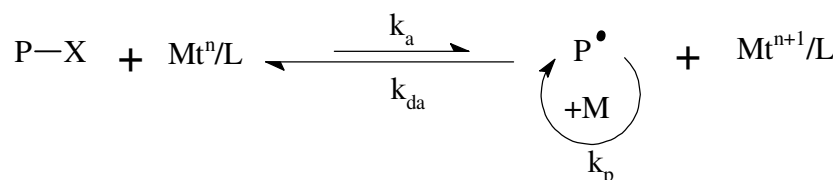


Scheme 1-2: Degenerative chain transfer equilibrium.

The controlled and living character of this system is achieved by reversible addition-fragmentation chain transfer (Scheme 1-2), which solely depends on the faster rate coefficient of chain transfer compared to that of propagation. This phenomenon results in polymer chains spending more time as dormant species relative to the time they spend in their active form.

1.2.2 ATRP

ATRP systems employ the use of an alkyl halide (P-X) together with a transition metal complex (Mt^n/L) as illustrated in Scheme 1-3. The homolytic cleavage of the alkyl halide is caused by the transition metal complex (Mt^n/L) resulting in the generation of an alkyl radical and the higher oxidation state metal halide complex (Mt^{n+1}/L).^{4,5}

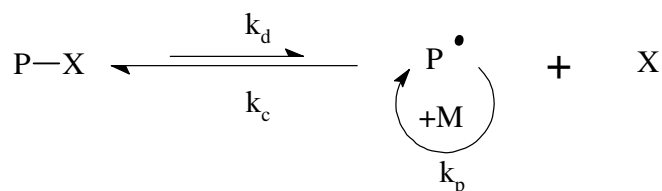


Scheme 1-3: ATRP equilibrium.

The alkyl radical generated adds monomer at a rate determined by the propagation rate coefficient (k_p) before undergoing reversible deactivation to form a dormant polymer chain end-capped with a halogen. In contrast to conventional FRP, the PRE largely minimizes irreversible radical–radical bimolecular termination in ATRP systems and the equilibrium in the system is shifted towards the dormant species.^{6, 7} The equilibrium should be optimized such that the propagating radical concentration is optimum to allow reasonable rates of propagation and minimize the amount of dead polymer chains formed.

1.2.3 NMP

NMP employs persistent radicals (X) which reversibly deactivate propagating alkyl radicals to form a dormant polymer chain (P–X), Scheme 1-4.



Scheme 1-4: NMP equilibrium.

Persistent radicals employed in this system are nitroxide compounds, which are stable radicals which will only react reversibly with the alkyl radicals to form a dormant species.

1.3 *In situ* NMR Spectroscopy

Recently, *in situ* NMR spectroscopy has proven to be a very useful and powerful technique in investigations of CRP. It is used to follow the concentration profile of one or several species in the reaction mixture and the information obtained can be very useful in elucidating and understanding the kinetic and mechanistic aspects of the reaction in question.⁸⁻¹⁰

1.4 Objectives of this work

The aims of the project were to study the kinetic and mechanistic features of homo- and copolymerization reactions of styrene and *n*-butyl acrylate mediated by persistent radical species in the form of nitroxides. *In situ* ¹H NMR was the primary technique for monitoring the

polymerization process. A unimolecular NMP system would be favoured over the bimolecular process, primarily because of the greater control over condition experienced in the unimolecular system. The alkoxyamine of choice is 2-methyl-2[N-tert-butyl-N-(1-diethoxyphosphoryl-2,2-dimethoxypropyl)aminoxy]propionic acid, abbreviated MAMA-DEPN. The use of *in situ* ^1H NMR allows for periodic acquisition of data so that the products, reactants and products of side reactions can be profiled as a function of polymerization time. Due the presence of the phosphorus in the nitroxide, *in situ* ^{31}P NMR would be used to follow the copolymerization of styrene and *n*-butyl acrylate and aid in the profile of the terminal unit of dormant chains with time as a function of initial feed composition. Simulation of both homo- and copolymerization reactions will be performed using the Predici software package (version 6.72.3) to help in the quest of explaining the experimentally observed kinetic features. A brief outline of this report is given in Section 1.5.

1.5 Outline

In Chapter II, a brief introduction on living radical polymerization is given with the focus is made on concepts of nitroxide mediated polymerization (NMP). The subject of mechanisms involved in both bimolecular and unimolecular NMP processes is touched on and a brief history on the development of nitroxides is given. A brief overview is given on the reported kinetic equations governing the different aspects of NMP, and also on methods reported in literature for the determination of kinetic constants involved in NMP.

In Chapter III, the concepts of homopolymerization of styrene and *n*-butyl acrylate as a building block for the copolymerization reactions that are dealt with in Chapter V are reported. Detailed outline for the optimized synthetic route of the nitroxide (DEPN) and the corresponding alkoxyamine (MAMA-DEPN) is reported in this chapter. The use of *in situ* ^1H NMR spectroscopy allows for respective homopolymerizations to be monitored in real time. The independence of rate of polymerization on the initial concentration of the alkoxyamine in the case of *n*-butyl acrylate homopolymerization is discussed.

Chapter IV addresses the side reactions experienced in the high temperature *n*-butyl acrylate homopolymerization in the presence of a nitroxide species via experimentation and theoretical models. The simulations of the polymerization were carried out with the Predici software package. The results obtained from simulations of the nitroxide mediated homopolymerization yielded valuable information which is able to explain a phenomenon of rate independence reported in Chapter III.

In Chapter V the copolymerizations of styrene and *n*-butyl acrylate will be studied using *in situ* ^1H and ^{31}P NMR techniques. The concept of differentiating between copolymerization models is introduced, defining both the terminal unit model (TUM) and the penultimate unit model (PUM) for copolymerization. From the data obtained from the *in situ* NMR copolymerizations, reactivity ratios of styrene and *n*-butyl acrylate were determined for the NMP system initiated by MAMA-DEPN. Simulations of styrene/*n*-butyl acrylate copolymerization are carried out with Predici software package, assuming the implicit penultimate unit model.

Chapter VI deals with the general findings and conclusions to the work reported in this dissertation. Recommendations for future studies are also provided.

References

1. Szwarc, M. *Nature* **1956**, 178, 1169-1170.
2. Braunecker, W. A.; Matyjaszewski, K. *Progr. Polym. Sci.* **2007**, 32, 93 - 146.
3. Matyjaszewski, K.; Davis, T. P., *Handbook of Radical Polymerization*. Wiley-Interscience: 2002.
4. Kamigaito, M.; Ando, T.; Sawamoto, M. *Chem. Rev.* **2001**, 101, (12), 3689 - 3745.
5. Matyjaszewski, K.; Xia, J. *Chem. Rev.* **2001**, 101, 2921 - 2990.
6. Tang, W.; Tsarevsky, N. V.; Matyjaszewski, K. *J. Am. Chem. Soc.* **2006**, 128, 1598 - 1604.
7. Fischer, H. *Chem. Rev.* **2001**, 101, (12), 3581 - 3610.
8. Aguilar, M. R.; Gallardo, A.; Fernández, M. d. M.; Román, J. S. *Macromolecules* **2002**, 35, (6), 2036-2041.
9. Abdollahi, M.; Mehdipour-Ataei, S.; Ziaee, F. *J. Appl. Polym. Sci.* **2007**, 105, 2588-2597.
10. Pound, G.; McLeary, J. B.; McKenzie, J. M.; Lange, R. F. M.; Klumperman, B. *Macromolecules* **2006**, 39, 7796-7797.

Chapter II: Controlled/Living Radical Polymerization Kinetics-An Overview

Synopsis

In this chapter a brief introduction on living radical polymerization is given with the focus on the concepts of nitroxide mediated polymerization (NMP). Mechanisms involved in both bimolecular and unimolecular NMP processes are described and a brief history of the nitroxide development is also given. A brief overview is given of the reported kinetic equations governing the different aspects of NMP, and also methods reported in literature used for the determination of kinetic constants involved in NMP.

2.1 Living Radical Polymerization; Concepts

The ideas behind controlled/living radical polymerization (CRP) for both degenerative transfer and persistent radical effect (PRE) based mechanisms were briefly introduced in the previous chapter. From this point, focus will mainly be on PRE based mechanisms, especially nitroxide mediated polymerization (NMP). Through controlled/living radical polymerization, specialized polymers of defined architecture, molecular weight and narrow molecular weight distribution are obtained with relative ease. The living character, control over molecular weight and molecular weight distribution characteristic of a CRP process are obtained because of minimized termination reactions combined with the fact that all polymer chains are allowed to grow at about the same rate since initiation is generally fast relative to the time of polymerization. In the case of NMP, the equilibrium between the propagating radicals and the persistent radical species is very important in determining the living character and control over a polymerization system. To attain a high degree of control and living character, the equilibrium constant ($K = k_d/k_c$, where k_d is the dissociation constant and k_c is the combination constant) of the system should be sufficiently small.¹ This will result in a low concentration of the propagating radicals, which will also be short lived before they reversibly terminate with persistent radical species. This will on average allow for addition of one or two monomer units to the propagating radical before transition into the dormant state.

The prediction of the average number of monomer units added per activation-deactivation cycle can be made by calculating the run length per activation cycle (RLPAC) as illustrated by Equation 2-1.²⁻⁴

$$RLPAC = \frac{R_p}{R_{deact}} = \frac{k_p [P\cdot][M]}{k_c [P\cdot][X]} = \frac{k_p [M]}{k_c [X]} \quad (2-1)$$

In Equation 2-1 the parameters used are explained as follows: R_p is the rate of polymerization, R_{deact} is the rate of deactivation of the transient radicals by the nitroxide, k_p is the coefficient of propagation, $[P\cdot]$ transient radical concentration, $[M]$ is the monomer concentration, and $[X]$ is the concentration of the nitroxide. From Equation 2-1, it can be seen that the relation $k_c > k_p$

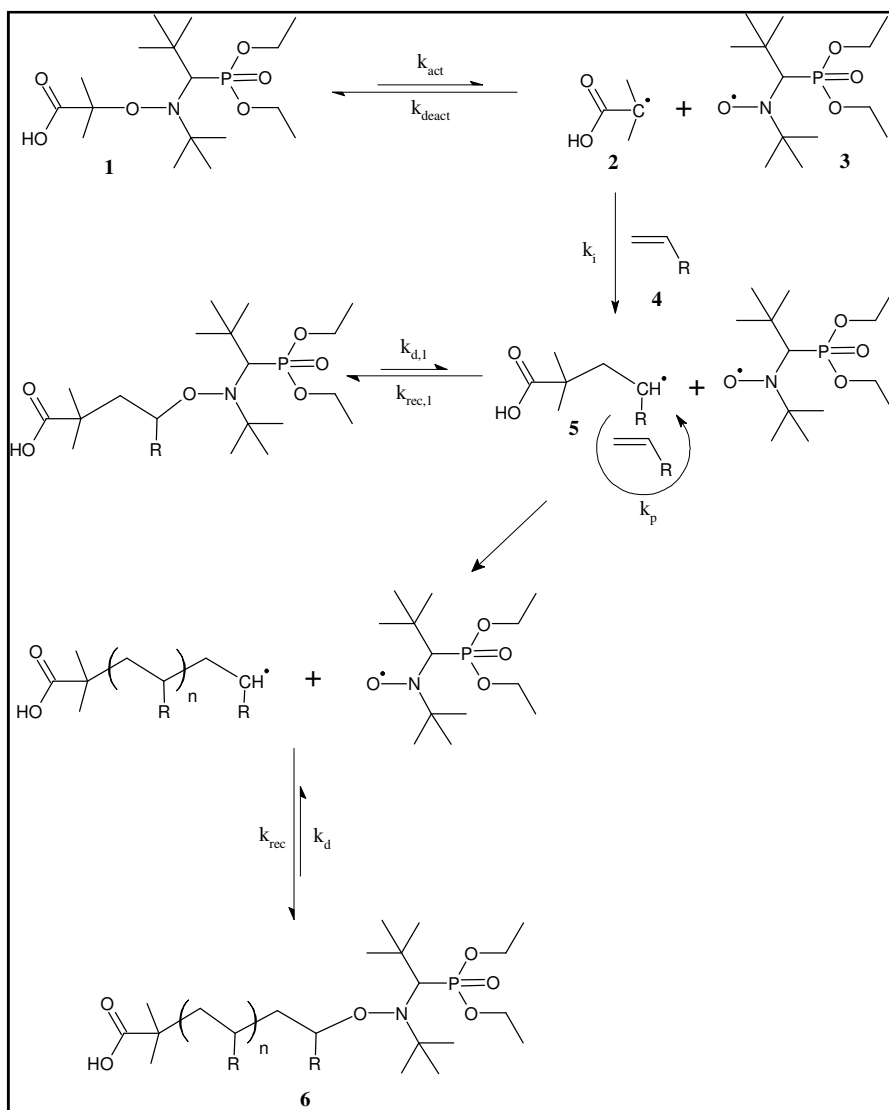
should be satisfied to attain the one or two monomer addition scenario per activation cycle for a typical monomer and nitroxide concentrations of the order 10^1 mol/L and 10^{-3} mol/L respectively.

2.2 Nitroxide Mediated Polymerization (NMP)

2.2.1 Basic Mechanism

The concepts behind the use of nitroxides in free radical polymerization date as far back as the 1980s, from the work of Solomon and coworkers^{5,6} with further advancement of the technique by Georges.⁷ Following Scheme 2-1, the dynamic equilibrium that exists between the active (**5**) and dormant (**6**) species in NMP is the major feature which is crucial to the degree of control of the polymerization process. The alkoxyamine initiator (**1**) is homolytically cleaved at the C–ON bond to give the transient radical (**2**) and the corresponding persistent nitroxide radical (**3**).

The transient radicals will add monomer units (**4**) before they are reversibly deactivated to the dormant form (**6**) by recombining with the nitroxide radicals. Due to the homolytic cleavage of the alkoxyamine, equal concentrations of persistent species (nitroxides) and transient radicals would normally be expected from the simple logic that for every transient radical formed a nitroxide is also formed. This is not the case that is observed in NMP, due to the fact that transient radicals will undergo irreversible bimolecular termination to some extent.⁸ In principle, nitroxides will not undergo any reaction other than reversible deactivation with the transient radical, thus the net result of the bimolecular termination of the transient radicals will be a buildup of excess nitroxide. The buildup of excess nitroxide radicals will favour the reversible deactivation of the transient radicals to form dormant polymer chains, and the irreversible bimolecular termination of the transient radicals is significantly decreased even though it never ceases completely. This phenomenon was termed the persistent radical effect (PRE),¹ which is discussed in detail later.

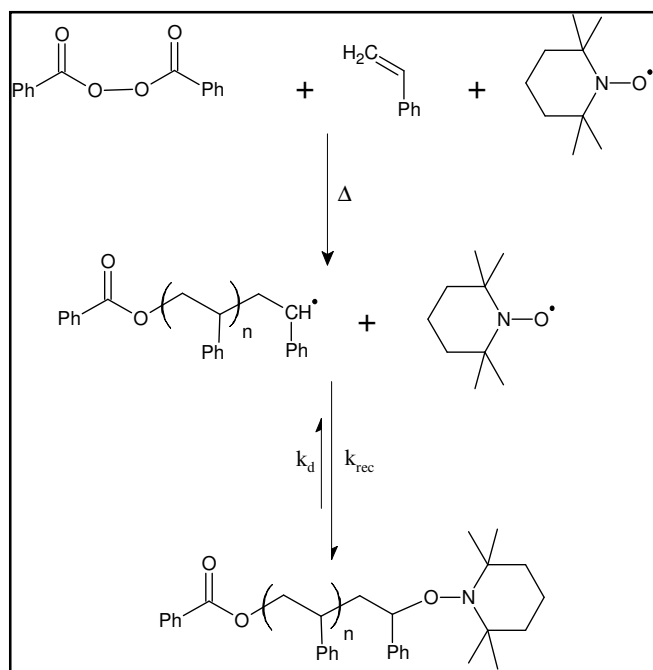


Scheme 2-1: Initiation and mediating steps in nitroxide mediated polymerization using MAMA-DEPN alkoxyamine.

2.2.2 Bimolecular vs Unimolecular NMP Processes

2.2.2.1 Bimolecular Process

In NMP, bimolecular processes refer to instances where a conventional free radical initiator, such as 2,2'-Azobis(isobutyronitrile) (AIBN) or benzoyl peroxide (BPO) is employed in conjunction with a free nitroxide in the presence of monomer and the result is an *in situ* generation of the alkoxyamine.



Scheme 2-2: A bimolecular NMP system.

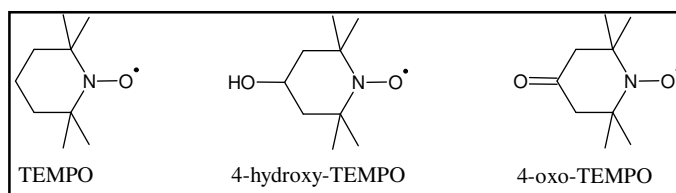
Scheme 2-2 illustrates a bimolecular process for the polymerization of styrene using BPO as the initiator and TEMPO as the controlling nitroxide as was applied by Georges and coworkers⁷ in the synthesis of narrow molecular weight distribution polymers with polydispersity indices (PDI) comparable to those obtained by anionic polymerization methods.

2.2.2.2 Unimolecular Process

The unimolecular process in NMP follows the mechanistic aspects as illustrated earlier in Scheme 2-1, in which alkoxyamines are made use of, as they homolytically cleave to give radicals that can initiate polymerization (transient radicals) and persistent radicals which will control the polymerization process. This system allows for the use of a single molecule to initiate and control the polymerization process. The drive towards the development of unimolecular systems was the poorly defined nature of the bimolecular process together with its unknown concentration of initiating species.⁹ The subject of alkoxyamine synthesis and the importance of the identity of the persistent radical (nitroxide) will be discussed in more details in coming sections.

2.2.3 Nitroxides Development: Review

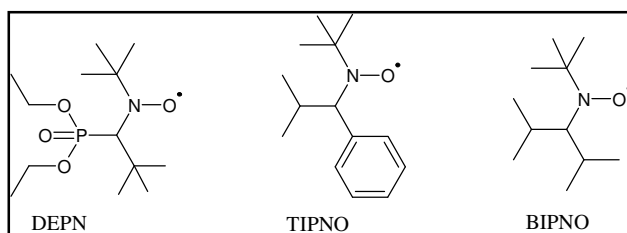
The degree to which control over a nitroxide mediated polymerization system is attained is strongly dependent on the structure of the persistent radical. The nitroxides TEMPO and TEMPO based derivatives (Scheme 2-3) together with their alkoxyamines are known to efficiently control only the polymerization of monomers such as styrene and its derivatives.



Scheme 2-3: Examples of first generation nitroxides (TEMPO and its derivatives).

However, TEMPO based nitroxides can also be used to control the random copolymerization of styrene with comonomers such as acrylates,^{10, 11} methacrylates¹¹⁻¹⁴ or acrylonitrile¹¹ yielding copolymers with low PDI, with number-average molecular weight, M_n , increasing linearly with monomer conversion and in good agreement with the theoretically expected values. Decreasing the molar fraction of the styrenic monomer in the feed resulted in the deviation between theoretical M_n and the experimentally obtained M_n increased and the PDI was also observed to increase.^{12, 15}

Shortcomings of TEMPO and other TEMPO based nitroxides, referred to as the first generation nitroxides, prompted the development of the second generation nitroxides (Scheme 2-4). In comparison with the first generation nitroxides, distinct features in the structure of the second generation nitroxides are that they are acyclic and that they bear hydrogen on one of the α -carbons, contrary to the two quaternary α -carbons found in the first generation nitroxides.



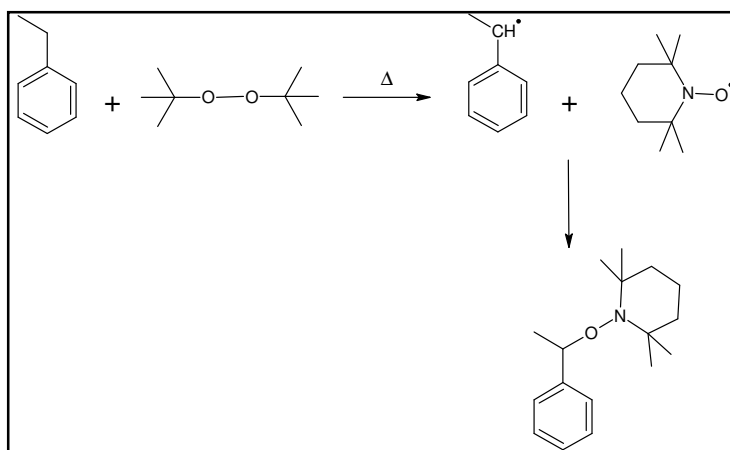
Scheme 2-4: Examples of second generation nitroxides.

These second generation nitroxides allowed for efficient polymerization of styrene and its derivatives in addition to a variety of other monomers such as acrylates¹⁶⁻¹⁸, acrylamides^{19, 20}, dienes²¹ and acrylonitrile¹⁹. Polymerization of styrene in the presence of DEPNO as the mediating radical was reported²² to proceed faster than in the case when TEMPO was used as a mediating radical. TIPNO and BIPNO were also applied successfully to the controlled polymerization of styrene.²³ Comparative studies between the first generation nitroxides and the second generation nitroxides showed not only advantages in terms of the versatility of monomers that can be polymerized under controlled conditions but also the kinetics were appreciably enhanced in the case of second generation nitroxides.^{23, 24}

2.2.4 Alkoxyamine Synthetic Approaches

2.2.4.1 Introduction

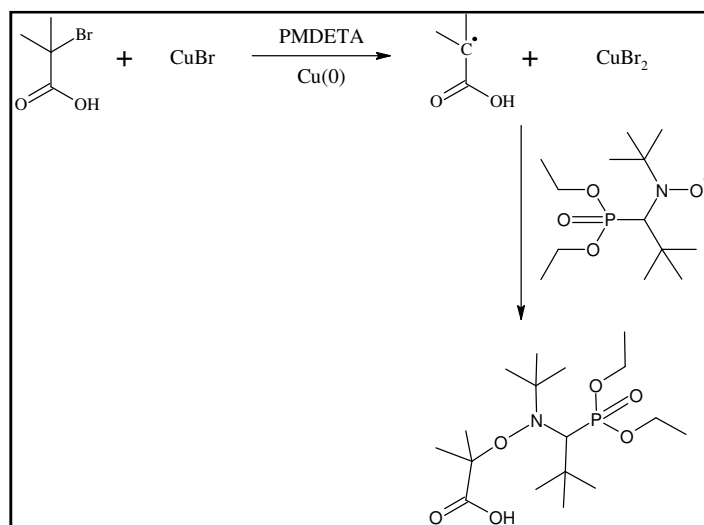
The development of functionalized unimolecular initiators in NMP was important, in that functionalized chain ends of polymers could readily be obtained on top of the already known advantages of the NMP system. The unimolecular initiators will be referred to as model alkoxyamines, to differentiate them from macro-alkoxyamines which refer to the polymer chains end capped with a nitroxide and capable of reinitiating a controlled polymerization process upon heating. The synthetic approach initially used for model alkoxyamines involved the generation of carbon centered radicals followed by trapping of the carbon centered radicals by the stable nitroxide radicals (Scheme 2-5). The major drawback of this synthetic procedure was low yields obtained due to many side reactions that occurred,⁹ which rendered the purification of the final product very difficult.



Scheme 2-5: Preparation of the alkoxyamine Styryl-TEMPO.

2.2.4.2 Tailoring the Right Alkoxyamine

Due to the drawbacks encountered in the initial synthetic routes of model alkoxyamines, efforts were made to improve the product yield and lower the side reactions by development of new strategies towards the synthesis of model alkoxyamines. Several reports have been made on the synthesis of TEMPO based alkoxyamines, and of several other new nitroxides. Hill²⁵ reported the synthesis of a new aryloethyl-functionalized N-alkoxyamine initiator for the preparation of end-functionalized polymer by NMP, and Pradhan²⁶ reported a highly selective route to allylic alkoxyamines applying an ene-like addition of an oxoammonium cation to alkenes. Flakus and coworkers²⁷ reported a synthetic route for the synthesis of phenylethyl-alkoxyamine of BIPNO with the aid of a Jacobsen-like manganese catalyst, with yields in excess of 90%. The application of atom transfer radical addition (ATRA) in the presence of Cu(0) to the synthesis of alkoxyamines by Matyjaszewski,²⁸ provided a facile low temperature route to the synthesis of model alkoxyamines (Scheme 2-6).



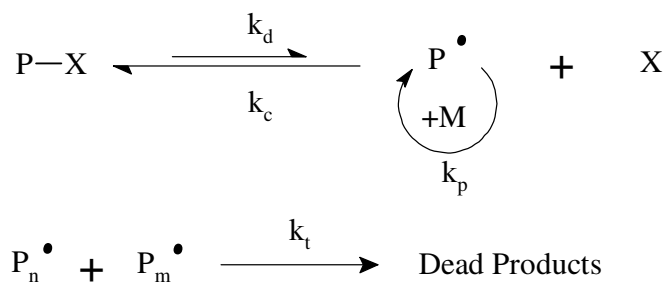
Scheme 2-6: Preparation of the alkoxyamine MAMA-DEPN via the ATRA technique.

The alkyl moiety in the alkoxyamine can be tailor-made to the desired group due to the wide availability of the alkyl halide compounds required for the synthetic procedures. In this procedure, an alkyl halide is treated with a copper(I) complex resulting in controlled generation of alkyl radicals and the corresponding copper(II) complex followed by trapping with a nitroxide of choice to give the corresponding alkoxyamine in very high yields. The use of copper(0) powder in the reaction aids in the reduction of the copper(II) to copper(I) in the presence of a stabilizing ligand such as N,N,N',N'',N''-pentamethyldiethylenetriamine (PMDETA).^{28, 29} This allows for complete conversion of the alkyl halide in the presence of a slight excess of the nitroxide to give high yields of the alkoxyamine.

2.2.5 Kinetic Aspects of NMP

2.2.5.1 The Persistent Radical Effect (PRE)

To explain the principles behind PRE, Scheme 2-7 will be considered.



Scheme 2-7: The NMP equilibrium and the termination step.

In unimolecular NMP systems, the concentration of transient radicals and persistent radical species generated at the initial stages of the reaction are equal, and the persistent radical species will only react reversibly with the transient radicals while on the other hand the transient radicals also react irreversibly in a bimolecular fashion resulting in dead products. The competition between the reversible deactivation and the irreversible bimolecular termination is present at early stages of the polymerization due to the low concentration of the persistent radical species. By applying simple stoichiometry it becomes clear that for every bimolecular termination of the transient radicals there is an excess buildup of two equivalents of the persistent radical species. The continuation of the irreversible bimolecular termination by the transient radicals will further result in buildup of excess persistent radical species to a point where the deactivation reaction in Scheme 2-7 will be more favored over the irreversible termination due to low radical concentration at any instant in the reaction. Despite the equilibrium being shifted towards the dormant species, irreversible bimolecular termination never ceases to occur even though it is highly suppressed.

2.2.5.2 Bimolecular NMP Systems

To describe the kinetics of these NMP systems, it is appropriate to consider the reaction illustrated by Scheme 2-7 and to take into account the persistent radical effect^{1, 8, 30} in the polymerization process. The rate of consumption of the monomer can be regarded as the prime factor in the kinetic description of the polymerization process and is expressed as:

$$-\left(\frac{d[M]}{dt}\right) = k_p [P^\bullet][M] \quad (2.1)$$

The expressions for the propagating and persistent radical concentrations in the polymerization system are defined by the following differential equations:

$$\left(\frac{d[X]}{dt}\right) = k_d[P-X] - k_c[P\cdot][X] \quad (2-2)$$

$$\left(\frac{d[P\cdot]}{dt}\right) = k_d[P-X] - k_c[P\cdot][X] + R_i - 2k_t[P\cdot]^2 \quad (2-3)$$

where R_i is the rate of conventional initiation in the case of bimolecular NMP systems and in the case of unimolecular processes R_i will only be significant in the case of styrene polymerization at high temperatures where spontaneous thermal initiation is quite significant. If any side reactions other than reactions defined by Equations 2-2 and 2-3 are neglected, the fraction of dead chains can be considered negligible. If the assumption that all the rate constants are chain length independent is valid, an expression for the transient radicals and the persistent species under quasi-equilibrium conditions can be written as:

$$[P\cdot][X] = K[P-X]_0 = KI_0 \quad (2-4)$$

with

$$K = k_d/k_c \quad (2-5)$$

where $I_0 = [P-X]_0 = [P_0 - X]$ represents the initial concentration of the model alkoxyamine initiator.

If R_i is significant, the NMP system will reach a stationary state after a certain period of time. At stationary state conditions both the concentration of $P\cdot$ and X are constant, thus $d[P\cdot]/dt = d[X]/dt = 0$ and the expressions for the concentrations of transient radicals and persistent species can be written as

$$[X] = (KI_0) \left(\frac{2k_t}{R_i} \right)^{1/2} \quad (2-6)$$

$$[P\cdot] = \left(\frac{R_i}{2k_t} \right)^{1/2} \quad (2-7)$$

From Equations 2-6 and 2-7 it can be deduced that the balance between initiation and termination rates will only determine the concentration of transient radicals typical of conventional polymerization systems, while on the other hand the equilibrium constant will affect the concentration of the persistent radical species.

The expression for the rate of polymerization is $R_p = k_p [P\cdot][M]$ and it is independent of the reversible activation-deactivation reaction (Scheme 1-4) which is also typical of the conventional polymerization system and the corresponding conversion index can be expressed as:

$$\ln \left(\frac{[M]_0}{[M]} \right) = k_p \left(\frac{R_i}{2k_t} \right)^{1/2} t \quad (2-8)$$

2.2.5.3 Unimolecular NMP Systems

In unimolecular NMP systems the generation of radicals, both transient and persistent will increase rapidly in the early stages of the polymerization reaction due the fact that the radical concentration is too small for the deactivation reaction (Scheme 1-4) to be significant. Due to the PRE explained in the previous section (2.2.5.1), the increase in the concentration of transient radicals will slow down and the concentration of the persistent radical species will continue to increase but at a slower rate. In this case, to solve the expressions of transient radicals and persistent radical species the term R_i in Equation 2-3 is taken as zero and Equation 2-4 is not used in Equation 2-3 when finding the solutions to the differential equations. Thus the resulting expressions for $[P\cdot]$ and $[X]$ are as illustrated by Equations 2-9 and 2-10, respectively.^{1,31}

$$[P\cdot] = (K[P - X]_0 / 6k_t)^{1/3} t^{-1/3} \quad (2-9)$$

$$[X] = \left(3k_t K^2 [P - X]_0^2\right)^{1/3} t^{1/3} \quad (2-10)$$

To find the expression for the conversion index, Equation 2-9 is substituted into Equation 2-1 to yield Equation 2-11, which upon rearrangement results in Equation 2-12.

$$-\left(\frac{d[M]}{dt}\right) = k_p [M] (K[P - X]_0 / 6k_t)^{1/3} t^{-1/3} \quad (2-11)$$

$$-\left(\frac{d[M]}{[M]}\right) = (k_p (K[P - X]_0 / 6k_t)^{1/3}) t^{-1/3} dt \quad (2-12)$$

Integrating Equation 2-12 with respect to $[M]$ and t in their respective limits of ($[M]_0$ to $[M]$) and ($t = 0$ to $t = t$), the expression for the conversion index is obtained as¹

$$\ln([M]_0/[M]) = (3k_p/2) (K[P - X]_0 / 6k_t)^{1/3} t^{2/3} \quad (2-13)$$

From Equation 2-13 it is evident that in the case of the nitroxide mediated polymerization system where a unimolecular initiator has been employed, the conversion index will show a one third and two thirds order dependence on the initial alkoxyamine concentration and time, respectively. Lutz and coworkers³² illustrated the experimental validity of the PRE theory by employing an alkoxyamine styryl-DEPN in the polymerization of styrene and obtained the conversion index which showed a two thirds order dependence on time according to Equation 2-13. On the other hand, the work of Benoit and coworkers¹⁶ where a free nitroxide and a conventional initiator are employed, the conversion index showed a first order dependence on time according to Equation 2-8. Also complementary is the work reported by Schierholz and coworker²⁰ showing first order dependence of the conversion index on time for the nitroxide mediated polymerization of *N,N*-dimethylacrylamide initiated by conventional initiator. Phan and coworkers³³ also reported polymerization of *n*-butyl acrylate using MAMA-DEPN as the unimolecular initiator and a slight excess of the free nitroxide DEPN and the conversion index showed a first order dependence on time.

An ideal system in NMP is the one where the concentration of transient radicals at any instance is at its lowest, thus limiting the undesired irreversible bimolecular termination. Thus from the expression of the equilibrium constant, Equation 2-5, for the reversible activation-deactivation reaction illustrated by Scheme 2-7, it is evident that for the equilibrium to be shifted more to the dormant species the equilibrium constant should be sufficiently small. This will allow for controlled growth of the polymer chains in a stepwise manner, where a unit or two are added on average per activation-deactivation cycle.

2.2.6 The NMP Equilibrium Constant (K)

The degree to which a nitroxide mediated polymerization system is controlled and the living character sustained/maintained is mainly dependent of the main NMP equilibrium (Scheme 1-4) governed the equilibrium constant K (Equation 2-5). As mentioned in Section 2.1, a high degree of control and living character is attainable for systems with sufficiently small values of the equilibrium constant. Systems with larger values of the equilibrium constant will lead to high concentration of transient radicals thereby leading to increased levels of irreversible bimolecular termination and as a consequence losing control and living character of the system.

However, exceedingly small values of the equilibrium constant will lead to inhibition of the polymerization process or bring it to a complete halt at low monomer conversions (typically < 10%). The inhibition or halt at low monomer conversion is a result of the formation of a stable C—ON bond between the propagating radical and the nitroxide that cannot cleave at the polymerization temperature. Vinyl acetate is such a monomer which cannot be polymerized by NMP due to the stable C—ON bond of the dormant species, and thus the chains of poly(vinyl acetate) end capped with the nitroxide will not be re-activated.^{34, 35}

If one considers methyl methacrylate from the family of methacrylic esters, the polymerization mediated by TEMPO is unsuccessful due to the dominant disproportionation reaction between the transient radical and the nitroxide. In the case where the polymerization is mediated by DEPN (second generation nitroxide) such disproportionation reactions are negligible. However even in the absence of disproportionation reactions, the polymerization of methyl methacrylate mediated by DEPN is still uncontrollable. The lack of control in the latter case can be attributed

solely to the large equilibrium constant governing the reversible activation-deactivation reaction between the nitroxide and the transient radical.^{36, 37} As a result of a large equilibrium constant, irreversible bimolecular termination becomes the dominant fate of the high concentration of the transient radicals.

Despite the difficulty in the nitroxide mediated polymerization of methyl methacrylate, the past few years have seen significant development towards this system. The polymerization of methyl methacrylate mediated by DEPN in the presence of a minimal amount of styrene or acrylonitrile has allowed the synthesis of well controlled polymers rich in methyl methacrylate by NMP.³⁸⁻⁴⁰

2.2.7 Rate Constants of Activation

One of the requirements for controlled radical polymerization is that initiation should be fast relative to the time of polymerization so as to allow polymer chains to start growing at the same time to give low polydispersity polymers. The knowledge of the decomposition rate of an alkoxyamine initiator is very important in giving a full kinetic description of a specific monomer(s) system. The alkoxyamine initiator can either be a model alkoxyamine compound or a preformed macro-alkoxyamine initiator. The preformed macro-alkoxyamines initiators are very important in the synthesis of block copolymers where mono- or di-functional model alkoxyamines can be used to prepare these precursors.^{20, 33, 41-43} Several methods have been used in the determination of activation rate constants of alkoxyamines and these include alkoxyamine homolysis in the presence of a radical scavenger.⁴⁴⁻⁴⁶ The second method for the determination of the activation rate constant, which is solely applied to macro-alkoxyamines is the SEC curve resolution method.^{16, 24, 47, 48}

The method of alkoxyamine homolysis in the presence of a radical scavenger has been undertaken where a different nitroxide or oxygen is used as the scavenger.⁴⁵ In the case of a different nitroxide being used as a scavenger, monitoring the disappearance of the original alkoxyamine (Alk_1) and the appearance of the new alkoxyamine (Alk_2) by offline HPLC can enable the use of Equation 2-14 to obtain the activation rate constant

$$\ln\left(\frac{[Alk_1]_t}{[Alk_1]_0}\right) = -k_d t \quad (2-14)$$

and from the knowledge that at any instant in the reaction

$$[Alk_1]_{t=0} = [Alk_1]_t + [Alk_2]_t \quad (2-15)$$

Therefore substituting Equation 2-15 into 2-14 results in the following expression⁴⁵

$$\ln\left(1 + \frac{[Alk_2]_t}{[Alk_1]_t}\right) = k_d t \quad (2-16)$$

Apart from the use of offline HPLC to determine alkoxyamine activation constant, quantitative ESR spectroscopy has also been used.^{44, 46} This is achieved by monitoring the concentration of the persistent radicals formed upon alkoxyamine homolysis in the presence of a radical scavenger such as oxygen and applying the following expressions

$$\ln\left(\frac{[nitroxide]_\infty - [nitroxide]_t}{[nitroxide]_\infty}\right) = -k_d t \quad (2-17)$$

$$[nitroxide]_t / [nitroxide]_\infty = k_d t \quad (2-18)$$

On the other hand, determination of activation rate constants of macro-alkoxyamine initiators using the SEC curve resolution method and SEC polydispersity method were introduced by Fukuda. In the curve resolution method, the concentration of the macro-alkoxyamine initiator is followed by SEC. Consider $[P_0-X]_0$ as the initial concentration of the macro-alkoxyamine initiator. Mixing the macro-alkoxyamine initiator with a precise amount of monomer and re-initiating the polymerization for a specific time, the persistent radical species will cleave allowing the transient radicals to add monomer before transforming into dormant species again. The result is the formation of new dormant species of higher molecular weight that is

distinguishable in the SEC curve from the initial macro-alkoxyamine. Therefore if the concentration of the initial macro-alkoxyamine at any instant is defined by $[P_0 - X]_t$, the following first order expression can be written,

$$\ln\left(\frac{I_0}{I_t}\right) = \ln\left(\frac{[P_0 - X]_0}{[P_0 - X]_t}\right) = k_d t \quad (2-19)$$

Thus following the concentration of $[P_0 - X]$ as a function of time using the area under the SEC curves enables the determination of the activation constant of the macro-alkoxyamine. Relatively easy as this method may seem, it is however quite difficult to resolve, quantitatively, the SEC curves of the dissociated and the non-dissociated fractions of the macro-alkoxyamine. A conventional radical initiator is added to the reaction medium to help improve the resolution between the SEC curves.

Drache et al.²³ reported an enhanced Fukuda's SEC curve resolution method, in which good curve resolutions are obtained within the low molecular weight range, which is applicable also to low molecular weight model alkoxyamines. In this enhanced method by Drache et al., a very sensitive UV detector is made use of, to determine the concentration of the model alkoxyamine and that of the free nitroxide. To determine the activation constant, Equation 2-19 is used, but with model alkoxyamine concentrations instead of that of macro-alkoxyamine.

2.2.8 Rate enhancement in NMP with the aid of additives

The ideas behind the addition of additives such as camphor sulfonic acid⁴⁹ to TEMPO-mediated polymerization of styrene were born to improve the rates of polymerization and shorten polymerization times which sometimes were in the order of days.^{49, 50} The additives have been applied mainly to systems mediated by TEMPO.⁴⁹⁻⁵¹ The additive of choice has seemed to be camphor sulfonic acid,⁴⁹⁻⁵³ even though compounds like 2-fluoro-1-methylpyridinium *p*-toluenesulfonate,⁵⁰ anhydrides⁵⁴ and certain organic acids⁵⁵ have successfully improved the rate of TEMPO-mediated styrene polymerization.

Malmström et al.⁵⁴ developed a new class of rate enhancing additives for use in nitroxide mediated polymerizations. The proposed explanation of the rate enhancement is that the reversible acylation of the nitrogen of the alkoxyamine induces a partial positive charge that results in the polarization of the N—O bond thus weakening the NO—C bond. In the light of the proposed explanation of the rate enhancement by Malmström et al.,⁵⁴ the application of such a series acylating agents to the second generation nitroxide mediated polymerization of monomers such as vinyl acetate seems ideal³⁵, in conjunction with further nitroxide development studies.

2.2.9 The potential of NMP, advantages over other living systems and the drawbacks of the technique

Relative to other polymerization techniques, NMP enjoys the benefits of being a relatively clean system. Copolymers produced by NMP need not undergo complicated purification processes like end group removal in RAFT to get rid of the sulphur moiety and the removal of the copper catalyst in ATRP. One disadvantage of NMP used to be the high polymerization temperatures required, but the development of new nitroxides and their respective alkoxyamine has opened a new window of endless possibilities towards low temperature polymerization in NMP. One such achievement comes at a price of course; the polymerization rates will be expected to be a bit lower at low temperatures. But a full understanding of the kinetic aspects coupled with mechanistic features of the technique can be of immense value in the achievement of the optimal conditions for different systems of commercial importance for future applications. With current development in new nitroxides coupled with the convenient ATRA method for alkoxyamine synthesis, polymers with desired chain ends can be achieved by use of an appropriate alkoxyamine. In the next chapters homopolymerization of styrene and *n*-butyl acrylate using the alkoxyamine MAMA-DEPN will be studied. Part of the information obtained from the homopolymerization will further be utilized, in trying to fully describe the copolymerization system of the same pair of monomers.

References

1. Fischer, H. *J. Polym. Sci., Part A: Polym. Chem.* **1999**, 37, 1885-1901.
2. Wang, Y.; Hutchinson, R. A.; Cunningham, M. F. *Macromol. Mater. Eng.* **2005**, 290, 230-241.
3. Nabifar, A.; McManus, N. T.; Vivaldo-Lima, E.; Lona, L. M. F.; Penlidis, A. *Can. J. Chem. Eng.* **2008**, 86, 879-892.
4. Zhou, M.; McManus, N. T.; Vivaldo-Lima, E.; Lona, L. M. F.; Penlidis, A. *Macromol. Symp.* **2010**, 289, 95-107.
5. Solomon, D. H.; Rizzardo, E.; Cacioli, P. Polymerization process and polymers produced thereby. 4581429, 1986.
6. Moad, G.; Rizzardo, E.; Solomon, D. H. *Macromolecules* **1982**, 15, 909-914.
7. Georges, M. K.; Veregin, R. P. N.; Kazmaier, P. M.; Hamer, G. K. *Macromolecules* **1993**, 26, 2987-2988.
8. Fischer, H. *Chem. Rev.* **2001**, 101, (12), 3581 - 3610.
9. Hawker, C. J.; Bosman, A. W.; Harth, E. *Chem. Rev.* **2001**, 101, 3661-3668.
10. Cuervo-Rodriguez, R.; Bordege, V.; Fernánde Monreal, M. C.; Fernánde Garcí'a, M.; Madruga, E. L. *J. Polym. Sci., Part A: Polym. Chem.* **2004**, 42, 4168-4176.
11. Zaremski, M. Y.; Plutalova, A. V.; Lachinov, M. B.; Golubev, V. B. *Macromolecules* **2000**, 33, 4365-4372.
12. Hawker, C. J.; Elce, E.; Dao, J.; Volksen, W.; Russell, T. P.; Barclay, G. G. *Macromolecules* **1996**, 29, (7), 2686-2688.
13. Miura, Y.; Nakamura, N.; Taniguchi, I.; Ichikawa, A. *Polymer* **2003**, 44, 3461-3467.
14. Cai, J.; Xu, L.; Mao, Z.; Chen, Z.; Liu, Y.; Jiang, X.; Cheng, R. *J. Appl. Polym. Sci.* **2006**, 102, 3118-3122.
15. Devonport, W.; Michalak, L.; Malmstro1m, E.; Mate, M.; Kurdi, B.; Hawker, C. J.; Barclay, G. G.; Sinta, R. *Macromolecules* **1997**, 30, 1929-1934.
16. Benoit, D.; Grimaldi, S.; Robin, S.; Finet, J.-P.; Tordo, P.; Gnanou, Y. *J. Am. Chem. Soc.* **2000**, 122, 5929-5939.
17. Chauvin, F.; Dufils, P.-E.; Gígmes, D.; Guillaneuf, Y.; Marque, S. R. A.; Tordo, P.; Bertin, D. *Macromolecules* **2006**, 39, 5238-5250.

18. Lacroix-Desmazes, P.; Lutz, J.-F.; Florence Chauvin; Severac, R.; Boutevin, B. *Macromolecules* **2001**, 34, 8866-8871.
19. Benoit, D.; Chaplinski, V.; Braslau, R.; Hawker, C. J. *J. Am. Chem. Soc.* **1999**, 121, 3904 - 3920.
20. Schierholz, K.; Givehchi, M.; Fabre, P.; Nallet, F.; Papon, E.; Guerret, O.; Gnanou, Y. *Macromolecules* **2003**, 36, 5995-5999.
21. Benoit, D.; Harth, E.; Fox, P.; Waymouth, R. M.; Hawker, C. J. *Macromolecules* **2000**, 33, 363-370.
22. Lacroix-Desmazes, P.; Lutz, J.-F.; Boutevin, B. *Macromol. Chem. Phys.* **2000**, 201, 662-669.
23. Drache, M.; Mandel, K.; Schmidt-Naake, G. *Polymer* **2007**, 48, 1875-1883.
24. Goto, A.; Fukuda, T. *Macromol. Chem. Phys.* **2000**, 201, 2138-2142.
25. Hill, N. L.; Braslau, R. *J. Polym. Sci., Part A: Polym. Chem.* **2007**, 45, (11), 2341-2349.
26. Pradhan, P. P.; Bobbitt, J. M.; Bailey, W. F. *Org. Lett.* **2006**, 8, (24), 5485-5487.
27. Flakus, S.; Mandel, K.; Bartsch, M.; Schmidt-Naake, G. *Macromol. Rapid Commun.* **2005**, 26, (21), 1698-1703.
28. Matyjaszewski, K.; Woodworth, B. E.; Zhang, X.; Gaynor, S. G.; Metzner, Z. *Macromolecules* **1998**, 31, 5955-5957.
29. Matyjaszewski, K.; Coca, S.; Gaynor, S. G.; Wei, M.; Woodworth, B. E. *Macromolecules* **1997**, 30, 7348-7350.
30. Fischer, H. *Macromolecules* **1997**, 30, 5666-5672.
31. Fukuda, T.; Goto, A.; Ohno, K. *Macromol. Rapid Commun.* **2000**, 21, 151 - 165.
32. Lutz, J.-F. o.; Lacroix-Desmazes, P.; Boutevin, B. *Macromol. Rapid Commun.* **2001**, 22, 189 - 193.
33. Phan, T. N. T.; Maiez-Tribut, S.; Pascault, J.-P.; Bonnet, A.; Gerard, P.; Guerret, O.; Bertin, D. *Macromolecules* **2007**, 40, 4516-4523.
34. Detrembleur, C.; Debuigne, A.; Jérôme, C.; Phan, T. N. T.; Bertin, D.; Gigmes, D. *Macromolecules* **2009**, 42, 8604-8607.
35. Lutz, J.-F.; Lacroix-Desmazes, P.; Boutevin, B.; Mercier, C. L.; Gigmes, D.; Bertin, D.; Tordo, P. *Polym. Prepr. (Am. Chem. Soc., Div. Polym. Chem.)* **2002**, 43, 287-288.

36. Ananchenko, G. S.; Souaille, M.; Fischer, H.; Mercier, C. L.; Tordo, P. *J. Polym. Sci., Part A: Polym. Chem.* **2002**, 40, 3264–3283.
37. Charleux, B.; Nicolas, J.; Guerret, O. *Macromolecules* **2005**, 38, 5485-5492.
38. Nicolas, J.; Brusseau, S.; Charleux, B. *J. Polym. Sci., Part A: Polym. Chem.* **2010**, 48, 34-47.
39. Nicolas, J.; Dire, C.; Mueller, L.; Belleney, J.; Charleux, B.; Marque, S. R. A.; Bertin, D.; Magnet, S.; Couvreur, L. *Macromolecules* **2006**, 39, 8274-8282.
40. Nicolas, J.; Mueller, L.; Dire, C.; Matyjaszewski, K.; Charleux, B. *Macromolecules* **2009**, 42, 4470-4478.
41. Diaz, T.; Fischer, A.; Jonquie`res, A.; Brebilla, A.; Lochon, P. *Macromolecules* **2003**, 36, 2235-2241.
42. Bian, K.; Cunningham, M. F. *J. Polym. Sci., Part A: Polym. Chem.* **2006**, 44, 414-426.
43. Dire, C.; Charleux, B.; Magnet, S. p.; Couvreur, L. *Macromolecules* **2007**, 40, 1897-1903.
44. Marque, S.; Fischer, H.; Baier, E.; Studer, A. *J. Org. Chem.* **2001**, 66, 1146-1156.
45. Bon, S. A. F.; Chambard, G.; German, A. L. *Macromolecules* **1999**, 32, 8269-8276.
46. Bertin, D.; Gigmes, D.; Marque, S. R. A.; Tordo, P. *Macromolecules* **2005**, 38, 2638-2650.
47. Fukuda, T. *J. Polym. Sci., Part A: Polym. Chem.* **2004**, 42, 4743-4755.
48. Goto, A.; Fukuda, T. *Macromolecules* **1999**, 32, 618-623.
49. Georges, M. K.; Veregin, R. P. N.; Kazmaier, P. M.; Hamer, G. K.; Saban, M. *Macromolecules* **1994**, 27, 7228-7229.
50. Odell, P. G.; Veregin, R. P. N.; Michalak, L. M.; Brousmiche, D.; Georges, M. K. *Macromolecules* **1995**, 28, 8453-8455.
51. Cunningham, M. F.; Tortosa, K.; Lin, M.; Keoshkerian, B.; Georges, M. K. *J. Polym. Sci., Part A: Polym. Chem.* **2002**, 40, 2828-2841.
52. Buzanowski, W. C.; Graham, J. D.; Priddy, D. B.; Shero, E. *Polymer* **1992**, 33, 3055-3059.
53. Veregin, R. P. N.; Odell, P. G.; Michalak, L. M.; Georges, M. K. *Macromolecules* **1996**, 29, 4161-4163.

54. Malmström, E.; Miller, R. D.; Hawker, C. J. *Tetrahedron* **1997**, 53, (45), 15225-15236.
55. Baldoví, M. V.; Mohtat, N.; Scaiano, J. C. *Macromolecules* **1996**, 29, 5497-5499.

Chapter III: Nitroxide Mediated Homopolymerization of Styrene and *n*-Butyl Acrylate

Synopsis

*This chapter deals with the concepts of nitroxide mediated homopolymerization of styrene and *n*-butyl acrylate as a building block towards the copolymerization reactions that are dealt with in Chapter V. A detailed outline for the synthesis of the nitroxide (DEPN) and corresponding alkoxyamine (MAMA-DEPN) is reported in this chapter. The use of MAMA-DEPN as an initiator in the polymerization of styrene and *n*-butyl acrylate is studied. The ideas behind the independent behaviour of the rate of polymerization as a function of initiator concentration in the case of *n*-butyl acrylate are dealt with and compared against the well-studied case of styrene.*

3.1 Introduction

3.1.1 Propagation and termination rate coefficients

Prior to the study of the copolymerization reactions of styrene and *n*-butyl acrylate, it is essential to first look at the homopolymerization of the respective monomers mediated by nitroxides. For the homopolymerization reactions, it should be investigated whether the expression shown in Equation 2-13 holds and from the homopolymerization reactions of the respective monomers very important kinetic information can be obtained. Of particular interest are the homopropagation rate coefficient of the respective monomers, being styrene¹ and *n*-butyl acrylate² which can be expressed as follows,

$$k_p^S = 10^{7.63} e^{-32.5 \times 10^3 / RT} \quad (3-1)$$

$$k_p^B = 10^{7.33} e^{-17.8 \times 10^3 / RT} \quad (3-2)$$

In the above expression *R* and *T* represent the gas constant (8.314 J·mol⁻¹·K⁻¹) and absolute temperature in Kelvin, respectively. Reliable propagation rate coefficients are obtained by pulsed laser polymerization (PLP), and Table 3-1 shows literature values of homopropagation rate coefficients for *n*-butyl acrylate obtained from PLP and the values obtained from Equation 3-2. Attention should be paid to the correlation of the values of *k_p* at lower temperatures and the subsequent deviation at elevated temperatures. The applicability of the PLP technique for the study of propagation rate coefficient in *n*-butyl acrylate polymerization is generally limited to temperatures of about 20°C³ due to the contribution from the mid-chain radicals at higher temperatures. The formation of such mid-chain radicals and their effect on the polymerization kinetics are dealt with later in this chapter.

Table 3-1: Literature homopropagation rate coefficients of *n*-butyl acrylate at different temperatures

Temperature (°C)	Beuermann et al. ⁴ $k_p^B / \text{L mol}^{-1} \text{s}^{-1}$	k_p^B (Generated from Equations 3-2) $\text{L mol}^{-1} \text{s}^{-1}$
10	12500	11 123
30	16300	18 317
50	20700	28 359

Despite the temperature limitation of the PLP technique, Barner-Kowollik and co-workers have recently demonstrated the use of PLP at high pulse rates at temperatures up to 70 °C.²

However, obtaining reliable homopropagation rate coefficient values for acrylate monomers can be quite a complicated task due to the fast propagating nature of such monomers. In addition to fast propagation, chain transfer to polymer is a well documented phenomenon for acrylates.⁵⁻⁷ Degirmenci and coworkers⁸ carried out density functional theory (DFT) calculations and reported that for monomers such as 2-dimethylaminoethyl acrylate chain transfer played a major role in the inhibition of the polymerization process. On the other hand, Table 3-2 compares literature values of homopropagation rate coefficients for styrene with the values obtained from Equation 3-1.

Table 3-2: Literature homopropagation rate coefficients of styrene at different temperatures

Temperature (°C)	Coote et al. ⁹ $k_p^S / \text{L mol}^{-1} \text{s}^{-1}$	Zammit et al. ¹⁰ $k_p^S / \text{L mol}^{-1} \text{s}^{-1}$	k_p^S (Generated from Equation 3-1) $\text{L mol}^{-1} \text{s}^{-1}$
17.9	62	60	62
27.7	93	-	97
37.6	117	136	146
47.4	213	193	215
57.2	275	290	309

One other important kinetic parameter is the bimolecular termination rate coefficient k_t , which can be taken from the existing values known from conventional free radical polymerization. It is well known that bimolecular termination is diffusion controlled. Thus using the Smoluchovski Equation,¹¹⁻¹³ the termination rate coefficient can be estimated as

$$k_t^{i,j} = 2\pi \cdot \sigma \cdot p(D_i + D_j)N_A \quad (3-3)$$

where σ is the capture radius of the termination reaction, p is the spin multiplicity factor, D_i is the diffusion coefficient of the polymeric radical with chain length i and N_A is Avogadro's number. The diffusion coefficient of the polymeric radical with chain length i can further be defined according to the expression¹⁴

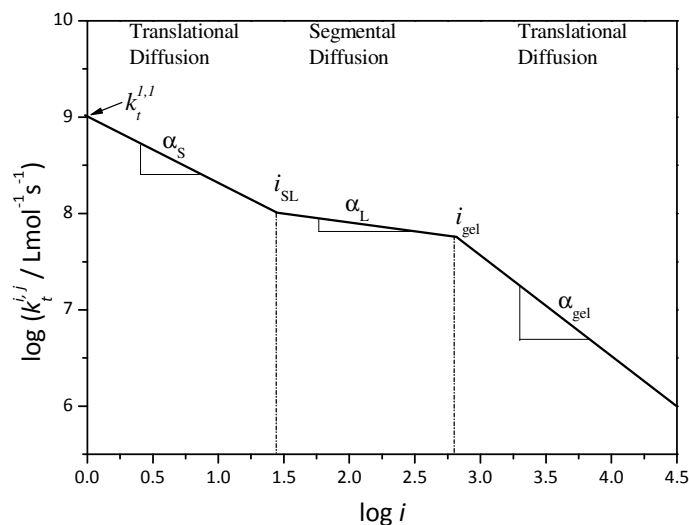
$$D_i = D_0 i^{-(0.664+2.02w_p)} \quad (3-4)$$

where w_p is the weight fraction of the polymer, and through this parameter it becomes clear that the diffusion coefficient is not only a function of chain length but also a function of viscosity. Equation 3-4 was first derived for methyl methacrylate and butyl methacrylate oligomers in methyl methacrylate and butyl methacrylate matrices, respectively for concentrations at which overlap starts. However, Equation 3-4 was found to hold for data obtained from styrene oligomers in a solution of polymer.^{13, 14}

In recent studies on termination kinetics, the description of termination rate coefficient as a function of continuously changing experimental conditions has been shown to be sufficiently described by composite models such as the one illustrated by Scheme 3-1. The power law expression illustrated by Equation 3-5 is then used for calculating the value of the termination rate coefficient depending on which regime of the composite model it corresponds to.

$$k_t^{i,i} = k_t^{1,1} i^{-\alpha_i} \quad (3-5)$$

where $k_t^{i,i}$ is the chain length dependent termination rate coefficient, $k_t^{1,1}$ is the termination rate coefficient for monomeric radicals (i.e. chain length of one), i is the chain length and α_i is the chain length dependent exponent. Equation 3-5 is based on the assumption that the two terminating radicals are of approximately the same chain length.



Scheme 3-1: The log-log plot of the chain length dependent termination rate coefficient ($k_t^{i,j}$) as a function of chain length (i), illustrating the generalized composite model for the termination process. The schematic also shows the chain length dependent exponents (α_i) and the crossover chain lengths (i_{SL} and i_{gel}). The corresponding value of the termination between two monomeric radicals ($k_t^{1,1}$) is also depicted.

In the composite model, at chain lengths below i_{SL} the termination is controlled predominantly by translational diffusion because of the relatively small sized polymer chain. In the chain length interval $i_{SL} < i < i_{gel}$, the termination is controlled by segmental diffusion due to the conformations of the polymer chains, and at chain lengths above i_{gel} the termination is again controlled by translational diffusion. The study of termination kinetics for a series of monomers with the RAFT-CLD-T (Reversible Addition-Fragmentation Transfer–Chain Length Dependent–Termination) method has been demonstrated in the literature.¹⁵⁻²⁰ Junkers et al.¹⁵ reported the chain length dependent power law exponents for the polymerization of *n*-butyl acrylate determined via two independent methods as $\alpha_S = 1.25$ and $\alpha_L = 0.22$ via RAFT-SP-PLP (Reversible Addition-Fragmentation Transfer–Single Pulse–Pulsed Laser Polymerization) and $\alpha_S = 1.04$ and $\alpha_L = 0.20$ via RAFT-CLD-T. Recently, Barth et al.²¹ reported a different set of power law exponents for the polymerization of *n*-butyl acrylate studied via SP-PLP-ESR (Single Pulse–Pulsed Laser Polymerization–Electron Spin Resonance). The reported short chain and long chain radicals’ power law exponents are 0.85 ± 0.09 and 0.16 ± 0.07 , respectively. The major advantage attributable to the latter technique is the direct access to the concentration profiles of

both the secondary propagating radical and mid-chain radicals. The upper limit of the short chain radical exponent (α_s) is one, which can be interpreted in terms of the centre of mass diffusion of rod-like species.²¹ On the basis of the description of the upper limit of the short chain radicals exponent, the interpretation of the value obtained for the same parameter via RAFT-CLD-T technique which is above unity becomes ambiguous.

The SP-PLP-ESR method has also been used in the past for the study of termination kinetics of monomers²²⁻²⁶ other than *n*-butyl acrylate.

3.1.2 Determination of the equilibrium constant

The calculation of the equilibrium constant (K) in NMP requires both the knowledge of the activation rate coefficient and the deactivation rate coefficient of the alkoxyamine in question, as was first shown through Equation 2-5 in Chapter II. The theory behind the determination of the activation rate coefficient was dealt with in Chapter II. The nitroxide exchange reactions²⁷ and Fukuda's SEC method²⁸ were introduced for determining activation rate coefficients for model- and macro-alkoxyamines, respectively. To build up to the determination of the equilibrium constant, let us first consider a phenomenon called persistent radical effect (PRE) that was introduced by Fischer.²⁹ The ideas behind the PRE theory were briefly introduced in the previous chapter. To improve on the PRE theory, Tang and coworkers³⁰ re-evaluated the PRE theory, to expand the applicability of the PRE equations to high monomer conversions. To predict the concentration of the persistent radical species as a function of time, Tang et al.³⁰ derived the following expression,

$$2K^2k_t t = \frac{[R-X]_0^2}{[R-X]_0 - [X]} + 2[R-X]_0 \ln \frac{[R-X]_0 - [X]}{[R-X]_0} - ([R-X]_0 - [X]) \quad (3-5)$$

where K is the equilibrium constant, k_t is the rate coefficient of termination, t is time, $[R-X]_0$ is the initial alkoxyamine concentration and $[X]$ is the concentration of the persistent radical species.

Taking a look at the right hand side of Equation 3-5, it is clear that the only parameter that is not constant is the concentration of the persistent radical species, thus the right hand side can be written as a function of $[X]$ in the form,

$$f([X]) = \frac{[R-X]_0^2}{[R-X]_0 - [X]} + 2[R-X]_0 \ln \frac{[R-X]_0 - [X]}{[R-X]_0} - ([R-X]_0 - [X]) \quad (3-6)$$

Therefore combining Equations 3-5 and 3-6, one can write

$$2K^2 k_t = f([X]) \quad (3-7)$$

Hence plotting $f([X])$ vs. time yields a first order plot, whereby

$$\text{slope} = 2K^2 k_t \quad (3-8)$$

Thus K can easily be deduced from Equation 3-8 with the knowledge of k_t . In the application of this concept of the re-evaluated PRE theory for the determination of the equilibrium constant, Drache et al.³¹ used the SEC column combination method to follow the decline in the concentration of the model alkoxyamine and the increase in the concentration of the persistent radical species (nitroxide) in accordance with the PRE theory. In this SEC combination method, they employed one Ultrastyrigel 100 Å and two Ultrastyrigel 500 Å columns to improve on separation within low molecular weight ranges. In contrast to Fukuda's SEC method,²⁸ Drache et al.³¹ obtained quite good SEC peak resolution between the model alkoxyamine and the free nitroxide. Inserting the information obtained into Equation 3-5, Drache et al.³¹ obtained equilibrium constants of 7.5×10^{-9} mol/L and 1.08×10^{-8} mol/L for styrene polymerization controlled by TIPNO and BIPNO (Scheme 2-4), respectively. In addition to the equilibrium constant, Equation 2-14 was used to determine the dissociation rate coefficients of the respective alkoxyamine PhEt-TIPNO and PhEt-BIPNO and obtained $3.2 \times 10^{-3} \text{ s}^{-1}$ and $6.8 \times 10^{-3} \text{ s}^{-1}$, respectively. Therefore, with the knowledge of both the equilibrium constant and the dissociation

rate coefficient it is now possible to calculate the value of the deactivation rate coefficient k_c via Equation 2-5.

For interest's sake, one might be interested in determining the crossover time (t_{cross}) it takes for a nitroxide mediated system, to reach the stationary state. The expression for the crossover time from non-stationary to the stationary state is represented by Equation 3-9.³²

$$t_{cross} = \frac{(k_i K^2 [R - X]_0^2)^{1/2}}{3R_i^{3/2}} \quad (3-9)$$

where R_i is the rate of initiation and all other symbols retain their meaning described earlier.

3.2 *In situ* ¹H NMR spectroscopy: Analysis

The NMR spectra were recorded with a 400 MHz Varian unity Inova spectrometer. The ¹H NMR spectra were acquired with a 3μs (40°) pulse width and a 4 seconds acquisition time. For the *in situ* kinetic experiments, samples were first inserted into the magnet at 25 °C and the magnet completely shimmed on the sample and the spectrum collected to serve as reference at 25 °C. This was followed by removal of the sample from the magnet and the cavity of the magnet was then heated to 120 °C and allowed to stabilize before introducing the sample again into the cavity of the magnet at elevated temperature.

Following the re-insertion of the sample, additional shimming was performed to acquire full optimum conditions and the first spectra were collected 3-7 minutes after the re-insertion. The phase correction of the spectra was performed automatically while baseline correction and integration of the spectra were carried out manually using ACD Labs 10.0 ¹H processor[®].

Figure 3-1 illustrates an array of spectra ($1 \leq \delta$ (ppm) ≤ 8.5) during the polymerization of *n*-butyl acrylate at 120 °C as a function of polymerization time. Figure 3-2 shows the enlarged region labelled "B" in Figure 3-1 together with the chemical shift where the peaks for each of the vinyl protons appear.

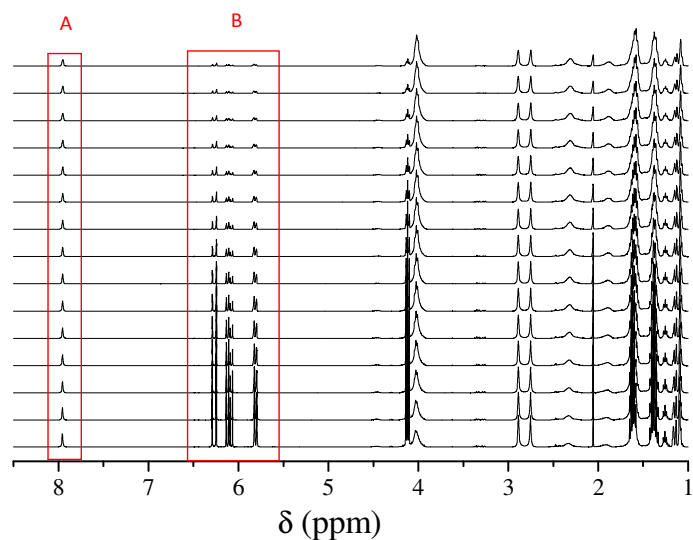


Figure 3-2: The ^1H NMR spectra (δ in the range 1 ppm to 8.5 ppm) at different times during the polymerization of *n*-butyl acrylate at 120 °C initiated by MAMA-DEPN in DMSO- d_6 . In the region labelled “B” are peaks due to the vinyl protons of *n*-butyl acrylate monomer and the peak labelled “A” is due to the $-\text{CHO}$ proton of the reference (DMF).

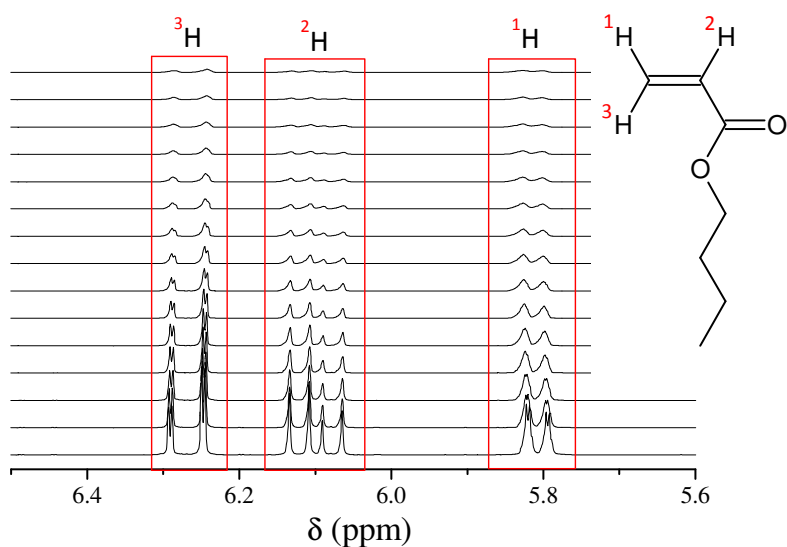


Figure 3-2: The enlarged region of the part labelled “B” in Figure 3-1 showing the spectral region of the vinyl protons of the *n*-butyl acrylate monomer, during the polymerization at 120 °C initiated by MAMA-DEPN in DMSO- d_6

3.3 Synthesis of the alkoxyamine 2-methyl-2[N-tert-butyl-N-(1-diethoxyphosphoryl-2,2-dimethoxypropyl)aminoxy]propionic acid (MAMA-DEPN)

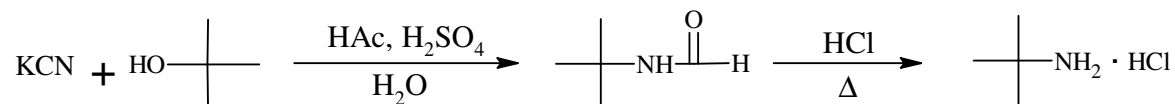
3.3.1 Experimental

3.3.1.1 Chemicals

Potassium cyanide (Merck, 97%), acetic acid (Saarchem), tert-butyl alcohol (ACE), sulphuric acid (Merck, 98%), hydrochloric acid (Merck, 37%), sodium hydroxide (Saarchem), isopropyl alcohol (Sasol), potassium carbonate (Merck, 99.5%), diethyl ether (Merck), pivalaldehyde (Fluka, $\geq 97\%$), diethyl phosphite (Acros Organics), dichloromethane (Merck), tetrahydrofuran (Kimix, CP grade), pentane, 2-bromo-2-methyl propionic acid (Aldrich), toluene (Merck), copper (I) bromide (Aldrich, 98%), copper (0) powder (Merck), N,N,N',N'',N''-pentamethyldiethylenetriamine (Aldrich, 99%), magnesium sulphate (Saarchem), ammonium chloride (Saarchem), boron trifluoride diethyl ether complex (Merck, 45% BF₃)

3.3.1.2 Procedures

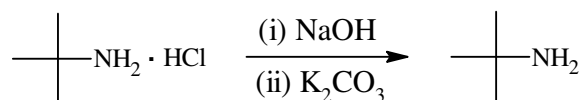
Tert-Butylamine hydrochloride



Tert-butylamine hydrochloride was synthesized according to the modified procedure of Talaty and coworkers.³³ To a round bottom flask equipped with a magnetic stirrer was charged KCN (20.0 g, 0.031 mol), glacial acetic acid (50 ml) and tert-butyl alcohol (22.7 g, 0.031 mol). To this mixture was slowly added, a mixture of concentrated H₂SO₄ (90 g) in glacial acetic acid (50 ml) and the reaction was allowed to proceed overnight. The reaction was stopped by slowly pouring the reaction mixture in ice cold distilled water (600 ml). The resultant solution was gradually neutralized with a NaOH solution (50 %), while maintaining the temperature at ~ 0 °C and tert-butyl formamide was extracted seven times with diethyl ether, followed by recovery of the formamide by removal of the solvent under vacuum. A mixture of tert-butyl formamide and 37% hydrochloric acid was then refluxed for 6 hours, followed by recovery under vacuum of tert-

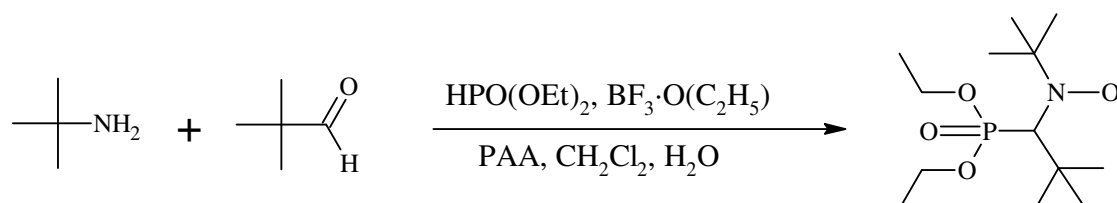
butylamine hydrochloride salt which was then purified by recrystallization from isopropyl alcohol. (Yield ~ 85 %)

Tert-Butylamine



Recovery of the free tert-butylamine from the amine hydrochloride salt was carried out as described by Smith and coworkers.³⁴ To an ice cold 40% solution of NaOH (8.5 ml) was added tert-butylamine hydrochloride (6.0 g, 56.3 mmol) with continuous stirring followed by addition of K₂CO₃ to saturate the solution allowing for the separation of the tert-butylamine layer. (Yield ~ 65%)

DEPN

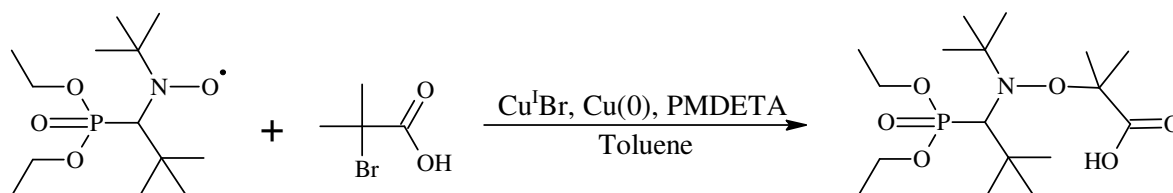


Synthesis of DEPN was achieved by employing the method invented by Guerret, O. and coworkers.³⁵ Pivalaldehyde (3.41 g, 41 mmol) was degassed with nitrogen for 10 minutes directly followed by drop-wise addition of tert-butylamine (3.0 g, 41 mmol) at ambient temperature and the resultant mixture was allowed to react for two hours at 35 °C. The reaction mixture was allowed to cool to room temperature followed by removal of the aqueous phase. To the organic phase (imine), diethyl phosphite (8.28 g, 60 mmol) was added drop-wise at 40 °C and immediately followed by drop-wise addition of BF₃·O(C₂H₅)₂ complex (~1 ml). The reaction

mixture was heated and allowed to react at 60 °C for one hour resulting in a colourless liquid (α -aminophosphonate or DEPP).

Peroxyacetic acid (PAA), dichloromethane and water were charged into a reactor and the mixture was neutralized to about pH 7.2 with 35 % K_2CO_3 . The temperature was maintained at 20 – 25 °C and the crude DEPP was added drop-wise while maintaining the pH at about 7.2 and the resultant reaction mixture was allowed to react for one hour while continuously maintaining the pH at 7.2. The pH of the reaction mixture was brought to 8 at the end of the reaction by further addition of 35 % solution of K_2CO_3 . The organic phase was recovered and washed three times with distilled water followed by removal of the solvent under vacuum to give DEPN (an orange liquid), which was then purified by silica gel chromatography (THF/ CH_2Cl_2 /pentane, 1:1:2). (Yield ~ 60%)

MAMA-DEPN (Alkoxyamine)



Synthesis of MAMA-DEPN was carried out using a method reported by Couturier and coworkers.³⁶ Under inert conditions a degassed solution of toluene (30 ml), 2-bromo-2-methyl propionic acid (3.34 g, 20 mmol) and DEPN (2.94 g, 10 mmol) was added to a mixture of degassed toluene (30 ml), CuBr (2.87 g, 20 mmol), copper powder (1.27 g, 20 mmol), N,N,N',N'',N''-pentamethyldiethylenetriamine (PMDETA) (6.93 g, 40 mmol) and at ambient temperature with continuous stirring. The reaction mixture was allowed to react for 90 minutes under nitrogen atmosphere at ambient temperature, followed by removal of the solids by filtration. The toluene filtrate was washed five times with a saturated aqueous solution of NH_4Cl and then dried over anhydrous $MgSO_4$. The dried organic phase was obtained by filtration and the solvent was removed under vacuum and the resultant solid was washed with pentane to yield a white powdery product (MAMA-DEPN). (Yield ~ 70%)

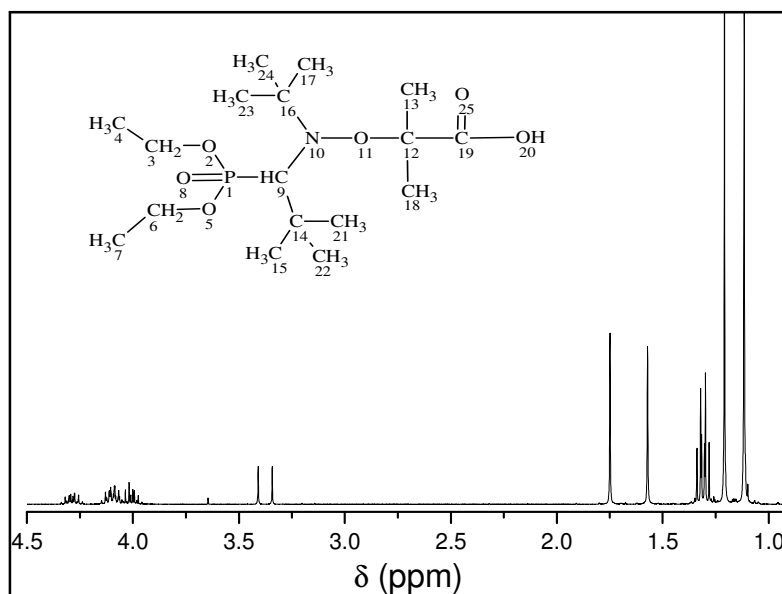


Figure 3-3: ^1H NMR spectrum of MAMA-DEPN.

^1H NMR (CDCl_3) Spectral peak assignments of MAMA-DEPN in Figure 3-3,

- δ 1.13 ppm (singlet, 9H on carbons 15, 21 and 22)
- δ 1.23 ppm (singlet, 9H on carbons 17, 23 and 24)
- δ 1.30-1.36 ppm (multiplet, 6H on carbons 4 and 7)
- δ 1.59 ppm (singlet, 3H on carbon 18)
- δ 1.77 ppm (singlet, 3H on carbon 13)
- δ 3.40 ppm (doublet, 1H on carbon 9)
- δ 3.97-4.36 ppm (multiplet, 4H on carbons 3 and 6)

The mass spectrum (Figure 3-4) of the synthesized MAMA-DEPN was obtained using the Waters API Quattro Micro with an ESI+ source at 3.5 kV capillary voltage. The peaks at 382 and 383 m/z are assigned to the alkoxyamine, and the peak at 295 m/z is assigned to the DEPN nitroxide fragment.

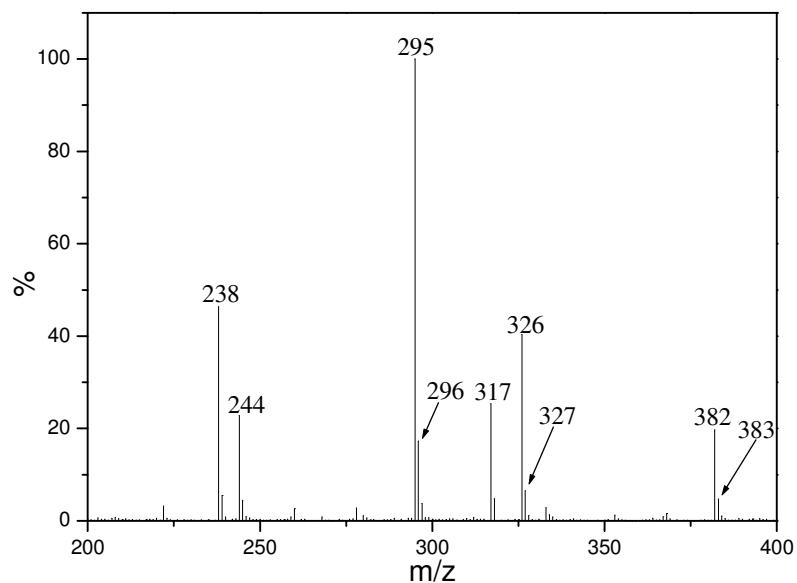


Figure 3-4: Mass spectrum of MAMA-DEPN.

3.4 Homopolymerization of styrene and *n*-butyl acrylate

3.4.1 Experimental

3.4.1.1 Chemicals

The alkoxyamine MAMA-DEPN was synthesized as described earlier in the chapter (Section 3.3). Styrene (Plascon research center, University of Stellenbosch) was repeatedly washed with aqueous 10% NaOH to remove inhibitors, then with distilled deionised water, dried for several hours with anhydrous MgSO₄ and distilled at 25°C under reduced pressure and stored at low temperatures. *n*-Butyl acrylate (Plascon research center, University of Stellenbosch) was washed repeatedly with aqueous 10% NaOH and distilled deionised water to remove inhibitors then distilled under vacuum and also stored at low temperatures. Deuterated dimethyl sulfoxide (DMSO-d₆, Cambridge Isotope Laboratories, 99%) and dimethyl formamide (DMF, Sigma-Aldrich) were used as received.

3.4.1.2 Procedure for styrene and *n*-butyl acrylate homopolymerizations

Styrene and *n*-butyl acrylate homopolymerizations were monitored via *in situ* ¹H NMR experiments at 120°C in DMSO-d₆. An internal reference (DMF) was added directly to the reaction mixture. A typical polymerization was conducted as follows; DMSO-d₆ (0.3021 g,

3.867×10^{-3} mol), MAMA-DEPN (30.7 mg, 8.05×10^{-5} mol), *n*-butyl acrylate (0.2035 g, 1.588×10^{-3} mol) and 20 μ L of DMF (internal reference) were thoroughly mixed and introduced into a J-Young type NMR tube. The sample was degassed by three freeze-pump-thaw cycles, followed by introduction of UHP nitrogen gas. The ^1H NMR spectra were recorded on a 400 MHz Varian Unity Inova spectrometer. The ^1H NMR spectra were acquired with a $3\mu\text{s}$ (40°) pulse width and a 4 seconds acquisition time. The NMR tube was first inserted into the magnet at 25 $^\circ\text{C}$ and the magnet fully shimmed on the sample and a spectrum collected to serve as reference at 25 $^\circ\text{C}$. This was followed by removal of the sample from the instrument and the cavity of the magnet was then heated to 120 $^\circ\text{C}$ and allowed to stabilize before introducing the sample again into the cavity of the magnet. After re-insertion of the sample, additional shimming was performed to acquire optimum conditions. The first spectrum was acquired 3–5 minutes after the re-insertion, followed by periodic spectra acquisition every two minutes for 60 minutes. The phase correction was performed automatically while baseline correction and integration of the spectra were carried out manually using ACD Labs 10.0 1D ^1H NMR processor[®]. Concentration profiles were constructed relative to a reference (DMF).

The same procedure was followed for the case of styrene homopolymerization, but the reaction time was 150 minutes, with periodic acquisition of spectrum every 5 minutes.

3.4.2 Results and discussion

Styrene and *n*-butyl acrylate homopolymerization reactions were conducted at 120 $^\circ\text{C}$ and followed by *in situ* ^1H NMR spectroscopy. Before the copolymerization reactions could be conducted, it was very important to look into the homopolymerization of the respective monomers under the chosen experimental conditions. Figures 3-5 and 3-6 illustrate the evolution of $\ln(1/(1-\xi))$ as a function of time (conversion index plot) for both styrene and *n*-butyl acrylate homopolymerization conducted at 120 $^\circ\text{C}$ in DMSO-d_6 with MAMA-DEPN as an initiator/mediator.

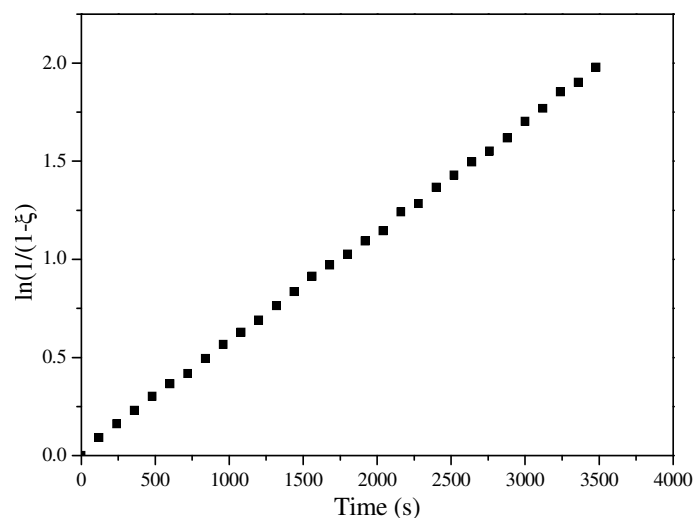


Figure 3-5: Evolution of $\ln(1/(1-\xi))$ as a function of time for the homopolymerization of *n*-butyl acrylate in DMSO- d_6 at 120 °C with MAMA-DEPN as the initiator/mediator agent.

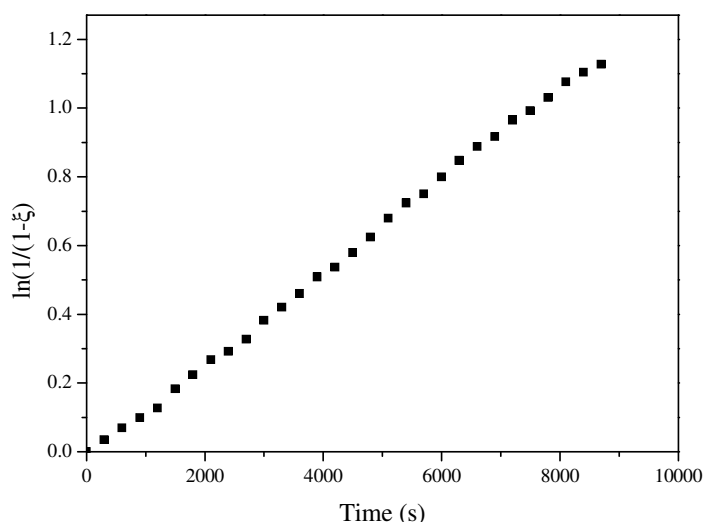


Figure 3-6: Evolution of $\ln(1/(1-\xi))$ as a function of time for the homopolymerization of styrene in DMSO- d_6 at 120 °C with MAMA-DEPN as the initiator/mediator agent.

Fairly linear plots of the conversion index as a function of time were obtained in both cases of styrene and *n*-butyl acrylate homopolymerization. The $-CHO$ proton of the dimethyl formamide at $\delta \sim 7.95$ ppm (in DMSO- d_6) was used as a reference for the signal integration to determine the relative concentration of the species of interest.

3.4.3 Conclusion

The polymerization reactions of styrene and *n*-butyl acrylate were successfully monitored via *in situ* ^1H NMR spectroscopy. The conversion index plots for the polymerization of styrene and *n*-butyl acrylate both showed a fairly linear evolution with polymerization time. However, in the case of styrene polymerization, a downward curvature is observed indicative of a reduction in the rate of polymerization at higher monomer conversion. Due to the labile nature of the C-ON bond of the MAMA-DEPN alkoxyamine, it is prone to spontaneous decomposition even at ambient temperature. Thus the alkoxyamine can contain traces of the free nitroxide, leading to deviation from expected behaviour as would be predicted by the PRE theory.

3.5 The Persistent Radical Effect (PRE) Theory: Experimental validity

The theory behind the PRE was introduced earlier in Chapter II (Section 2.2.5.1), and this section will briefly look at the validity of the theory in styrene homopolymerization. In the absence of free nitroxide, the conversion index is expected to show a two-thirds order dependence on time and one-third order dependence on the alkoxyamine concentration according to Equation 2-13. In reality, there is no alkoxyamine based NMP system that can be regarded as completely nitroxide free, due to the fact that alkoxyamine can decompose resulting in the presence of free nitroxide, regardless of how minute the quantity may be. In this case a nitroxide free system implies a system where no additional free nitroxide has been intentionally added. In this section the PRE theory is tested for the homopolymerization of styrene using a preformed DEPN end capped polystyrene (PS-DEPN) macro-alkoxyamine.

3.5.1 Experimental

3.5.1.1 Chemicals

The alkoxyamine MAMA-DEPN was synthesized as described earlier (Section 3.3). Styrene (Plascon research center, University of Stellenbosch) was washed with aqueous 10% NaOH to remove inhibitors, then with water, dried for several hours with anhydrous MgSO_4 and distilled at 25°C under reduced pressure and stored at low temperatures. Deuterated dimethyl sulfoxide (DMSO-d_6 , Cambridge Isotope Laboratories, 99%) and dimethyl formamide (DMF, Sigma-Aldrich) were used as received.

3.5.1.2 Macro-initiator synthesis

In contrast to the styrene and *n*-butyl acrylate homopolymerization reaction procedures described in Section 3.4 in which homopolymerization reactions were carried out in a J-Young type NMR tube, the PS-DEPN macro-initiator synthesis was carried out in a Schlenk flask. In a typical synthetic procedure for the macro-initiators, monomer (5.0 g of Styrene), and MAMA-DEPN (100 mg, 0.262mmol) were thoroughly mixed in a 100 ml Schlenk flask. The sample mixture was then degassed by three freeze-pump-thaw cycles and UHP nitrogen gas introduced. The mixture was placed in a preheated oil bath, thermostated at 120 °C. After 45 minutes, the reaction mixture was quenched in liquid nitrogen followed by precipitation of the polymer in excess of chilled methanol. The synthesized macro-initiator was then re-dissolved and re-precipitated twice to ensure removal of free DEPN before completely drying.

3.5.1.3 Procedure styrene polymerization

An accurately weighed quantity of the macro-alkoxyamine (PS-DEPN) was dissolved in monomer (Styrene) and DMSO- d_6 followed by thorough mixing and the mixture introduced in a J-Young type NMR tube. 25 μ L of DMF were added to serve as an internal reference. The sample was degassed by three freeze-pump-thaw cycles and UHP nitrogen atmosphere introduced. The *in situ* polymerization reaction was carried out as previously described for homopolymerization reactions (Section 3.4.1.2). In a typical experiment, 52.5 mg of PS-DEPN ($M_n = 3490 \text{ g mol}^{-1}$ by SEC), 0.3041 g styrene and 0.3595 g DMSO- d_6 were thoroughly mixed with acquisition of the first spectrum 4 minutes 13 seconds after insertion of the sample at 120°C. The reaction was allowed to run for two and a half hours acquiring spectra every five minutes.

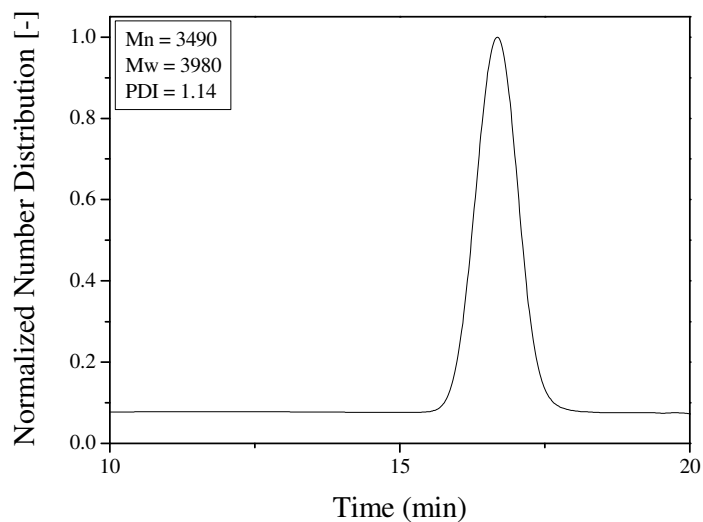


Figure 3-7: Molecular weight distribution of the DEPN end capped polystyrene macro-alkoxyamine (PS-DEPN).

Figure 3-7 shows the SEC chromatogram of the DEPN end capped polystyrene macro-initiator with a narrow molecular weight distribution.

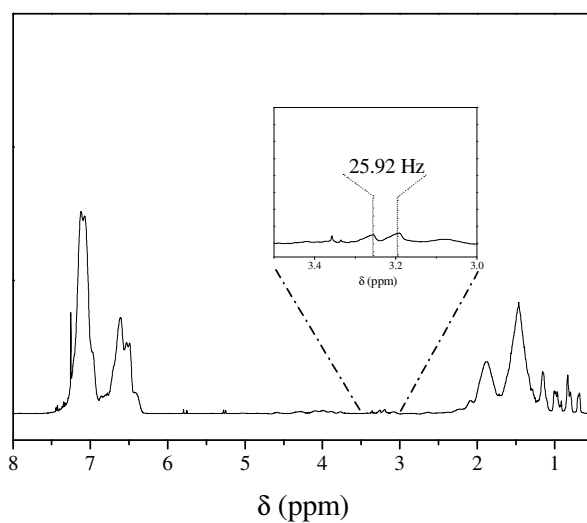


Figure 3-8: The ^1H NMR spectrum of the DEPN end capped polystyrene (PS-DEPN) with the insert showing the doublet signal of the proton attached to the α -carbon of the end group DEPN.

Figure 3-8 illustrates the ^1H NMR spectrum of the preformed polystyrene based macro-alkoxyamine, with the insert showing the doublet of the α -proton on the nitroxide moiety

end capping the polymer. The 25.92 Hz splitting of the α -proton signal is in good agreement with the splitting observed for the DEPN based alkoxyamine.

3.5.2 Results and discussion

If the PRE theory is valid for a system, the plot of the conversion index as a function of $t^{2/3}$ should yield a straight line in accordance with Equation 2-13. Figures 3-9 and 3-10 illustrate the plots of conversion index as a function of time (t) and $t^{2/3}$, respectively. It is evident that the plot of conversion index as a function time is not linear (Figure 3-9). The two-thirds order dependence of the conversion index on time observed is thus in accordance with the expected behaviour for a PRE governed system, where a unimolecular initiator is employed. In the case of a macro-alkoxyamine as in the case of PS-DEPN, the amount of free nitroxide can be highly minimized by several cycles of re-dissolving and re-precipitating the polymer. The spontaneous decomposition of the macro-alkoxyamine is also not as likely to occur as in the case of a model alkoxyamine like MAMA-DEPN, basically due the difference in their values of the dissociation rate coefficients. The model alkoxyamine (MAMA-DEPN) with a higher k_d will suffer a great degree of spontaneous decomposition relative to the macro-alkoxyamine with a lower value of the dissociation rate coefficient at ambient temperature.

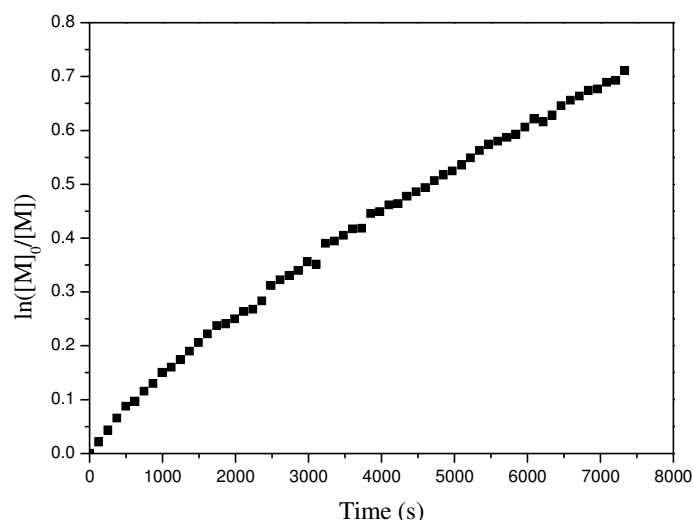


Figure 3-9: Evolution of $\ln([M]_0/[M])$ as a function of time for the homopolymerization of styrene in DMSO- d_6 initiated by PS-DEPN at 120 °C.

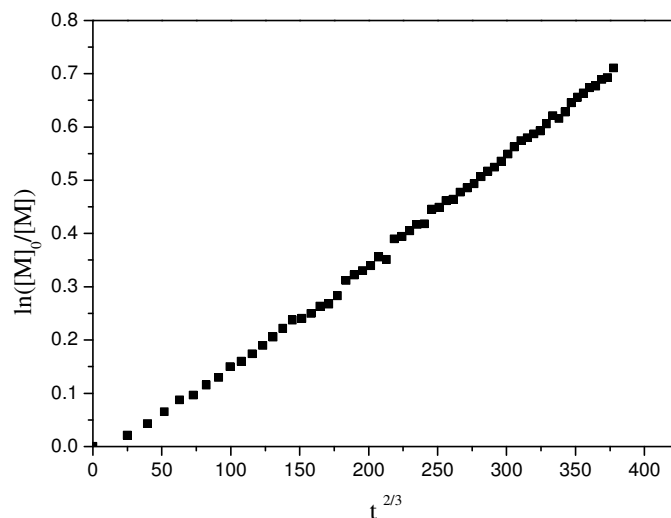


Figure 3-10: Evolution of $\ln([M]_0/[M])$ as a function of $t^{2/3}$ for the homopolymerization of styrene in DMSO- d_6 initiated by PS-DEPN at 120 °C.

The plot of conversion index as a function of $t^{2/3}$ (Figure 3-10) shows a fairly linear plot, thus proving the validity of the PRE. With the knowledge of the dissociation rate coefficient (k_d) of the macro-alkoxyamine (*e.g.* PS-DEPN), the PRE theory can be used to determine the equilibrium constant (K) thus enabling the determination of the combination rate coefficient (k_c).

3.5.3 Conclusion

In accordance with the PRE theory, the polymerization of styrene using a PS-DEPN macro-alkoxyamine yielded a conversion index that showed a two-third order dependence on time. The evolution of the conversion index with time, showed a non linear profile with a downward curvature as polymerization time increased. Therefore, the concept of the persistent radical effect has been illustrated for the polymerization of styrene.

The applicability of the PRE theory to the polymerization of *n*-butyl acrylate using a macro-alkoxyamine of DEPN capped poly(*n*-butyl acrylate) (PBA-DEPN) was not conducted in this study due to the difficulty associated with the handling and purification of low molecular weight poly(*n*-butyl acrylate). The purification of the macro-alkoxyamine is a crucial process since all (or most) of the free nitroxide should be removed from the pre-formed macro-alkoxyamine.

3.6 Systematic study of the effect of varying the alkoxyamine concentration in styrene and *n*-butyl acrylate homopolymerization reactions

The effect of alkoxyamine concentration on the polymerization of styrene is of particular interest because of the pronounced thermal auto-initiation of the monomer at elevated temperatures. It would be expected that in the polymerization of styrene initiated by an alkoxyamine, the rate of polymerization would increase with increasing concentration of the alkoxyamine. In contrast with this expectation, Catala³⁷ reported that the rate of polymerization of styrene was independent of the concentration of the alkoxyamine. The authors then attributed this observation to the aggregation of dormant species that possess a high degree of association. However, Greszta and Matyjaszewski³⁸ re-evaluated the report by Catala³⁷ and reached a conclusion that thermal auto-initiation of styrene was the responsible factor for the observed phenomenon. The conclusion reached by Greszta and Matyjaszewski³⁸ meant that thermal auto-initiation was accountable for the production of the majority of the propagating radicals. Fukuda et al.³⁹ also reported the independence of the polymerization rate on the initial concentration of the alkoxyamine for the nitroxide mediated styrene polymerization, with TEMPO as the mediator. The polymerization rate of the nitroxide mediated styrene polymerization was observed to be equal to the polymerization of the alkoxyamine free system, which can be explained in terms of thermal auto-initiation of styrene. Gray et al.⁴⁰ reported the effect of initial alkoxyamine concentration on the limitations of preparation of controlled high molecular weight polystyrene via unimolecular nitroxide mediated polymerization. In the case where polystyrene macro-initiator was used to polymerize styrene, the effect of thermal auto-initiation of styrene resulted in approximately constant conversion as a function of the alkoxyamine concentration. Kruse et al.⁴¹ reported modeling studies of nitroxide mediated styrene polymerization, indicating the importance of the thermal auto-initiation of styrene in fitting the simulated data to the experimental data. To test the general applicability of the theory drawn from results reported by Catala,³⁷ Gray et al.⁴⁰ and Kruse et al.⁴¹ an investigation was conducted by Schulte⁴² on the effect of varying alkoxyamine concentration for three NMP systems of styrene. The results obtained from this study indicated that for highly efficient alkoxyamines at high concentrations (≥ 0.5 mol %) only a slight decrease in conversion was observed with decreasing alkoxyamine concentrations. On the other hand, at low alkoxyamine concentrations (≤ 0.1 mol %), the

conversion obtained for an efficient alkoxyamine were below those obtained for styrene auto-polymerization. However, conversion values in the region of those obtained for styrene auto-polymerization were observed when alkoxyamine with quite small values of K ($< 10^{-11}$ M) were used in the styrene polymerization. Thus, according to Schulte, the use of low concentrations of highly efficient alkoxyamines in styrene polymerization results in the retardation of the polymerization process. Part of this work will involve the investigation of the effect of the initial concentration of the alkoxyamine on the kinetics of styrene and *n*-butyl acrylate polymerizations.

3.6.1 Experimental

3.6.1.1 Chemicals

The alkoxyamine MAMA-DEPN was synthesized as described earlier (Section 3.3). Styrene (Plascon research center, University of Stellenbosch) was repeatedly washed with aqueous 10% NaOH to remove inhibitors, then with distilled deionised water, dried for several hours with anhydrous MgSO₄ and distilled at 25°C under reduced pressure and stored at low temperatures. *n*-Butyl acrylate (Plascon research center, University of Stellenbosch) was washed repeatedly with aqueous 10% NaOH and distilled deionised water to remove inhibitors, dried for several hours with anhydrous MgSO₄ and then distilled under vacuum and stored at low temperatures. Deuterated dimethyl sulfoxide (DMSO-d₆, Cambridge Isotope Laboratories, 99%) and dimethyl formamide (DMF, Sigma-Aldrich) were used as received.

3.6.1.2 Procedure

The polymerizations were carried out as previously described in Section 3.4.1.2.

3.6.2 Results and Discussion

The evolution of conversion (ξ [-]) with polymerization time as a function of the initial concentration of the alkoxyamine in the case of styrene polymerization is presented in Figure 3-11. Figure 3-12 depicts the evolution of the conversion index with time in the polymerization of *n*-butyl acrylate at different initial concentration of the alkoxyamine initiator.

In both styrene and *n*-butyl acrylate polymerization it was observed that there was apparent independence of the rate of polymerization on the initial concentration of the alkoxyamine.

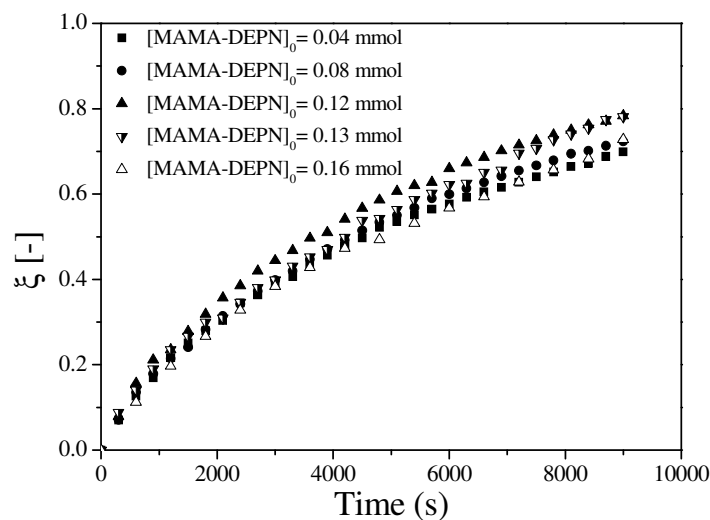


Figure 3-11: The evolution of conversion (ξ [-]) as function of the initial concentration of the alkoxyamine for the polymerization of styrene in DMSO- d_6 at 120°C.

The conversion versus time profiles for the styrene homopolymerization show no apparent dependence of the rate of polymerization on the initial concentration of the alkoxyamine is indicative of the fact that thermal auto-initiation at high temperatures is dominant, overcoming the effect of the initial alkoxyamine concentration.

The independence of rate of polymerization towards the initial alkoxyamine/initiator concentration in the case of styrene has been extensively studied before and well reported in the literature.³⁷⁻⁴² In the case of styrene it is well accepted that the apparent independence of the rate of polymerization as a function of initiator concentration can be explained by the significant thermal auto-initiation of the styrene monomer. Could the same explanation be applicable in the case of *n*-butyl acrylate polymerization with MAMA-DEPN? If indeed thermal auto-initiation plays a role in the observed phenomenon, conducting the polymerization at lower temperatures would result in a system with minimal contribution from thermal auto-initiation.

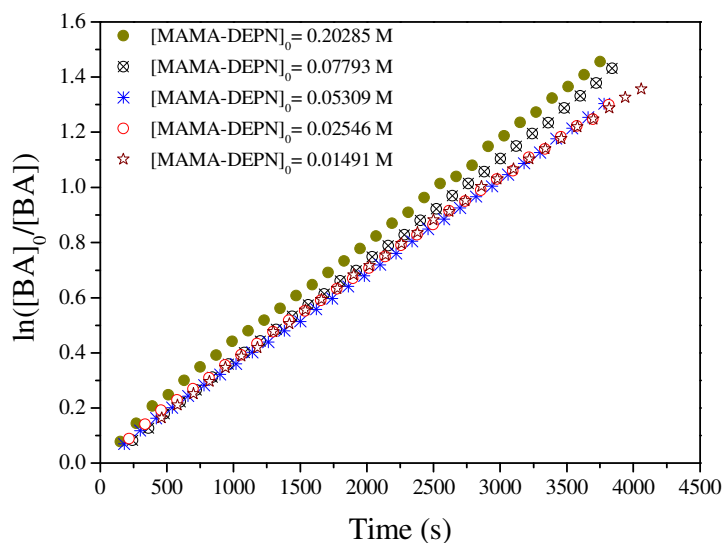


Figure 3-12: Semi-logarithmic plot for *n*-butyl acrylate polymerization initiated with different initial alkoxyamine concentrations in DMSO- d_6 at 120 °C.

Thus, this would allow the effect due to the initial concentration of the alkoxyamine to be pronounced in the kinetic profiles. Figure 3-13 depicts the evolution of monomer conversion as a function of time in the polymerization of *n*-butyl acrylate conducted at 100 °C. No apparent effect was observed that could be attributed to the initial concentration of the alkoxyamine.

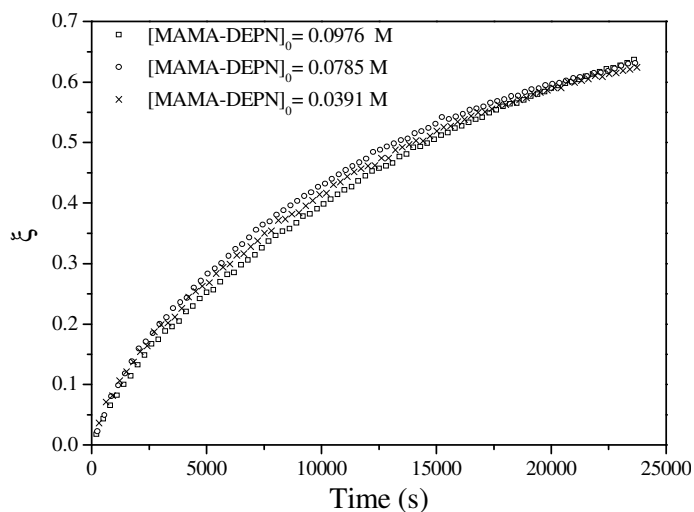


Figure 3-13: Conversion versus time plots for *n*-butyl acrylate polymerization initiated with different initial alkoxyamine concentrations in DMSO- d_6 at 100 °C.

The consistency with temperature of the apparent independence of the rate of polymerization, within the temperature range studied suggested that the explanation of the observed phenomenon is not conclusively attributable to thermal auto-initiation as in the case of styrene. This independence of rate within the temperature range studied could be indicative of an underlying mechanistic feature apart or in addition to thermal auto-initiation.

With the observed independence of rate on initiator concentration, it is important to further assess quantitatively the possible contribution of thermal auto-initiation to the observed phenomenon. When neat *n*-butyl acrylate was degassed and immersed in an oil bath at 120°C, the system gelled within minutes. However, in the presence of TEMPO (0.02 mol %), without added initiator no polymer formed even after 48 hours at 100°C. The C-ON bond between the *n*-butyl acrylate derived radical and TEMPO would be expected to be stable enough to allow complete consumption of TEMPO by thermally initiated monomer derived radicals. The system would then be expected to behave as in the case of neat *n*-butyl acrylate after all or most of the TEMPO is consumed. Contrary to the expected results, over the whole range of TEMPO to *n*-butyl acrylate mole ratios studied, no polymer formed. *In situ* ¹H NMR experiments were then conducted to follow in real time the rate of monomer consumption in the presence of DEPN without initiator at 120°C.

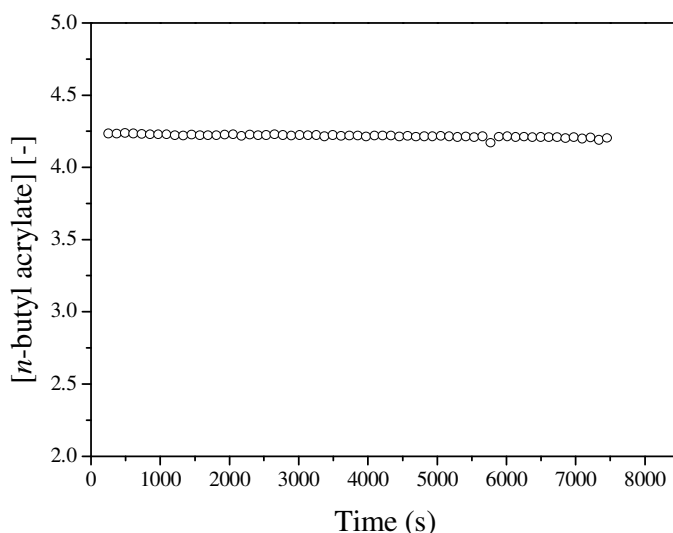


Figure 3-14: The evolution of *n*-butyl acrylate concentration with time for thermally initiated polymerization in DMSO-*d*₆ in the presence of 4.52×10^{-02} mol L⁻¹ free DEPN at 120 °C.

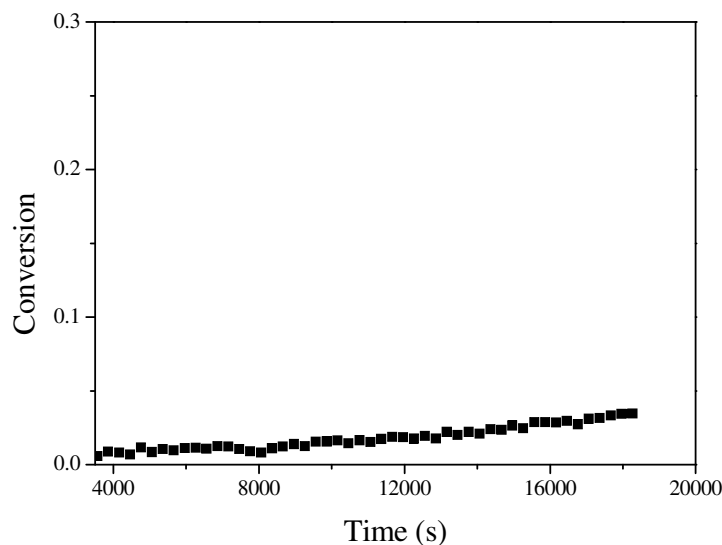
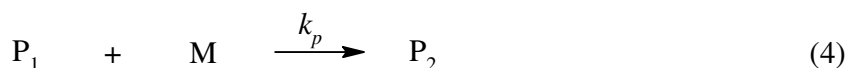
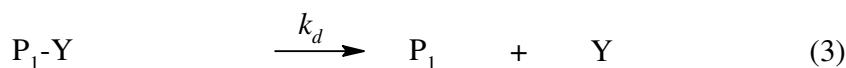
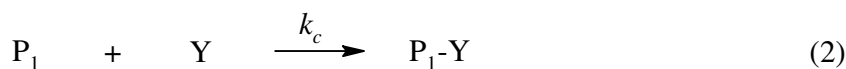
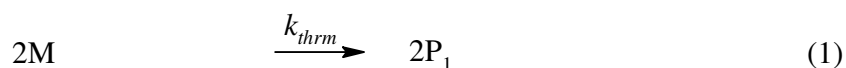


Figure 3-15: The evolution of *n*-butyl acrylate conversion with time for thermally initiated polymerization in DMSO- d_6 in the presence of $5.30 \times 10^{-02} \text{ mol L}^{-1}$ free DEPN at 120 °C.

Figure 3-14 illustrates the evolution of the relative monomer concentration with time, for which free DEPN added was equivalent to DEPN derived from a unimolecular experiment for which 8.94 mg of the MAMA-DEPN alkoxyamine was employed. No significant consumption of *n*-butyl acrylate is observed and analysis of the ^1H NMR spectra did not reveal peaks characteristic of poly(*n*-butyl acrylate). The experimental setup were similar to the previously described *in situ* ^1H NMR homopolymerization of *n*-butyl acrylate with MAMA-DEPN, and with everything kept similar, the MAMA-DEPN was replaced with DEPN. The polymerization of *n*-butyl acrylate in the presence of free DEPN was repeated with polymerization time increased to five hours (Figure 3-15). Figure 3-15 shows the evolution of monomer conversion with polymerization time, and only after ca. 2½ hours does significant monomer consumption occur. Nonetheless the monomer consumption occurs at a rate far less than in a system with a radical initiator.

To quantify the thermal auto-initiation of *n*-butyl acrylate, Scheme 3-2 is considered. At early reaction times, reactions (4) and (5) from Scheme 3-2 can be considered negligible.



Scheme 3-2: Schematic representation of thermally initiated *n*-butyl acrylate (M) polymerization in the presence of a free nitroxide (Y).

Due to the large excess of free DEPN at these early reaction times, the thermally generated radicals (reaction (1)) will react mainly according to reactions (2) and (3). In this time regime where propagation and termination reactions are negligible, the rate of consumption of the monomer can be defined by Equation (3-10) which upon integration yields Equation (3-11).

$$d[M]/dt = -k_{thrm}[M]^2 \quad (3-10)$$

$$\left(\frac{1}{[M]} - \frac{1}{[M]_0} \right) = k_{thrm}t \quad (3-11)$$

The plot of the left hand side of Equation (3-11) with time yields a straight line (Figure 3-16) whose slope must equal the rate coefficient of thermal auto-initiation in the case where propagation and termination reactions are negligible. The deviation from linearity will signify the occurrence of propagation and termination reactions. The data obtained via *in situ* ¹H NMR will be subject to scatter due to the minute difference in monomer concentration being measured, thus care should be exercised in the treatment of data. The rate coefficient of thermal auto-initiation ($k_{thrm} = 3.54 \times 10^{-07} \text{ L mol}^{-1} \text{ s}^{-1}$) extracted from Figure 3-16 was in good agreement with $k_{thrm} = 1.578 \times 10^{-07} \text{ L mol}^{-1} \text{ s}^{-1}$ determined from the Arrhenius parameters reported by Rantow et al.⁴³ at 120 °C.

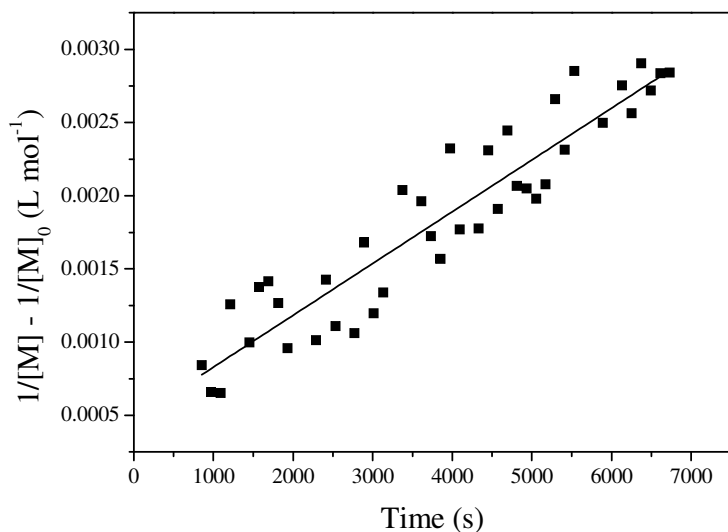


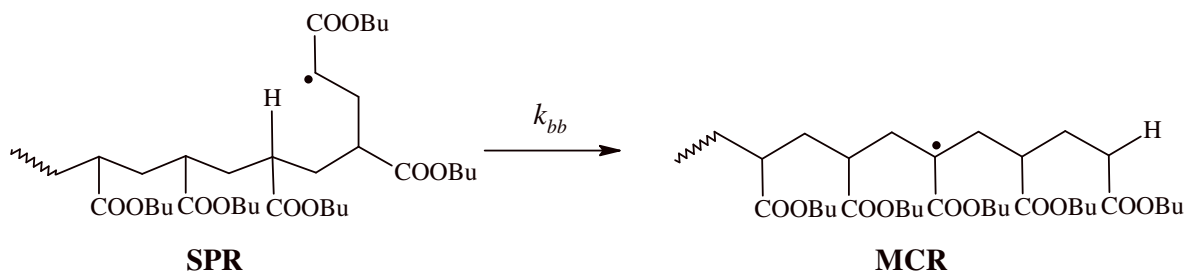
Figure 3-16: The plot of the negative inverse monomer consumption with time (■) in the linear range with the solid line as the linear fit to the data with a slope = $3.54 \times 10^{-07} \text{ L mol}^{-1} \text{ s}^{-1}$ and adjusted $R^2 = 0.87$. $[n\text{-butyl acrylate}] = 3.12 \text{ mol L}^{-1}$ and $[\text{DEPN}] = 0.0452 \text{ mol L}^{-1}$ at $120 \text{ }^\circ\text{C}$ with DMSO-d_6 as the solvent.

The rate coefficient of thermal auto-initiation determined in this work at $120 \text{ }^\circ\text{C}$ is approximately an order of magnitude less than that of styrene.⁴⁴ Thermal auto-initiation in the case of high temperature *n*-butyl acrylate polymerization does occur, but cannot be the sole cause of the observed phenomenon of rate independence towards initiator concentration.

Thus to try explain the phenomenon reported in this work, a thorough consideration of the co-existence of the secondary propagating radicals and mid-chain radicals, and their implications on the kinetics and mechanistic of the system with regard to varying initial alkoxyamine concentration is considered. In Chapter IV a further attempt to address the matter of the co-existence of the mid-chain radicals and secondary propagating radicals in the presence of a persistent radical species will be made from a theoretical point of view.

Before explaining the observed phenomenon, the matter of the co-existing radicals in the case of *n*-butyl acrylate should further be expanded on. Acrylate type monomers show more complex behaviour in their polymerization mechanistic and kinetic features relative to other vinyl monomers such as styrene. Deviations from ideal behaviour with respect to polymerization kinetics have previously been reported in the literature, with monomer reaction orders ranging from 1.4 to 1.8.⁴⁵ *n*-Butyl acrylate can undergo chain transfer to monomer and/or polymer. The

former restricts the molar mass and the latter results in branched polymer structures. Chain transfer to polymer can occur either intermolecularly or intramolecularly.⁴⁵ Intermolecular chain transfer involves transfer of a radical reactive site from a chain end position of a growing polymer chain to a mid-chain position of another polymer chain by hydrogen abstraction.



Scheme 3-3: The intramolecular chain transfer to polymer via the 1,5-hydrogen shift from the antepenultimate unit resulting in the transformation of a secondary propagating radical (SPR) into the mid-chain radical (MCR) at a rate determined by the rate coefficient of backbiting (k_{bb}).

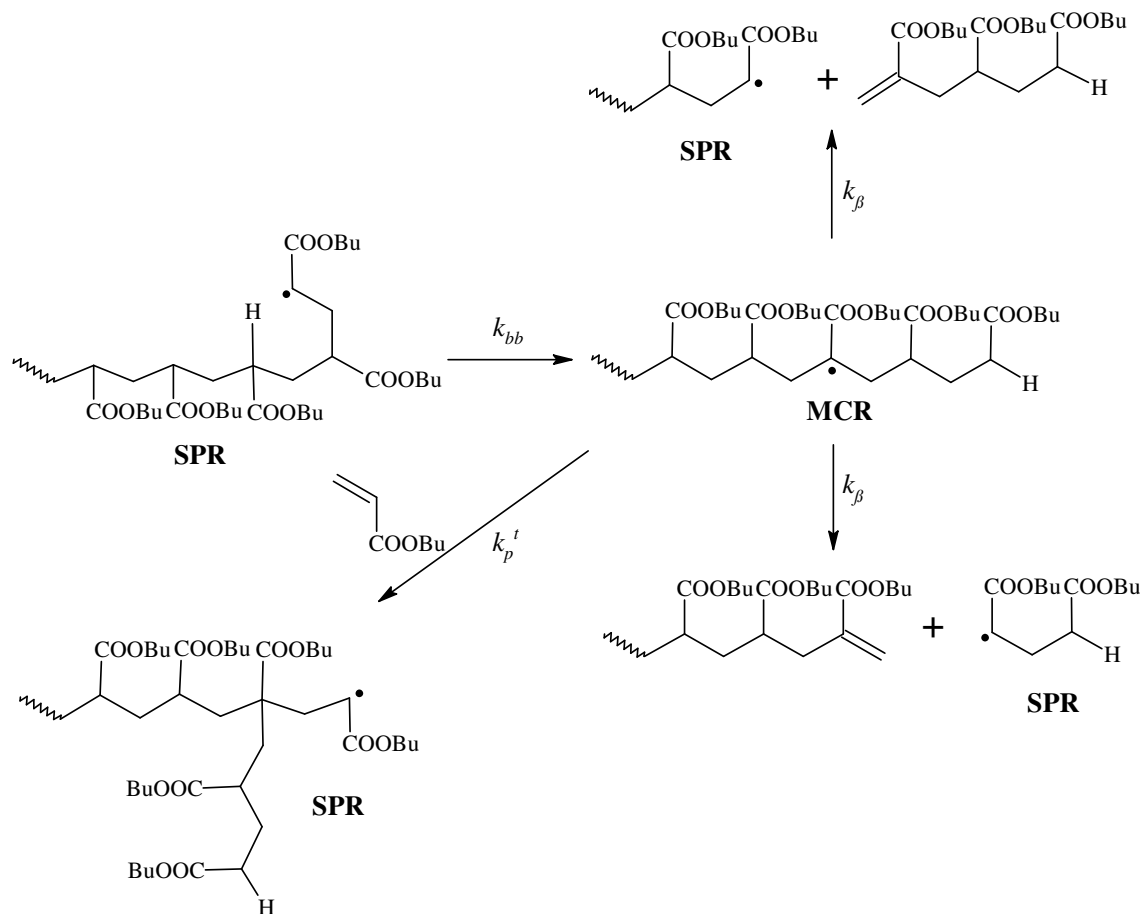
Intramolecular chain transfer (so-called backbiting) occurs by hydrogen abstraction from a unit in the proximity (the antepenultimate unit) of the propagating radical, via the formation of an intermediate six-membered ring structure (Scheme 3-3).⁴⁶ Intramolecular chain transfer is governed by the rate coefficient of backbiting (k_{bb}). It should however be noted that intramolecular chain transfer can occur at any position in the polymer backbone with slightly different governing rate coefficients. However, the most probable and more favoured position is on the third unit from the chain end radical via the intermediate six membered ring structure.⁴⁶ Thus k_{bb} can be assumed within good approximation as the sole rate coefficient of intramolecular chain transfer. The result of the chain transfer to polymer process is the transformation of secondary propagating radicals (SPRs) into tertiary mid-chain radicals (MCRs). Intramolecular chain transfer has been reported as the main cause for the branched structure of poly(*n*-butyl acrylate) prepared via nitroxide mediated polymerization in bulk and mini-emulsion polymerization.⁴⁷ The MCRs exhibit a higher level of stability relative to the SPRs and as a result tend to add monomer at a rate an order of magnitude lower than the rate at which monomer is added to the SPRs.^{7, 48} Scheme 3-4 shows the formation of the MCR from a SPR together with the possible reactions the MCR can undergo. Thus due to the chain transfer

process and the possible reaction pathways the MCRs can undergo, the result is a system with two distinct co-existing transient radical species.

Two types of transient radicals exist in the system, *i.e.* the SPRs and MCRs, with k_p and k_p^t as their respective propagation rate coefficients. The average propagation rate coefficient (k_p^{av}) can be defined by the weighted average of the propagation rate coefficients of the SPRs and MCRs. If θ is defined as the fraction of MCRs in the system, and if $\lim_{\theta \rightarrow 0} f(\theta)$, then $k_p^{av} \rightarrow k_p$, while on the other hand if $\lim_{\theta \rightarrow 1} f(\theta)$, then $k_p^{av} \rightarrow k_p^t$. From the analytical expressions derived by Nikitin,^{7, 49, 50} the rate of polymerization (R_p) can be expressed by Equation 3-12.

$$R_p = k_p^{av} [M]([Q] + [P]) \quad (3-12)$$

The fraction of MCRs, which is temperature dependent,^{51, 52} should have a strong influence on R_p , due to the large difference between k_p and k_p^t . The effect of the polymerization temperature on the ratio of SPRs to MCRs will thus tend to have a larger influence on the apparent average rate of propagation, relative to the effect of the initial concentration of the alkoxyamine. In the expression for the rate of polymerization (R_p), $[M]$, $[Q]$ and $[P]$ represent concentrations of monomer, MCRs and SPRs, respectively. In the case of *n*-butyl acrylate, the main factors that affect θ are backbiting, β -fragmentation and addition of monomer to the MCR. These processes are illustrated in Scheme 3-4. The rate coefficients of these three processes, k_{bb} , k_β and k_p^t , respectively, can all be represented by Arrhenius expressions.^{7, 43} The reaction pathways (Scheme 3-4) that will determine the fate of MCRs include (i) addition of monomer to the MCR (which will transform the MCRs to SPRs with a short branch chain) at a rate determined by k_p^t , (ii) β -fragmentation, which will result in the formation of an SPR and a chain bearing a 1,1-disubstituted alkene end group at a rate determined by the rate coefficient of β -fragmentation (k_β), and (iii) termination with either an SPR or another MCR at rates determined by k_t^t and k_t'' , respectively.^{21, 53}



Scheme 3-4: Formation of mid-chain radicals (MCRs) from secondary propagating radicals (SPRs) via backbiting and the subsequent transformation of the MCR to SPR via β -fragmentation and monomer addition.

In addition to the re-generation of the SPR, β -fragmentation also result in chains bearing the 1,1-disubstituted alkene end group. According to the work of Chiefari⁶ on the synthesis of macromonomers via chain transfer to polymer, the 1,1-disubstituted alkene end group can be identified by the signal at $\delta \sim 5.5$ ppm. Figure 3-17 shows a signal increasing with polymerization time at $\delta \sim 5.5$ ppm identified as due to one of the protons of the 1,1-disubstituted alkene end group resulting from the β -fragmentation of the MCR. The second peak expected at $\delta \sim 6.1$, due to the second vinyl proton of the 1,1-disubstituted alkene end group could not be observed due to overlap with the signal of the monomer proton labelled ²H in Figure 3-2.

The *n*-butyl acrylate polymerization reactions initiated by MAMA-DEPN were also carried out at 90 °C, 100 °C and 110 °C. A proton signal at $\delta \sim 5.5$ ppm was not observed at 90 °C and

100 °C, implying that the concentration of species bearing 1,1-disubstituted alkene end group could be below the detection limit of the NMR spectrometer. However at 110 °C, the signal at $\delta \sim 5.5$ ppm due to one of the protons of the 1,1-disubstituted alkene end group was observed at high monomer conversion (Figure 3-18). At 110 °C, the species bearing the 1,1-disubstituted alkene end group accumulate with polymerization time and only at higher monomer conversion is the concentration of the species above the threshold detection value of the NMR instrument.

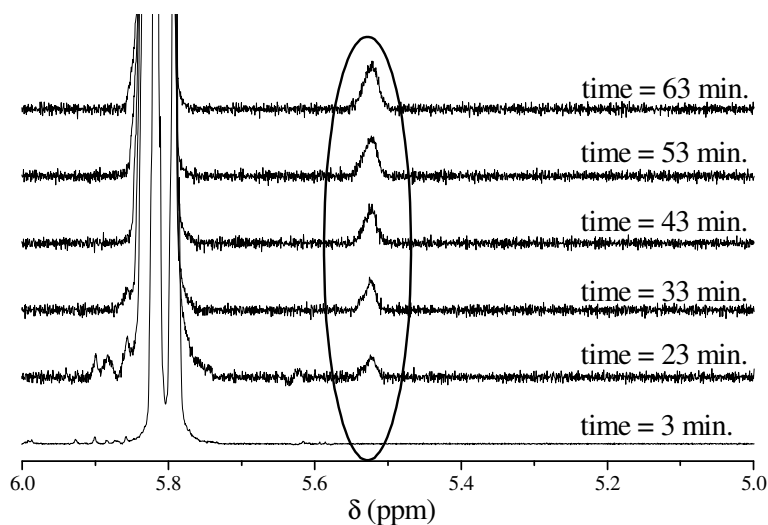


Figure 3-17: ^1H NMR spectra at different reaction times illustrating the increasing intensity of the peak at around $\delta \sim 5.5$ ppm that is due to an increasing concentration of 1,1-disubstituted alkene end groups as a result of β -fragmentation of the MCRs in the polymerization of *n*-butyl acrylate at 120 °C with $[\text{MAMA-DEPN}]_0 = 0.156$ M, $[\textit{n}\text{-butyl acrylate}]_0 = 3.0$ M and $\text{DMSO-}d_6 = 65$ % v/v.

Thus Figures 3-17 and 3-18 indicate the existence of polymer chains bearing the 1,1-disubstituted alkene end group at 120 °C and 110 °C, respectively. However, no ^1H NMR evidence could be found at 100 °C and temperatures below. The absence of such evidence should not be used to draw a conclusion that β -fragmentation is non-existent or insignificant. Several studies in the literature⁵⁴⁻⁵⁶ have reported on the presence of the polymer chains bearing the 1,1-disubstituted alkene at temperatures lower than 100°C.

Figure 3-19 shows the evolution of the concentration of the species bearing the 1,1-disubstituted alkene end group with polymerization time. The concentration profile depicts that the overall rate

of accumulation of the alkene bearing species is constant. The most likely explanation for the observed phenomenon is a constant rate of β -fragmentation.

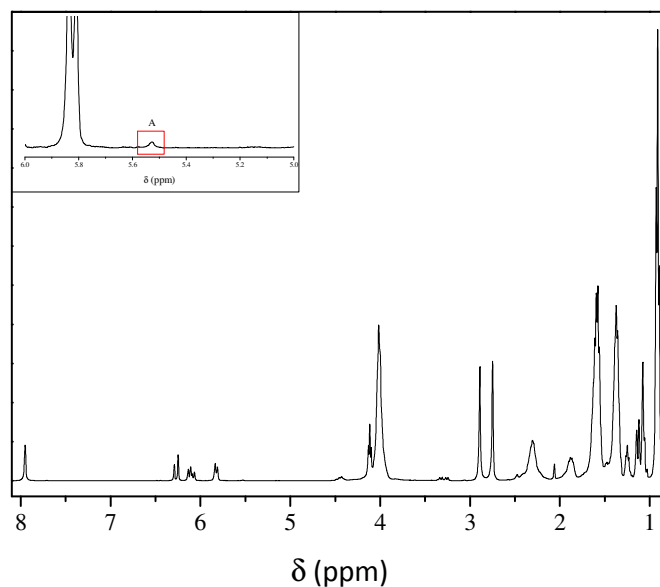


Figure 3-18: The ¹H NMR spectrum taken after 2 hours of polymerization of n-butyl acrylate at 110 °C with [MAMA-DEPN]₀ = 0.1494 M, [*n*-butyl acrylate]₀ = 3.0 M and DMSO-d₆ = 65 % v/v. The insert shows the expanded region in the range 6.0 > δ (ppm) > 5.0 with the marked peak, labelled **A**, assigned to one of the protons of the 1,1-disubstituted alkene end group resulting from the β -fragmentation of the MCRs.

Alternatively, but less likely, the constant rate of accumulation of the species bearing the 1,1-disubstituted alkene end group might be the result of a balance of two processes, namely the generation of the species and their incorporation in the growing polymer chain.^{57, 58}

The implication of the latter process is that in addition to the formerly mentioned modes of generation of the MCRs, the incorporation of the species bearing the 1,1-disubstituted alkene end group would also result in the formation of MCRs.

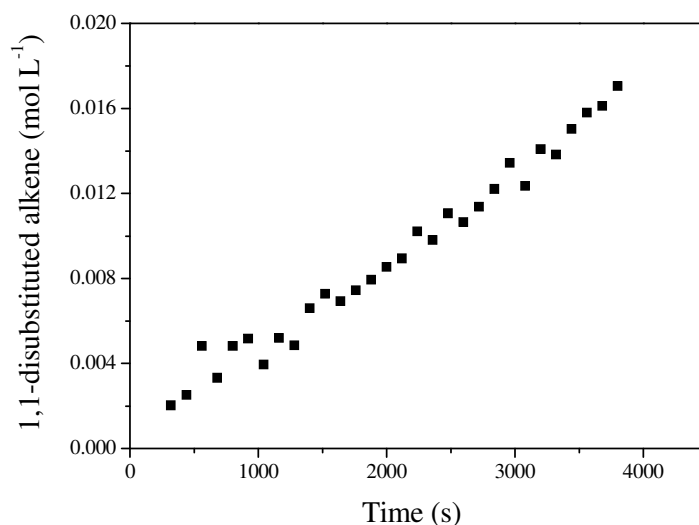


Figure 3-19: The evolution of concentration of 1,1-disubstituted alkene end group vs. polymerization time during *n*-butyl acrylate polymerization at 120 °C with $[MAMA-DEPN]_0 = 0.156$ M, $[n\text{-butyl acrylate}]_0 = 3.0$ M and DMSO- $d_6 = 65$ % v/v.

Figure 3-20 shows the effect of the initial alkoxyamine concentration on the concentration profiles of the species bearing the 1,1-disubstituted alkene end group as a function of monomer conversion. It can be observed that the concentration profiles are independent of initial alkoxyamine concentration. This means that there is a constant rate of β -fragmentation, independent of initial alkoxyamine concentration. This observation is in agreement with the constant rate of polymerization as observed in Figure 3-12.

If the process of the incorporation of the 1,1-alkene species in the growing polymer is assumed negligible, the differential describing the concentration of the species bearing the 1,1-alkene end group with time can be expressed by Equation 3-13 which upon integration yields Equation 3-14. It should be noted that Equation 3-14 is valid only for a constant concentration of MCRs.

$$\frac{d[1,1 - alkene]}{dt} = k_{\beta}[Q] \quad (3-13)$$

$$[1,1 - alkene] = k_{\beta}[Q]t \quad (3-14)$$

The linear evolution with time of the species bearing the 1,1-alkene end group as a result of β -fragmentation observed in Figure 3-19, is in agreement with the first order dependence predicted by Equation 3-14. The linear evolution can be used to estimate whether the incorporation of the species bearing the 1,1-alkene end group in the growing polymer is negligible or not. In the case where the incorporation of the species bearing the 1,1-alkene end group is significant, a deviation from linearity of the profile in Figure 3-19 would be expected. The gradient of the linear plot in Figure 3-19 can then be related to the concentration of the mid-chain radicals in the system with the knowledge of the β -fragmentation rate coefficient.

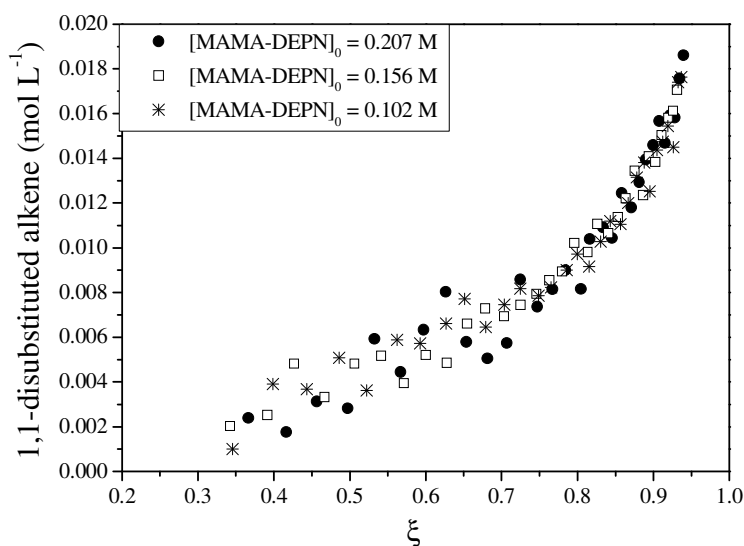


Figure 3-20: The evolution of relative concentration of 1,1-disubstituted alkene end group vs. monomer conversion during *n*-butyl acrylate polymerization at 120 °C for different initial concentrations of the alkoxyamine MAMA-DEPN. $[n\text{-butyl acrylate}]_0 = 3.0 \text{ M}$ and $\text{DMSO-d}_6 = 65 \text{ \% v/v}$.

The constant rate of polymerization observed is synonymous with a constant concentration of propagating radicals, which would translate to overall propagating radicals (mid-chain and secondary propagating radicals) in the case of *n*-butyl acrylate polymerization. This constant concentration of overall radicals leads to constant concentration of mid-chain radicals and hence (at a fixed temperature) to a constant increase in the species bearing the 1,1-alkene end group (Figure 3-19).

A stationary concentration of the mid-chain radicals is thus maintained that is similar in the range of the initial alkoxyamine concentration studied as illustrated by Figure 3-20. The fraction of MCR is known to be temperature dependent.⁵¹ Figure 3-13 in conjunction with Figure 3-20 and Equation 3-14 would further suggest that a similar steady state concentration of MCR is attained in all experiments undertaken. It would then seem logical to think that the concentration of SPR is also similar. However, thorough considerations of the reactions the mid-chain radicals undergo, including the reversible deactivation with the nitroxide, are described in Chapter IV. The effect of thermal auto-initiation and the equilibrium involving the mid-chain radicals on the kinetics of *n*-butyl acrylate polymerization are assessed in Chapter IV via modelling of the system with the Predici software package.

3.6.3 Conclusion

The unimolecular nitroxide mediated homopolymerization of both styrene and *n*-butyl acrylate using the alkoxyamine MAMA-DEPN has shown that the rate of polymerization is independent of the initial concentration of the alkoxyamine. In the case of styrene, the independence is well in agreement with previous literature reports on the same subject. This phenomenon of the rate independence on initiator concentration has been explained in terms of the pronounced thermal auto-initiation in the polymerization of styrene. However, in the case of *n*-butyl acrylate, where thermal initiation is not expected to be that significant, the issue of the rate independence has not been addressed in the literature to date, to the best of our knowledge. The nature of the complexity of the system with two distinct co-existing transient radicals has complicated matters in the complete quest of understanding the kinetics and mechanistic features of acrylate type polymerization systems. At this point, no cause can be singled out attributable to the observed behaviour in *n*-butyl acrylate polymerization. But the co-existence of the two types of transient radicals and their temperature dependence is believed to have an effect to some extent on the observed phenomenon.

3.7 Summary

Unimolecular nitroxide mediated homopolymerization reactions of styrene and *n*-butyl acrylate were conducted successfully. The persistent radical effect theory was validated in the case of

styrene polymerization at 120 °C using a DEPN end capped polystyrene macro-alkoxyamine as initiator. In line with literature, the rate of polymerization in the case of styrene showed no apparent dependence on the initial concentration of the alkoxyamine.

It was also demonstrated that the rate of polymerization of *n*-butyl acrylate shows no dependence on the concentration of the alkoxyamine. For *n*-butyl acrylate polymerization conducted at 120 °C, the accumulation of the β -fragmentation product (chains bearing the 1,1-disubstituted alkene end group) occurred at a constant rate independent of the initial alkoxyamine concentration. No ¹H NMR evidence of the species bearing the 1,1-disubstituted alkene end group could be observed when the polymerization was carried at 100 °C or lower.

The absence of evidence of species bearing the 1,1-disubstituted alkene end group can be used to support approximations that the contribution of β -fragmentation to the polymerization kinetics of *n*-butyl acrylate is minimal at 100 °C and lower temperatures, validating exclusion of β -fragmentation in polymerization models at moderate polymerization temperatures.

References

1. Buback, M.; Gilbert, R. G.; Hutchinson, R. A.; Klumperman, B.; Kuchta, R. D.; Manders, B. G.; O'Driscoll, K. F.; Russell, G. T.; Schweer, J. *Macromol. Chem. Phys.* **1995**, 196, 3267-.
2. Barner-Kowollik, C.; Günzler, F.; Junkers, T. *Macromolecules* **2008**, 41, 8971-8973.
3. Asua, J. M.; Beuermann, S.; Buback, M.; Castignolles, P.; Charleux, B.; Gilbert, R. G.; Hutchinson, R. A.; Leiza, J. R.; Nikitin, A. N.; Vairon, J.-P.; Herk, A. M. v. *Macromol. Chem. Phys.* **2004**, 205, 2151-2160.
4. Beuermann, S.; D. A. Paquet, J.; McMinn, J. H.; Hutchinson, R. A. *Macromolecules* **1996**, 29, 4206-4215.
5. Chiefari, J.; Jeffery, J.; Krstina, J.; Moad, C. L.; Moad, G.; Postma, A.; Rizzardo, E.; Thang, S. H. *Macromolecules* **2005**, 38, 9037-9054.
6. Chiefari, J.; Jeffery, J.; Mayadunne, R. T. A.; Graeme Moad; Rizzardo, E.; Thang, S. H. *Macromolecules* **1999**, 32, 7700-7702.
7. Nikitin, A. N.; Hutchinson, R. A.; Buback, M.; Hesse, P. *Macromolecules* **2007**, 40, 8631-8641.
8. Degirmenci, I.; Avci, D.; Aviyente, V.; Cauter, K. V.; Speybroeck, V. V.; Waroquier, M. *Macromolecules* **2007**, 40, 9590 - 9602.
9. Coote, M. L.; Zammit, M. D.; Davis, T. P.; Willett, G. D. *Macromolecules* **1997**, 30, 8182-8190.
10. Zammit, M. D.; Coote, M. L.; Davis, T. P.; Willett, G. D. *Macromolecules* **1998**, 31, 955-963.
11. Chambard, G. Control of Monomer Sequence Distribution; Strategic Approach based on Novel Insights in Atom Transfer Radical polymerization. PhD, Technische Universiteit Eindhoven, Eindhoven, 2000.
12. Fischer, H.; Paul, H. *Acc. Chem. Res.* **1987**, 20, 200-206.
13. Piton, M. C.; Gilbert, R. G.; Chapman, B. E.; Kuchel, P. W. *Macromolecules* **1993**, 26, 4472-4477.
14. Griffiths, M. C.; Strauch, J.; Monteiro, M. J.; Gilbert, R. G. *Macromolecules* **1998**, 31, 7835-7844.

15. Junkers, T.; Theis, A.; Buback, M.; Davis, T. P.; Stenzel, M. H.; Vana, P.; Barner-Kowollik, C. *Macromolecules* **2005**, *38*, 9497-9508.
16. Johnston-Hall, G.; Monteiro, M. J. *J. Polym. Sci., Part A: Polym. Chem.* **2008**, *46*, 3155-3173.
17. Theis, A.; Feldermann, A.; Charton, N.; Davis, T. P.; Stenzel, M. H.; Barner-Kowollik, C. *Polymer* **2005**, *46*, 6797-6809.
18. Johnston-Hall, G.; Stenzel, M. H.; Davis, T. P.; Barner-Kowollik, C.; Monteiro, M. J. *Macromolecules* **2007**, *40*, 2730-2736.
19. Theis, A.; Feldermann, A.; Charton, N.; Stenzel, M. H.; Davis, T. P.; Barner-Kowollik, C. *Macromolecules* **2005**, *38*, 2595-2605.
20. Johnston-Hall, G.; Theis, A.; Monteiro, M. J.; Davis, T. P.; Stenzel, M. H.; Barner-Kowollik, C. *Macromol. Chem. Phys.* **2005**, *206*, 2047-2053.
21. Barth, J.; Buback, M.; Hesse, P.; Sergeeva, T. *Macromolecules* **2010**, *43*, 4023-4031.
22. Buback, M.; Müller, E.; Russell, G. T. *J. Phys. Chem. A* **2006**, (110), 3222-3230.
23. Buback, M.; Egorov, M.; Junkers, T.; Panchenko, E. *Macromol. Rapid Commun.* **2004**, (25), 1004-1009.
24. Buback, M.; Egorov, M.; Junkers, T.; Panchenko, E. **2005**, *206*, 333-341.
25. Barth, J.; Buback, M. *Macromol. Rapid Commun.* **2009**, *30*, 1805-1811.
26. Barth, J.; Buback, M.; Hesse, P.; Sergeeva, T. *Macromolecules* **2009**, *42*, 481-488.
27. Bon, S. A. F.; Chambard, G.; German, A. L. *Macromolecules* **1999**, *32*, 8269-8276.
28. Fukuda, T. *J. Polym. Sci., Part A: Polym. Chem.* **2004**, *42*, 4743-4755.
29. Fischer, H. *Macromolecules* **1997**, *30*, 5666-5672.
30. Tang, W.; Fukuda, T.; Matyjaszewski, K. *Macromolecules* **2006**, *39*, 4332-4337.
31. Drache, M.; Mandel, K.; Schmidt-Naake, G. *Polymer* **2007**, *48*, 1875-1883.
32. Goto, A.; Fukuda, T. *Prog. Polym. Sci.* **2004**, *29*, 329 - 385.
33. Talaty, E. R.; Boese, C. A.; Adewale, S. M.; Ismail, M. S.; Provenzano, F. A.; Utz, M. J. *J. Chem. Educ.* **2002**, *79*, (2), 221-224.
34. Smith, L. I.; Emerson, O. H. *Org. Synth.* **1949**, *29*, 18-21.
35. Guerret, O.; Couturier, J.-L.; Le Mercier, C. Method for preparing beta-phosphorus nitroxide radicals. 7126021, 2006.

36. Couturier, J. L.; Guerret, O.; Bertin, D.; Gignes, D.; Marque, S.; Tordo, P. Alkoxyamines originating from β -phosphorylated nitroxides and use thereof in radical polymerisation. 20060142511, 2006.
37. Catala, J. M.; Bubel, F.; Hammouch, S. O. *Macromolecules* **1995**, 28, 8441-8443.
38. Greszta, D.; Matyjaszewski, K. *Macromolecules* **1996**, 29, 5239-5240.
39. Fukuda, T.; Terauchi, T.; Goto, A.; Ohno, K.; Tsujii, Y.; Miyamoto, T.; Kobatake, S.; Yamada, B. *Macromolecules* **1996**, 29, 6393-6398.
40. Gray, M. K.; Zhou, H.; Nguyen, S. T.; Torkelson, J. M. *Macromolecules* **2003**, 36, 5792-5797.
41. Kruse, T. M.; Souleimonova, R.; Cho, A.; Gray, M. K.; Torkelson, J. M.; Broadbelt, L. J. *Macromolecules* **2003**, 36, 7812-7823.
42. Schulte, T.; Knoop, C. A.; Studer, A. *J. Polym. Sci., Part A: Polym. Chem.* **2004**, 42, 3342-3351.
43. Rantow, F. S.; Soroush, M.; Grady, M. C.; Kalfas, G. A. *Polymer* **2006**, 47, 1423-1435.
44. Hui, A. W.; Hamielec, A. E. *J. Appl. Polym. Sci.* **1972**, 16, 749-769.
45. Junkers, T.; Barner-kowollik, C. *J. Polym. Sci., Part A: Polym. Chem.* **2008**, 46, 7585-7605.
46. Dossi, M.; Storti, G.; Moscatelli, D. *Macromol. Symp.* **2010**, 289, 119-123.
47. Farcet, C.; Belleney, J.; Charleux, B.; Pirri, R. *Macromolecules* **2002**, 35, 4912-4918.
48. Buback, M.; Hesse, P. *Polym. Prepr.* **2008**, 49, (2), 217-218.
49. Nikitin, A. N.; Hutchinson, R. A. *Macromolecules* **2005**, 38, 1581-1590.
50. Nikitin, A. N.; Hutchinson, R. A. *Macromol. Theory Simul.* **2006**, 15, 128-136.
51. Willemse, R. X. E.; Herk, A. M. v.; Panchenko, E.; Junkers, T.; Buback, M. *Macromolecules* **2005**, 38, 5098-5103.
52. Barth, J.; Buback, M.; Hesse, P.; Sergeeva, T. *Macromol. Rapid Commun.* **2009**, 30, 1969-1974.
53. Junkers, T.; Koo, S. P. S.; Davis, T. P.; Stenzel, M. H.; Barner-Kowollik, C. *Macromolecules* **2007**, 40, 8906-8912.
54. Koo, S. P. S.; Junkers, T.; Barner-Kowollik, C. *Macromolecules* **2009**, 42, 62-69.

55. Junkers, T.; Bennet, F.; Koo, S. P. S.; Barner-Kowollik, C. *J. Polym. Sci., Part A: Polym. Chem.* **2008**, 46, 3433-3437.
56. Günzler, F.; Junkers, T.; Barner-Kowollik, C. *J. Polym. Sci., Part A: Polym. Chem.* **2009**, 47, 1864-1876.
57. Postma, A.; Davis, T. P.; Li, G.; Moad, G.; O'Shea, M. S. *Macromolecules* **2006**, 39, 5307-5318.
58. Sato, E.; Emoto, T.; Zetterlund, P. B.; Yamada, B. *Macromol. Chem. Phys.* **2004**, 205, 1829-1839.

Chapter IV: Secondary Reactions in *n*-Butyl Acrylate Polymerization and Theoretical Considerations

Synopsis

*A theoretical consideration of high temperature *n*-butyl acrylate polymerization is presented in this chapter. The possibility of a reversible deactivation-activation equilibrium reaction between the mid-chain radical (MCR) and the nitroxide (DEPN) is investigated and shown to exist via in situ ¹H NMR. The estimated values of the deactivation and activation rate coefficients of the MCR and MCR-DEPN respectively, are also presented. The effects of the MCR/MCR-DEPN equilibrium and thermal auto-initiation on the polymerization kinetics of *n*-butyl acrylate were investigated by simulation of the *n*-butyl acrylate polymerization with the Predici software package.*

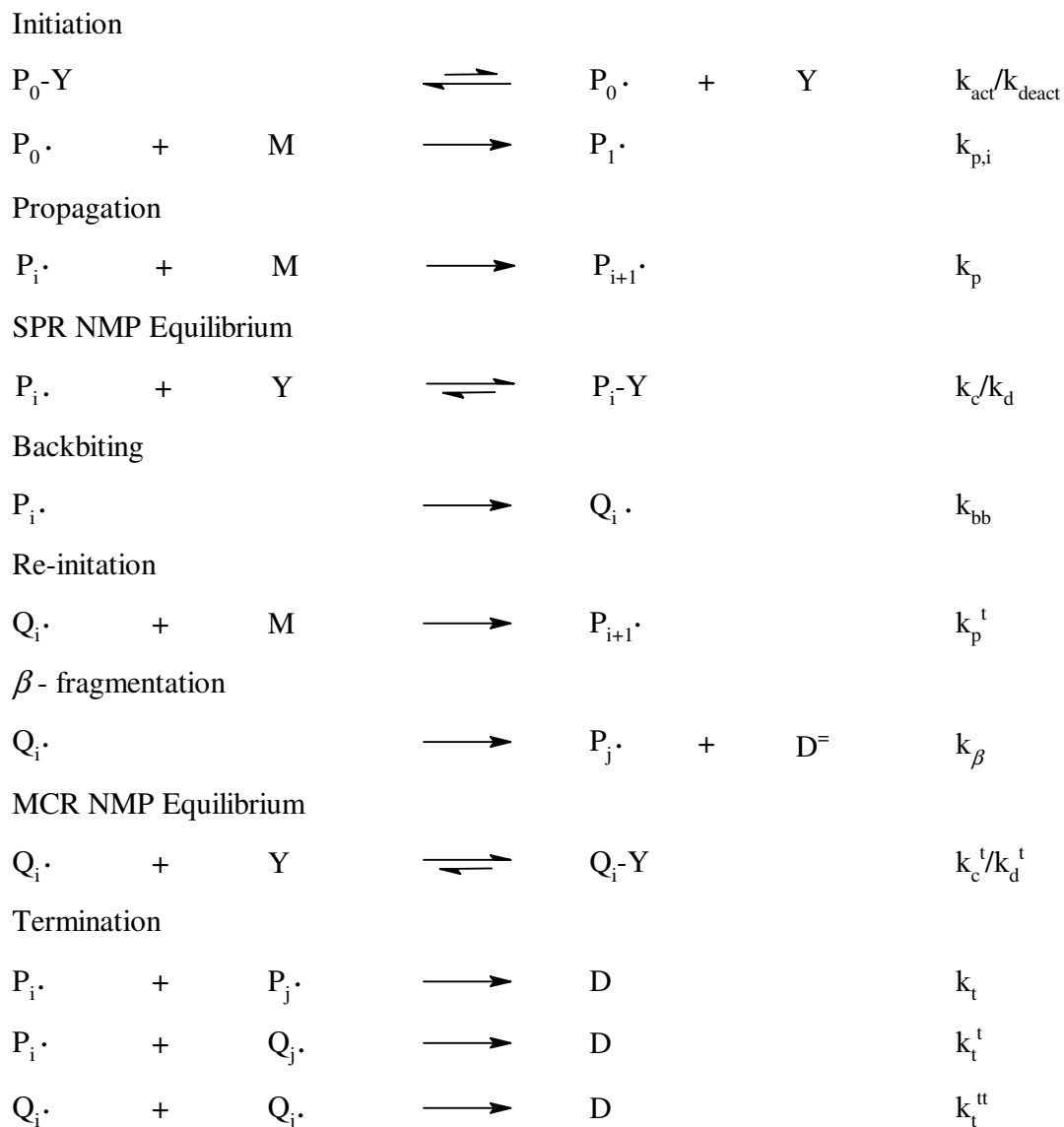
4.1 Introduction

The complexity of the *n*-butyl acrylate homopolymerization system has led to reports of inaccurate values of some experimentally determined kinetic parameters over the past years. Developments in experimentation have allowed for a better understanding of the system and reports of continuously improving kinetic data. This current chapter will serve as an extension of the homopolymerization of *n*-butyl acrylate reported in Chapter III, with the emphasis on complexities introduced by the secondary reactions in high temperature *n*-butyl acrylate polymerization. As already mentioned in Chapter III, the chain transfer process to polymer in *n*-butyl acrylate polymerization results in a system in which two types of transient radicals [the secondary propagating radical (SPR) and tertiary mid chain radical (MCR)] exist. In the case of NMP, a matter which to the best of our knowledge has not been addressed in the literature, is the possibility of a reversible deactivation reaction of the MCR with the stable free nitroxide (persistent radical), if any. The confirmation of the existence or non-existence of such a reaction is critical in explicitly describing the polymerization of *n*-butyl acrylate and in the construction of a kinetic model, representative of the system.

It should however be noted that the choice of NMP in the assessment of the possibility of the reversible deactivation-activation reaction between the MCR and the mediating species, was solely based on the simplicity of the system in consideration relative to other controlled radical polymerization (CRP) techniques such as RAFT and ATRP. In the case of NMP, the adduct that forms from the coupling of the MCR and DEPN (forming the dormant species) can be detected with relative ease even during the course of the polymerization process monitored via *in situ* ¹H NMR.

If one was to consider a nitroxide mediated polymerization of *n*-butyl acrylate in which the sole mode of chain transfer to polymer was via intra-molecular chain transfer, the model for the polymerization can be described as illustrated by Scheme 4-1. In Scheme 4-1, two equilibrium reactions are considered together with respective bimolecular termination between two SPRs and two MCRs including the cross termination of the respective transient radicals. The reaction of β -fragmentation is included to cover high temperature polymerization of *n*-butyl acrylate where the reaction cannot be regarded as negligible. The inclusion of the equilibrium between MCR-

DEPN and the MCR in Scheme 4-1 does not imply the existence of such a reaction but merely serves as a starting point for the investigation of such an equilibrium reaction.



Scheme 4-1: Model for nitroxide mediated polymerization of *n*-butyl acrylate with the inclusion of intra-molecular chain transfer to polymer and the reversible deactivation-activation reaction between the MCR and the nitroxide. P and Q symbolise the SPR and MCR, respectively.

From Scheme 4-1, the following differential equations can be derived:

$$\frac{d[P_0]}{dt} = k_d[P_0 - X] - k_c[P_0][X] - k_{p,i}[P_0][M] \quad (4-1)$$

$$\frac{d[P_1]}{dt} = k_i[P_0][M] - k_p[P_1][M] + k_d[P_1 - X] - k_c[P_1][X] - (k_t[P_1] + k_t'[Q_1])[P_1] \quad (4-2)$$

$$\begin{aligned} \frac{d[P_i]}{dt} = & k_p[M][P_{i-1}] - k_p[M][P_i] - k_{bb}[P_i] + k_p'[M][Q_{i-1}] + k_d[P_i - X] \\ & - k_c[P_i][X] + k_\beta[Q_i] - (k_t[P_i] + k_t'[Q_i])[P_i] \end{aligned} \quad (4-3)$$

$$\begin{aligned} \frac{d[Q_i]}{dt} = & k_{bb}[P_i] - k_p'[M][Q_i] - (k_t''[Q_i] + k_t'[P_i])[Q_i] + k_d'[Q_i - X] \\ & - k_c'[Q_i][X] - k_\beta[Q_i] \end{aligned} \quad (4-4)$$

Due to relatively fast initiation, the polymer chains are of relative similar lengths, so that Equations 4-5 can be assumed valid. The chain length distribution of poly(*n*-butyl acrylate) produced via CRP techniques indicate relatively narrow distributions,^{1, 2} which means that the radical concentrations can be expressed by Equations 4-5. Applying Equation 4-5 in Equations 4-1 – 4-3 allows for the omission of the chain length subscript “*i*” for simplification purposes.

$$[P] = \sum_{i=1}^{\infty} [P_i] \quad [Q] = \sum_{i=1}^{\infty} [Q_i] \quad (4-5)$$

Assuming steady state conditions, adding Equations 4-3 and 4-4 yields

$$k_d[P - X] + k_d'[Q - X] = k_t[P]^2 + 2k_t'[P][Q] + k_t''[Q]^2 + (k_c[P] + k_c'[Q])[X] \quad (4-6)$$

After a certain initial period in a free radical polymerization, a constant concentration of transient radicals is maintained (stationary-state conditions). In the case of *n*-butyl acrylate polymerization, the constant concentration is maintained with respect to both the MCR and SPR.

As a result both the differentials of SPR and MCR concentrations with respect to time, taken after this initial period, can be set to zero. Thus, setting Equation 4-4 to zero yields,

$$k_{bb}[P] - k_p^t[M][Q] - (k_i^u[Q] + k_i^t[P])[Q] + k_d^t[Q - X] - k_c^t[Q][X] - k_\beta[Q] = 0 \quad (4-7)$$

and re-arranging,

$$[Q] = \frac{k_{bb}[P] + k_d^t[Q - X]}{k_p^t[M] + k_i^u[Q] + k_i^t[P] + k_c^t[X] + k_\beta} \quad (4-8)$$

One of the characteristics of the CRP techniques is the minimal extent to which termination reactions occur. In the case of the unimolecular NMP system as governed by the PRE theory, termination occurs predominantly at the early stages of the polymerization. As the concentration of nitroxide builds up relative to the transient radicals, the reversible deactivation reaction is favoured over the activation reaction. The result is a high concentration of dormant polymer chains relative to active transient radicals, therefore minimizing termination. Termination reactions can thus be assumed to be negligible such that the inequality $k_p^t[M] + k_c^t[X] + k_\beta \gg k_i^u[Q] + k_i^t[P]$ is valid. The expression for the concentration of MCR expressed by Equation 4-8 can be reduced to a simpler form expressed by Equation 4-9.

$$[Q] = \frac{k_{bb}[P] + k_d^t[Q - X]}{k_p^t[M] + k_c^t[X] + k_\beta} \quad (4-9)$$

Equation 4-9 expresses the complex relation between the secondary propagating radicals and the mid-chain radicals in the presence of the persistent radical species with the assumption that there exists a reversible deactivation-activation reaction between the nitroxide and MCR. Thus from Equation 4-9, it can be observed that if there exists such an equilibrium between the MCR-DEPN and the MCR, this will affect the active concentration of MCR and consequently the transitions between SPR and MCR. It should be noted that this interpretation is based on the assumption

that in the presence of the mediating species the termination reactions are minimal and thus negligible, a fair approximation for CRP processes.

If the steady state conditions are assumed, the differential for the total concentration of transient radicals can be written as follows,

$$\frac{d([P]+[Q])}{dt} = 0 \quad (4-10)$$

From Equations 4-3, 4-5 and 4-10, Equation 4-11 can be derived.

$$k_d[P-X] + k'_d[Q-X] = k_c[P][X] + k'_c[Q][X] \quad (4-11)$$

According to Equation 4-11, the concentration of the active radicals will be controlled by two equilibrium reactions involving the reversible activation-deactivation cycles between the persistent radical species and the two respective transient radical species. In a typical polymerization system with a single type of transient radical, the equilibrium can be described by Equation 4-12. However, the observed equilibrium in a system with two distinct transient radicals assumed to both undergo reversible deactivation-activation reaction with the nitroxide cannot be described adequately by Equation 4-12. In this case the equilibrium can be described by the observed or effective dissociation (activation) and combination (deactivation) rate coefficients according to Equation 4-13.

$$K = \frac{k_d}{k_c} = \frac{[P][X]}{[P-X]} \quad (4-12)$$

$$K^{eff} = \frac{k_d^{eff}}{k_c^{eff}} = \frac{([P]+[Q])[X]}{[P-X]+[Q-X]} \quad (4-13)$$

However, the existence of the reversible deactivation of the MCR by the nitroxide is not an easy reaction to prove. The use of mass spectrometry techniques has previously been reported for polymer chains bearing multiple nitroxides in the polymerization of *n*-butyl acrylate mediated by DEPN.³ However the information derived from such a study cannot distinguish whether adducts were formed between an MCR and the nitroxide or a SPR and the nitroxide. The information that can be derived from such studies is that due to intra- and inter-molecular chain transfer to polymer, there can be multiple active sites on a single polymer chain.

Based on the fact that the larger fraction of transient radicals in the system are MCR,^{4, 5} one would expect the nitroxide to react reversibly with the MCR. However, due to the greater stability of such radicals relative to SPR, the rate coefficients governing such a reversible deactivation would be expected to differ for those that govern the reversible deactivation of the SPR. If the reversible deactivation reaction between the MCR and the nitroxide is considered negligible, Equation 4-9 can be further reduced to Equation 4-14.

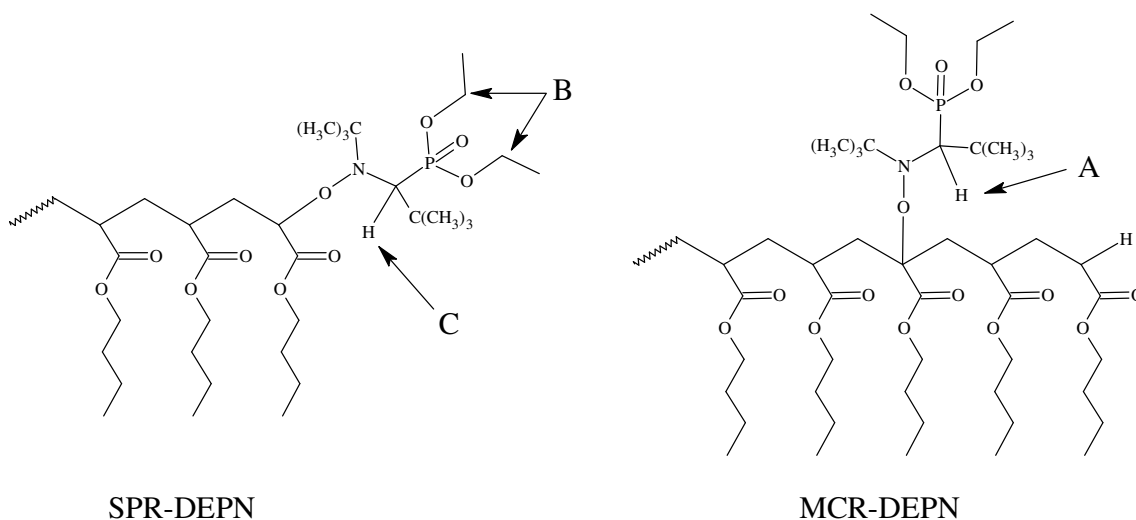
$$[Q] = \frac{k_{bb}[P]}{k'_p[M] + k_\beta} \quad (4-14)$$

Equation 4-14 has several important implications, one of which is that the fraction of the MCR in the system is mainly dependent on three processes which are intra-molecular chain transfer to polymer, addition of the monomer to the MCR and β -fragmentation.

4.2 Investigating the NMP equilibrium involving the MCR

To fully understand and describe a polymerization system, the knowledge of all primary and side reactions is important. Scheme 4-1 illustrated reactions during a high temperature *n*-butyl acrylate polymerization, in which an assumption has been made that an equilibrium exists between the MCR and MCR-DEPN. According to Equation 4-8 the presence of such an equilibrium will have an effect on the active concentration of MCRs. This will in turn have an effect on the quantity of accumulated β -fragmentation products (and rate thereof) and the branching density.

This section will address the existence or non-existence of such an equilibrium, by searching for the adduct (MCR-DEPN) of the MCR with the nitroxide DEPN, illustrated in Scheme 4-2. The existence of MCR-DEPN in the final polymer can serve as an indirect proof of the existence of equilibrium between the MCR and MCR-DEPN.



Scheme 4-2: The possible dormant structures of poly(*n*-butyl acrylate) illustrating the adducts of the SPR and the MCR with the nitroxide DEPN.

To assess whether the reversible deactivation of the MCR does occur, experiments were carried out in which the ratio of MAMA-DEPN to free nitroxide (DEPN) was varied in the polymerization of *n*-butyl acrylate.

4.2.1 Experimental

4.2.1.1 Chemicals

The alkoxyamine MAMA-DEPN and the nitroxide DEPN were synthesized as described in Chapter III (Section 3.3). *n*-Butyl acrylate (Plascon Research Centre, Stellenbosch University) was washed with 10% aqueous solution of sodium hydroxide and then with distilled deionised water before drying over anhydrous magnesium sulphate. The monomer was distilled under reduced pressure and stored at low temperature.

4.2.1.2 Procedure for the polymerization

In a typical polymerization, *n*-butyl acrylate (2.00 g, 15.6 mmol), MAMA-DEPN (40.5 mg, 0.106 mmol) and DEPN (7.9 mg, 0.0268 mmol) were added to a Schlenk flask. The mixture was degassed by three freeze-pump-thaw cycles followed by introduction of nitrogen atmosphere. The Schlenk flask was immersed in a preheated oil bath at 120 °C and the reaction was allowed to proceed for 7 hours.

4.2.2 Results and discussion

Figure 4-1 shows a ¹H NMR spectrum of poly(*n*-butyl acrylate) prepared from MAMA-DEPN with additional free DEPN added. An unconventionally large fraction of free DEPN relative to MAMA-DEPN was employed with the aim of increasing the chance of the reversible deactivation-activation reaction of the MCR with the nitroxide (DEPN). This would also lead to an improved detection of the products of such a reversible deactivation.

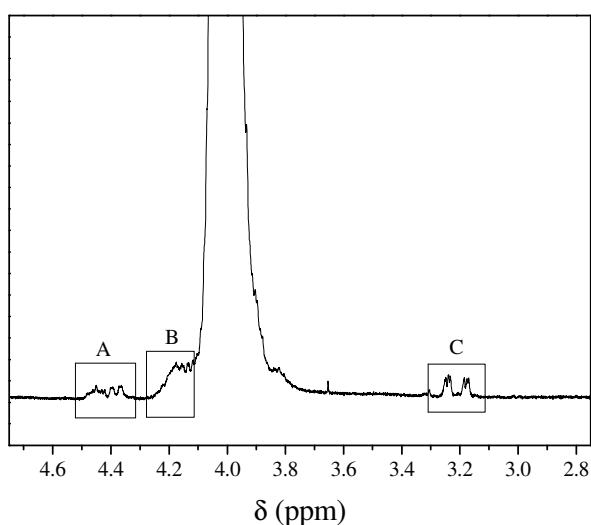


Figure 4-1: ¹H NMR spectrum of poly(*n*-butyl acrylate) in the region 4.7 – 2.8 ppm with the peaks labelled A, B and C assigned to signals of the protons labelled in Scheme 4-2.

The prime area of interest in Figure 4-1 is the area of peaks labelled A. This signal has been assigned to the α -proton of DEPN in a dormant structure in which the MCR is reversibly terminated by DEPN. The α -proton of DEPN in the case where the dormant structure is a result of a reversible termination between the SPR and DEPN appears in the region labelled C in

Figure 4-1. The assignment of the peaks in Figure 4-1 was aided by predicting the ^1H NMR spectra of the species of interest (Scheme 4-2). In the predicted ^1H NMR spectrum (not shown) of the SPR-DEPN adduct, the proton labelled C was observed in its expected region (3.2-3.4 ppm). The expected chemical shift for the peak due to the proton labelled A was then predicted.

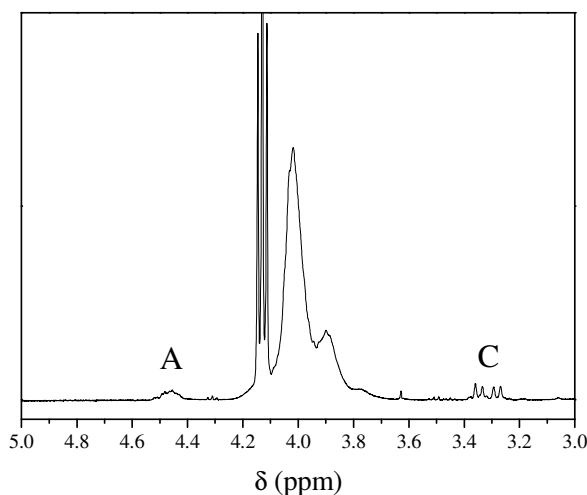


Figure 4-2: ^1H NMR spectrum of styrene/*n*-butyl acrylate copolymerization mixture in the region 5.0 – 3.0 ppm with the peaks labelled A and C assigned to signals of the protons labelled in Scheme 4-2. ($f_s = 0.1$).

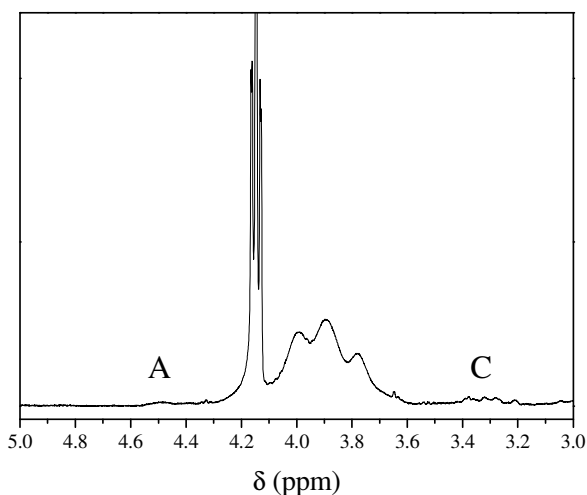


Figure 4-3: ^1H NMR spectrum of styrene/*n*-butyl acrylate copolymerization mixture in the region 5.0 – 3.0 ppm with the peaks labelled A and C assigned to signals of the protons labelled in Scheme 4-2. ($f_s = 0.4$).

The resolution of the doublet of multiplets is lost from region C to A. The loss in the resolution can be ascribed to the fact that chain transfer to polymer does not exclusively occur via the 1,5-hydrogen shift. Chain transfer to remote positions along the backbone of the chains together with intermolecular chain transfer results in MCRs that are chemically non-equivalent depending on their position on the backbone. The subtle differences in the chemical environments of such MCRs is thus observed in loss of resolution in the peaks labelled A in Figure 4-1. The existence of the reversible deactivation-activation reaction between DEPN and MCR in the nitroxide mediated *n*-butyl acrylate polymerization has several implications.

If indeed the signal (at ca. 4.4 ppm) in Figure 4-1 is due to the α -proton labelled A in Scheme 4-2, inhibition of intra-molecular chain transfer to polymer should result in the disappearance of the peak. The inhibition of intra-molecular chain transfer to polymer (mainly backbiting) in *n*-butyl acrylate polymerization can be done by simply copolymerizing with a second monomer, such as styrene. At feed compositions with a considerable amount of styrene, the intra-molecular chain transfer process should be cancelled out. When $f_s = 0.1$ (Figure 4-2), uninterrupted long sequences of *n*-butyl acrylate can form making it possible for backbiting to occur. The result is the formation of a MCR and consequently its adduct with DEPN. The presence of the signal labelled “A” in Figure 4-2 is indicative of the existence of such a macro-alkoxyamine. However, upon an increase of the feed composition of styrene in the copolymerization mixture, signal “A” disappears in Figure 4-3 ($f_s = 0.4$).

The implication of the existence of the equilibrium involving the MCR is that the equilibrium rate constant normally reported in the literature is in actual fact the effective equilibrium constant that is more accurately described by Equation 4-13 as opposed to Equation 4-12.

The second implication is that the effective concentration of MCRs is not only dependent on backbiting, addition of monomer to MCR and β -scission as predicted by Equation 4-14. A rather more accurate evolution of the MCRs should then be predicted by Equation 4-8. Under controlled/living radical polymerization conditions, Equation 4-8 should lead to similar evolution of the MCRs as its simplified form (Equation 4-9), due to negligible termination reactions.

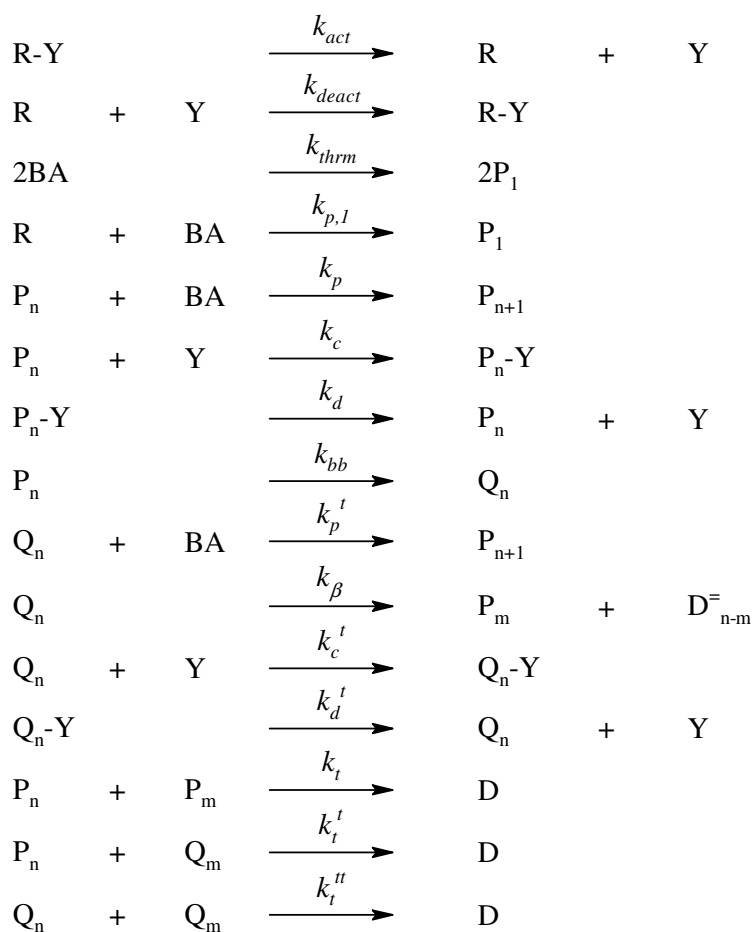
The evidence of a reversible deactivation-activation reaction between the MCR and a mediating species is for the first time explicitly reported in this work. As a result there are no literature values for the rate coefficients of deactivation and activation of MCR and MCR-DEPN, respectively. Estimated values for the rate coefficients of deactivation and activation of MCR and MCR-DEPN will be proposed in this chapter.

4.2.4 Conclusion

Evidence from ^1H NMR has shown the existence of an adduct of MCR with DEPN, a structure from which it can be inferred that there exists a reversible deactivation-activation reaction between the MCR and DEPN. As a result, to adequately describe the kinetic model for the

polymerization of *n*-butyl acrylate mediated by nitroxides, the reversible deactivation-activation reaction between the nitroxide and the MCR should be included. The awareness of the importance of the inclusion of the reversible reaction involving the MCR and nitroxide does not come without a cost, as it introduces uncertainties in the model due to the unknown values of the kinetic rate coefficients of the reactions in question (k_d^t and k_c^t).

4.3 Kinetic model for *n*-butyl acrylate polymerization mediated by persistent radical species



Scheme 4-3: Nitroxide mediated *n*-butyl acrylate polymerization model implemented into Predici.

In high temperature *n*-butyl acrylate polymerization in the presence of a persistent radical species, additional effects exist that contribute to the observed experimentally determined values

of rate coefficient of activation of the macro-alkoxyamine and equilibrium rate constant. The reported equilibrium rate constant for *n*-butyl acrylate polymerization at 120 °C in the presence of DEPN are $K = 1.7 \times 10^{-10}$ and $K = 6.95 \times 10^{-11}$.^{6,7} Due to the well established co-existence of SPR and MCR in *n*-butyl acrylate polymerization, care is required in the interpretation of the equilibrium rate constants in the existing reports. The equilibrium rate constant should in actual fact be resolved into two components. The first component is the reversible reaction between the SPR and persistent radical species and secondly the reversible reaction between the MCR and the persistent radical species.

Table 4-1: Rate coefficients used in the kinetic modelling of *n*-butyl acrylate using the Predici simulation package

	A	E _a (KJ mol ⁻¹)	Value at 120 °C	Refs
k_{act}	$2.4 \times 10^{14} \text{ s}^{-1}$	112.3	0.289 s^{-1}	8
k_{deact}			$5.0 \times 10^6 \text{ L mol}^{-1} \text{ s}^{-1}$	2
$k_{p,1}$	$4.0 \times 10^6 \text{ L mol}^{-1} \text{ s}^{-1}$	19.8	$9.36 \times 10^3 \text{ L mol}^{-1} \text{ s}^{-1}$	9
k_p	$2.31 \times 10^7 \text{ L mol}^{-1} \text{ s}^{-1}$	18.1	$9.10 \times 10^4 \text{ L mol}^{-1} \text{ s}^{-1}$	10
k_c			$2.80 \times 10^7 \text{ L mol}^{-1} \text{ s}^{-1}$	2,11
k_d			$1.55 \times 10^{-3} \text{ s}^{-1}$	2
k_t			$7.34 \times 10^7 \text{ L mol}^{-1} \text{ s}^{-1}$	2
k_{bb}	$3.50 \times 10^7 \text{ L mol}^{-1} \text{ s}^{-1}$	29.3	$4.48 \times 10^3 \text{ L mol}^{-1} \text{ s}^{-1}$	12
k_p^t	$1.52 \times 10^6 \text{ L mol}^{-1} \text{ s}^{-1}$	28.9	$2.20 \times 10^2 \text{ L mol}^{-1} \text{ s}^{-1}$	13
k_β	$8.60 \times 10^{10} \text{ L mol}^{-1} \text{ s}^{-1}$	71.5	$2.72 \times 10^1 \text{ s}^{-1}$	14
k_c^t			Unknown	
k_d^t			Unknown	
k_t^t			$3.90 \times 10^7 \text{ L mol}^{-1} \text{ s}^{-1}$	15
k_t^{tt}			$2.80 \times 10^6 \text{ L mol}^{-1} \text{ s}^{-1}$	15
k_{thrm}			$3.54 \times 10^{-7} \text{ L mol}^{-1} \text{ s}^{-1}$	Chapter III

Both these components are embedded in the current values of the equilibrium rate constant reported in the literature. A similar phenomenon should affect the determination of the

dissociation rate constant of a poly(*n*-butyl acrylate) macro-alkoxyamine. Relative to the SPR, the MCR is expected to have a lower rate coefficient of deactivation, because of the relatively higher stability. The rate coefficient of the activation of the MCR-DEPN dormant species will be expected to be higher than that of the SPR-DEPN dormant species.

4.3.1 Methodology

The simulations carried out in this work were performed with the Predici simulation package (version 6.72.3) on a standard desktop computer. The simulations were carried out in the distribution mode. The polymerization model and kinetic parameters used are summarized in Scheme 4-3 and Table 4-1, respectively.

4.3.2 Results and discussion

No reports in the literature exist on the investigation of the possibility of a reversible reaction between a mediating species and a MCR. As a result no rate coefficients for such a reaction exist in the current literature. Scheme 4-3 was implemented into Predici with the aim of reporting the first approximate values for the rate coefficients of deactivation (k'_c) of the MCR with DEPN and activation (k'_d) of the resulting macro-alkoxyamine (MCR-DEPN). To fully resolve the two equilibrium reactions into their respective equilibrium rate constants is a very complicated task. For instance, if a parameter variation study is undertaken for the four rate coefficients (k_c , k_d , k'_c and k'_d), there exists no possibility of a unique solution. The values determined for the equilibrium rate constant (K) and the dissociation rate coefficient (k_d) are in actual fact composite values including the equilibrium between MCR and MCR-DEPN and the dissociation of MCR-DEPN, respectively. It is assumed in this study that the values of k_c and k_d reported in the literature can be adapted to describe the equilibrium between the SPR and SPR-DEPN. For a comparison of simulation and experimental data, the evolution of the concentrations of *n*-butyl acrylate and the 1,1-alkene species with time were considered. Based on the relative stability of MCR in comparison to SPR, one can speculate that the rate coefficient of deactivation of MCR (k'_c) should be lower than that of the deactivation of SPR (k_c) by DEPN. Based on the same

analogy of stability, the rate coefficient of activation of MCR-DEPN would be expected to lie between activation rate coefficients of MAMA-DEPN and SPR-DEPN (i.e. $k_{act} > k_d^t > k_d$).



Scheme 4-4: General structures of an adduct of a SPR and a nitroxide (Structure A) and a MCR and a nitroxide (Structure B)

The rate coefficient of activation of DEPN based alkoxyamine can be shown to be dependent on the nature of the carbon centre attached to the nitroxide ($*C - ON$). When the nitroxide is attached to a secondary carbon, the corresponding alkoxyamine will show a lower rate coefficient of activation than an alkoxyamine formed from a tertiary carbon centre. For model alkoxyamines, the DEPN based alkoxyamine will show $k_d(120^\circ C) \geq 10^{-1} s^{-1}$ for adducts with tertiary carbons, with lower values for secondary and even lower for primary carbons.¹⁶ The rate coefficient of activation of MAMA-DEPN at 120 °C is $2.88 \times 10^{-1} s^{-1}$.⁸ Ananchenko et al.¹⁷ estimated k_d (100 °C) of poly(methyl methacrylate) based macro-alkoxyamine (PMMA-DEPN) as $8 \times 10^{-2} s^{-1}$. In general, the rate coefficient of activation (homolytic cleavage) is higher in the case where the C – ON bond of the alkoxyamine is formed between a nitroxide radical and a radical of a tertiary carbon atom of the alkyl group.¹⁷⁻²⁰ The rate coefficients of activation for the structures in Scheme 4-4 ('A' and 'B' representing SPR-DEPN and MCR-DEPN, respectively) will thus be expected to differ by an order of magnitude or two, due to the differences in the macro-alkoxyamine structures.

Figure 4-4 illustrates the evolution of the concentration of *n*-butyl acrylate with time. A good agreement between experimental and simulated data was obtained when k_c^t and k_d^t values were set to $1.0 \times 10^6 L mol^{-1} s^{-1}$ and $5.32 \times 10^{-2} s^{-1}$, respectively. A reasonable correlation was also obtained for the specified values of k_c^t and k_d^t in the evolution with time of concentration of species bearing the 1,1-disubstituted alkene end group (Figure 4-5). The values of k_c^t and k_d^t

reported are mere initial guess values. It should be noted that the values of k_c and k_d , do not exclusively describe the deactivation and activation of SPR and SPR-DEPN, respectively, but do in fact include the effects of the equilibrium involving the MCR.

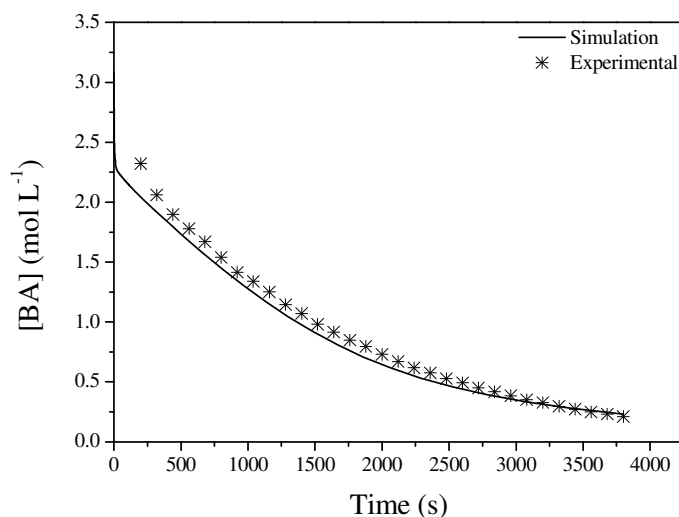


Figure 4-4: The experimental evolution of *n*-butyl acrylate concentration with time compared with simulation data according to Scheme 4-3 for which $k_c^t = 1.0 \times 10^6 \text{ L mol}^{-1} \text{ s}^{-1}$ and $k_d^t = 5.32 \times 10^{-2} \text{ s}^{-1}$ and all other parameters are as listed in Table 4-1.

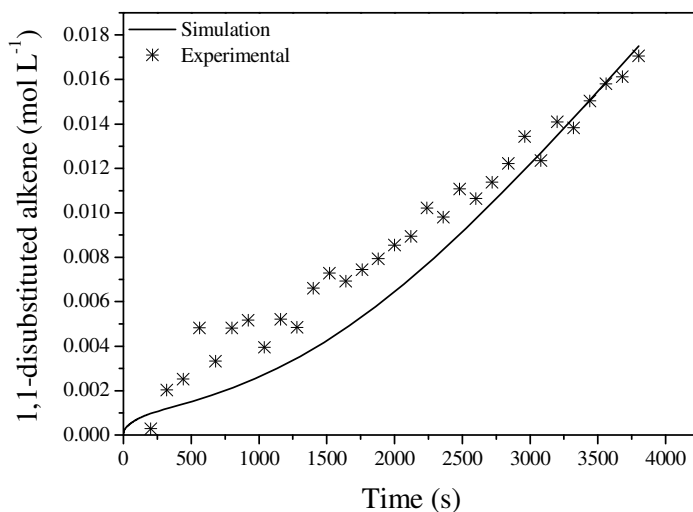


Figure 4-5: The experimental evolution of the concentration of 1,1-disubstituted alkene species with time compared with simulation data according to Scheme 4-3 for which $k_c^t = 1.0 \times 10^6 \text{ L mol}^{-1} \text{ s}^{-1}$ and $k_d^t = 5.32 \times 10^{-2} \text{ s}^{-1}$ and all other parameters are as listed in Table 4-1.

The effect of the initial concentration of the alkoxyamine on the rate of polymerization and the evolution of concentration of the 1,1-disubstituted alkene species was investigated for the polymerization model. The kinetic parameters in Table 4-1 together with the estimated values of k_c^t and k_d^t were implemented in the polymerization model (Scheme 4-3). Figure 4-6 illustrates the simulated and experimental conversion index plots of *n*-butyl acrylate polymerization with different initial concentrations of the alkoxyamine (MAMA-DEPN). The rate of polymerization shows no dependence on the initial concentration of the alkoxyamine, in agreement with the experimental results reported in Chapter III. A good correlation between experimental and simulated data is observed for the range of initial concentrations of the alkoxyamine studied.

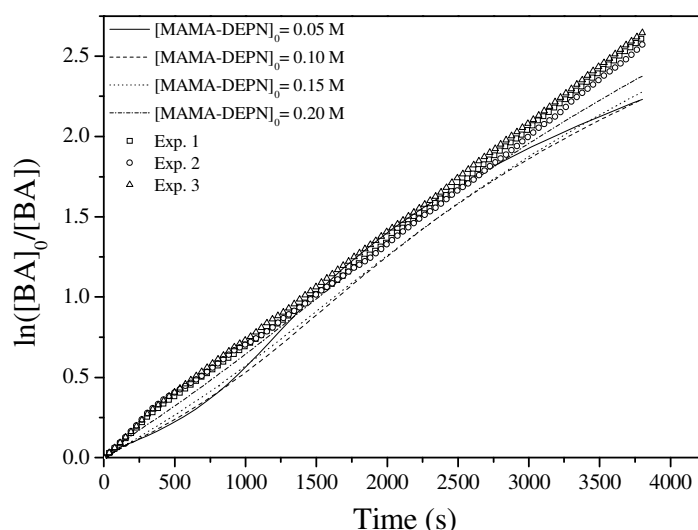


Figure 4-6: Simulated conversion index plots of *n*-butyl acrylate polymerization at different indicated initial concentrations of the alkoxyamine (MAMA-DEPN) vs. experimental data for which $[MAMA-DEPN]_0$ for Experiments 1 (Exp. 1), 2 (Exp. 2) and 3 (Exp. 3) are 0.2, 0.15 and 0.10 mol L⁻¹, respectively.

The simulated evolution of the concentration of the 1,1-disubstituted alkene species as a function of initial alkoxyamine (MAMA-DEPN) concentration, is illustrated in Figure 4-7. A relatively good correlation between experimental and simulated data was obtained for the evolution of the alkene species. As observed in the experimental results (Chapter III), no apparent dependence of evolution of the concentration of the alkene species on the initial concentration of the alkoxyamine was observed. Likewise, the simulated profiles showed no dependence on initial

concentration of the alkoxyamine. Figure 4-8 illustrates the agreement between model and experimental data for the evolution of the concentration of *n*-butyl acrylate as a function of time.

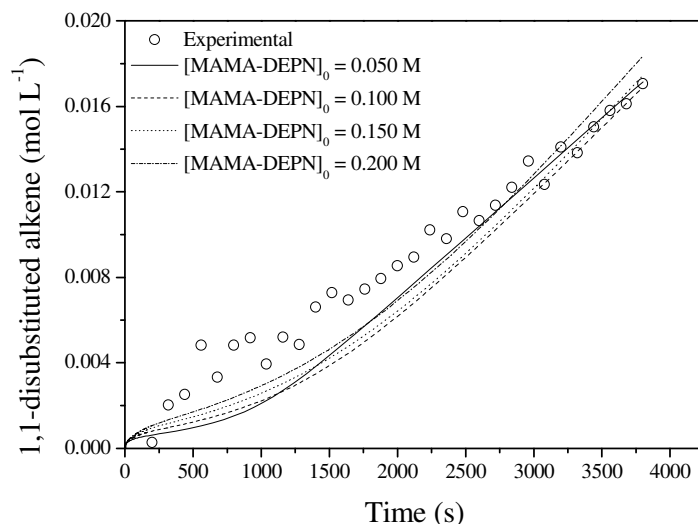


Figure 4-7: The evolution of the concentration of species bearing 1,1-disubstituted alkene end group as a function of the initial concentration of MAMA-DEPN for *n*-butyl acrylate polymerization conducted at 120 °C with all profiles simulated except for the labelled experimental data points (○), for which $[MAMA-DEPN]_0 = 0.16 \text{ mol L}^{-1}$.

As predicted by Equation 3-14, the evolution of the concentration of the alkene species will depend on the product of the MCR and rate coefficient of β -fragmentation (k_β). With the β -fragmentation rate coefficient a constant at the specific polymerization temperature, the only variable the evolution of the alkene species depends on is the MCR concentration. However, the fraction of MCR in *n*-butyl acrylate polymerization has previously been shown to be constant at a particular polymerization temperature.⁵ As a result, at a specific polymerization temperature both the concentration of the MCRs and the rate coefficient of β -fragmentation are constants and a similar accumulation of the alkene species will be observed irrespective of the initial concentration of the alkoxyamine.

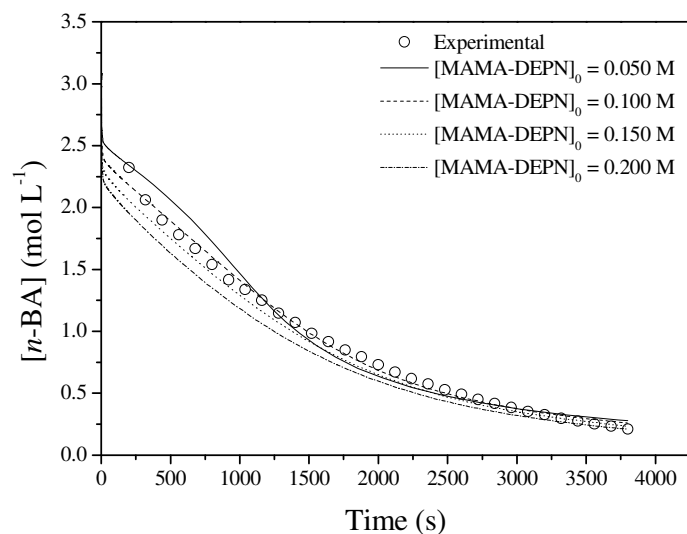


Figure 4-8: The evolution of the concentration of *n*-butyl acrylate as a function the initial concentration of MAMA-DEPN for the polymerization conducted at 120 °C with all data simulated except for the labelled experimental data points (\circ), for which $[\text{MAMA-DEPN}]_0 = 0.16 \text{ mol L}^{-1}$.

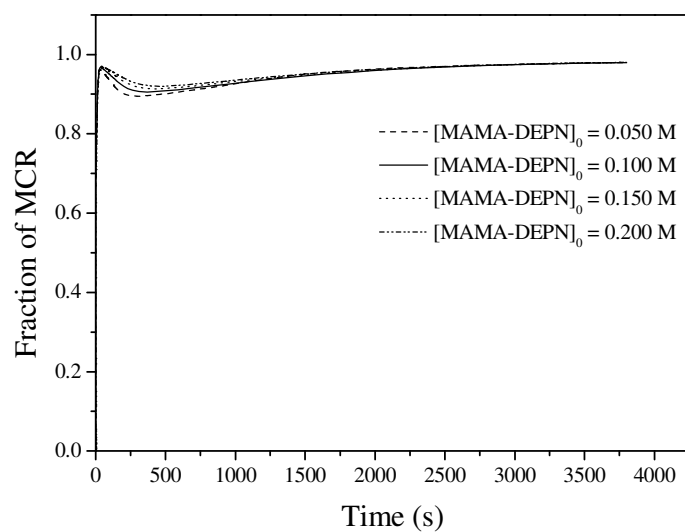


Figure 4-9: Simulated fraction of MCR in *n*-butyl acrylate polymerization at 120 °C, as function of the initial concentration of the alkoxyamine.

In Figure 4-9, the fraction of MCRs relative to the total concentration of active transient radicals remains constant for the entire polymerization. A high fraction of MCR is observed (exceeding 90%) according to the simulated data. However this figure comes as no surprise as a fraction of about 80% have been reported in ESR studies of *n*-butyl acrylate polymerization at 70 °C.⁵ Barth

et al.⁴ also reported that the fraction of MCRs relative to the total transient radical concentration is about 90% at temperatures exceeding 60 °C. To assess the effect of the equilibrium involving the MCR and MCR-DEPN on reaction kinetics, simulations of *n*-butyl acrylate polymerization were carried out with and without the reversible deactivation of the MCR with DEPN. The simulations were carried out as a function of the initial concentration of the alkoxyamine. The results of the simulations are summarized in Figure 4-10. For both models with and without the equilibrium step, no apparent dependence of rate of polymerization on the initial concentration of the alkoxyamine was observed. The lower rate of polymerization in the model without the reversible deactivation of the MCR with DEPN can be explained in terms of loss of radicals as a result of transient radical termination reactions due to their high concentration in the medium.

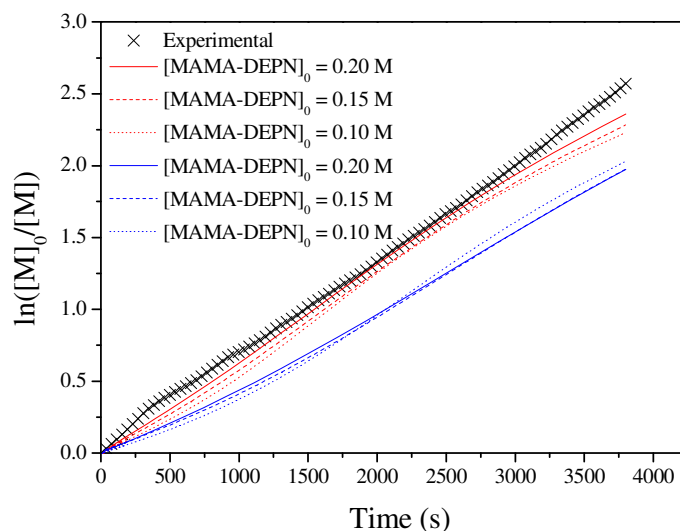


Figure 4-10: Comparison of simulated conversion index plots of *n*-butyl acrylate polymerization model including (red lines) and excluding (blue lines) the equilibrium involving the MCR as a function of initial concentration of the alkoxyamine. Experimental conversion index plot is included for which the employed $[MAMA-DEPN]_0 = 0.15 \text{ mol L}^{-1}$.

The inclusion or exclusion of the reversible deactivation of the MCR with DEPN in the *n*-butyl acrylate polymerization model only has an effect on the rate of polymerization while preserving the observed phenomenon of rate independence with changing initiator concentration.

The effect of thermal auto-initiation of *n*-butyl acrylate on the polymerization kinetics was also investigated. The data presented to this point in this chapter has included the thermal

auto-initiation of *n*-butyl acrylate in the polymerization model. With all reactions in Scheme 4-3 considered except for the thermal auto-initiation, the simulations were carried out with different initial concentrations of the alkoxyamine. The results for the evolution of the concentration of the species bearing the 1,1-disubstituted alkene end group and the conversion index are illustrated in Figures 4-11 and 4-12, respectively.

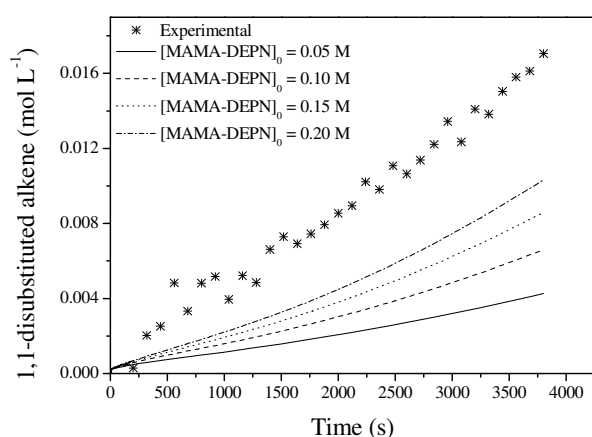


Figure 4-11: Simulated evolution of 1,1-disubstituted alkene bearing species without thermal auto-initiation as a function of the initial concentration of the alkoxyamine. Experimental data for the evolution of the species is included for which the employed $[MAMA-DEPN]_0 = 0.15 \text{ mol L}^{-1}$.

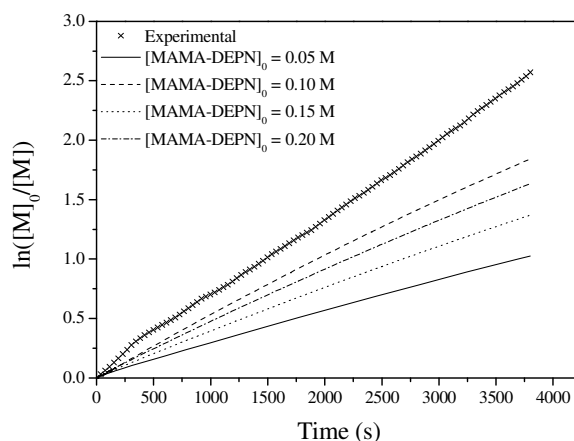


Figure 4-12: Simulated conversion index plots of *n*-butyl acrylate without thermal auto-initiation as a function of the initial concentration of the alkoxyamine. Experimental data for the evolution of the species is included for which the employed $[MAMA-DEPN]_0 = 0.15 \text{ mol L}^{-1}$.

A clear dependence of both the conversion index and the concentration of the species bearing the 1,1-disubstituted alkene end group on the initial concentration of the alkoxyamine is apparent in the absence of thermal auto-initiation of *n*-butyl acrylate. According to the conversion index plots, the observed increase in rate of polymerization with increasing concentration of the MAMA-DEPN is in line with results that would be expected for an ideal case. However, introduction of thermal auto-initiation in the polymerization model yields the profiles reported in Figure 4-6. Thus by comparison of Figures 4-6 and 4-12, the observed phenomenon of lack of dependence of the rate of polymerization on initial concentration of the alkoxyamine can be explained in terms of thermal auto-initiation in *n*-butyl acrylate polymerization. Like in the case

of styrene polymerization, thermal auto-initiation plays a vital role in the kinetics of *n*-butyl acrylate polymerization at high polymerization temperatures.

Another matter of interest is the presence of free DEPN at the onset of polymerization and its effect on the kinetics. Alkoxyamines such as MAMA-DEPN with high activation rate coefficients are prone to spontaneous decomposition at ambient temperatures. The result of the decomposition is the presence of free DEPN at the onset of the reaction. As a result, the system is no longer a unimolecular NMP system. The effect of such free DEPN on the reaction kinetics is illustrated in Figures 4-13 – 4-15 (simulations).

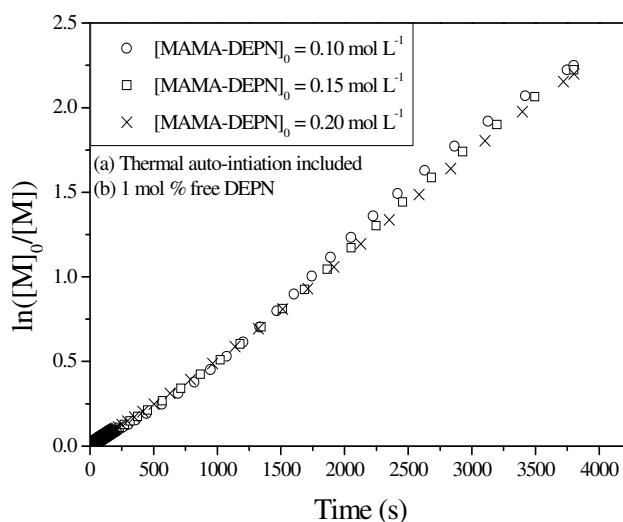


Figure 4-13: Simulated conversion index plots for *n*-butyl acrylate polymerization in the presence of 1 mol % free DEPN relative to MAMA-DEPN added with the thermal auto-initiation step taken into account, for different initial concentration of MAMA-DEPN.

Based on the experimentally achieved overall concentration of the 1,1-alkene species and the monomer conversion, it can be argued in conjunction with simulation results that no more than 1 mol % free DEPN relative to MAMA-DEPN is present at onset of polymerization in the system. This can be explained by the fact that for simulations with greater than 1 mol % initial free DEPN, the achieved final monomer conversion and concentration of the 1,1-alkene species, are below those experimentally obtained. Comparing simulations and experiments, the retardation of the polymerization process can be used to estimate the threshold concentration of initial free DEPN.

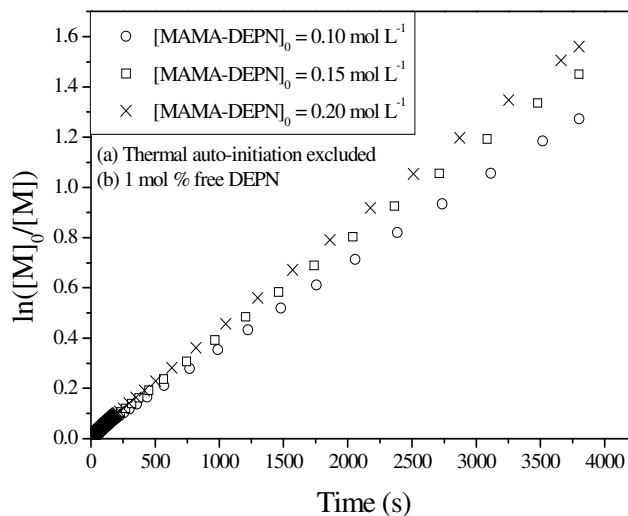


Figure 4-14: Simulated conversion index plots for *n*-butyl acrylate polymerization in the presence of 1 mol % free DEPN relative to MAMA-DEPN added with the thermal auto-initiation step excluded, for different initial concentration of MAMA-DEPN.

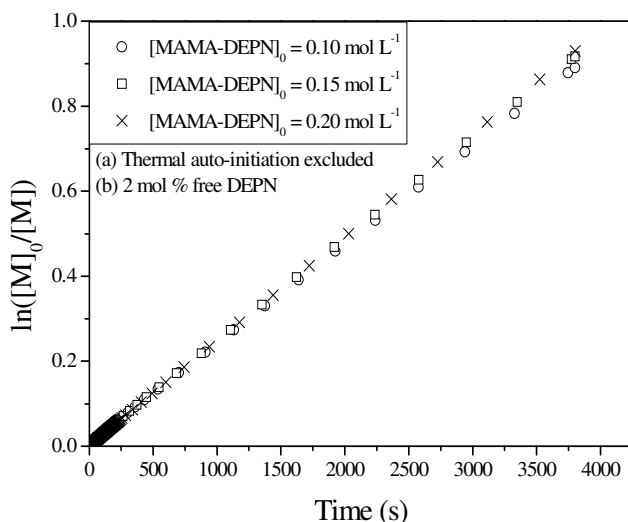


Figure 4-15: Simulated conversion index plots for *n*-butyl acrylate polymerization in the presence of 2 mol % free DEPN relative to MAMA-DEPN added with the thermal auto-initiation step excluded, for different initial concentration of MAMA-DEPN.

In addition, without the thermal auto-initiation step the experimentally obtained final conversion could not be obtained theoretically, highlighting the importance of such a reaction step. Therefore, for such concentrations of free DEPN (< 1 mol %), the independence of rate of polymerization can still be ascribed to the thermal auto-initiation of *n*-butyl acrylate

(Figure 4-13). When the thermal auto-initiation step in the kinetic model is deactivated, with 1 mol % free DEPN present at polymerization onset, the rate of polymerization is observed to increase with increasing concentration of the alkoxyamine (Figure 4-14). From Figure 4-15 it becomes apparent that the effects of free nitroxide on rate of polymerization become significant from about 2 mol % free DEPN relative to MAMA-DEPN. At concentrations lower than 2 mol %, the independence of rate of polymerization should then be ascribed to thermal auto-initiation.

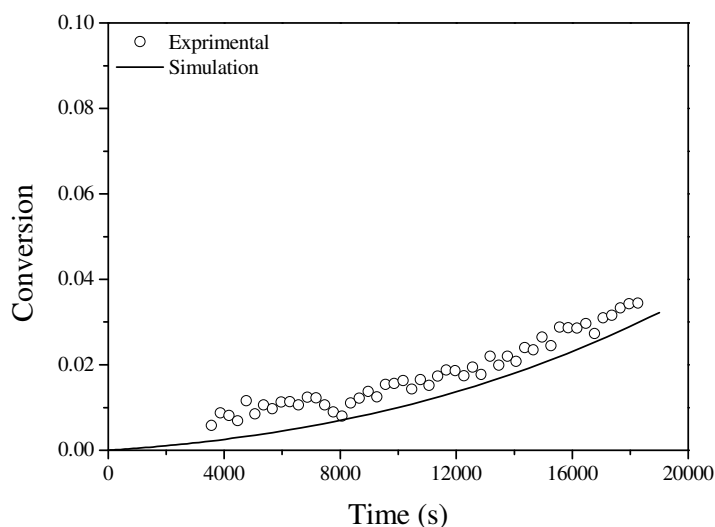


Figure 4-16: Simulated and experimental evolution of monomer conversion in thermally initiated *n*-butyl acrylate polymerization in the presence of free DEPN. $[n\text{-butyl acrylate}]_0 = 3.09 \text{ mol L}^{-1}$ and $[\text{DEPN}]_0 = 0.053 \text{ mol L}^{-1}$.

The validity of the constructed polymerization model was further assessed by comparison of experimental data and simulated data for thermally initiated *n*-butyl acrylate polymerization at 120 °C in the presence of free DEPN.

From Figure 4-16, a reasonable agreement between the model and the experimental data is observed. Thus, the rate coefficients of deactivation (k'_c) and activation (k'_d) of MCR and MCR-DEPN, respectively estimated in this work are further supported as good estimates.

4.3.3 Conclusion

Through simulations of the *n*-butyl acrylate polymerization model shown in Scheme 4-3 via the Predici software package, the values of the rate coefficients of deactivation (k_c^t) and activation (k_d^t) of the equilibrium involving the MCR and DEPN have been estimated by comparison with experimental data. It has also been demonstrated that the exclusion of the equilibrium between MCR and MCR-DEPN will result in a lower rate of polymerization in comparison with the model in which the equilibrium is included. The inclusion or exclusion of such equilibrium also showed no dependence of rate of polymerization on the initial concentration of the alkoxyamine. The inclusion or exclusion of thermal auto-initiation of *n*-butyl acrylate in the polymerization model yielded interesting results. When thermal auto-initiation reaction was omitted from the polymerization model, the rate of polymerization was observed to increase with increasing concentration of the alkoxyamine. When the thermal auto-initiation reaction was included in the model, the rate of polymerization showed no dependence on the initial concentration of the alkoxyamine, in line with the data reported in Chapter III. Thus, as in case of styrene polymerization the apparent independence of rate of polymerization in the case of *n*-butyl acrylate polymerization can also be explained in terms of thermal auto-initiation of the monomer. Good agreement between experimental and theoretical data was obtained for the evolution of monomer conversion with time for thermally initiated *n*-butyl acrylate polymerization in the presence of free DEPN.

4.4 Summary

The existence of a reversible deactivation of the MCR by DEPN has been deduced from the ^1H NMR spectrum of poly(*n*-butyl acrylate) prepared with MAMA-DEPN. Preliminary estimated values of the deactivation rate coefficient (k_c^t) of the MCR with DEPN, and activation rate coefficient (k_d^t) of the resulting macro-alkoxyamine are also reported. A full parameter estimation of the four rate coefficients of interest (k_c , k_d , k_c^t and k_d^t) should however be carried out with fitting to three or more reaction species to further increase the accuracy of the estimated values. The apparent independence of the rate of polymerization on the initial

concentration of the alkoxyamine reported in Chapter III can be explained in terms of thermal auto-initiation of *n*-butyl acrylate as deduced from simulated data.

References

1. Phan, T. N. T.; Maiez-Tribut, S.; Pascault, J.-P.; Bonnet, A.; Gerard, P.; Guerret, O.; Bertin, D. *Macromolecules* **2007**, *40*, 4516-4523.
2. Chauvin, F.; Dufils, P.-E.; Gignes, D.; Guillaneuf, Y.; Marque, S. R. A.; Tordo, P.; Bertin, D. *Macromolecules* **2006**, *39*, 5238-5250.
3. Farcet, C.; Belleney, J.; Charleux, B.; Pirri, R. *Macromolecules* **2002**, *35*, 4912-4918.
4. Barth, J.; Buback, M.; Hesse, P.; Sergeeva, T. *Macromol. Rapid Commun.* **2009**, *30*, 1969-1974.
5. Willemse, R. X. E.; Herk, A. M. v.; Panchenko, E.; Junkers, T.; Buback, M. *Macromolecules* **2005**, *38*, 5098-5103.
6. Benoit, D.; Grimaldi, S.; Robin, S.; Finet, J.-P.; Tordo, P.; Gnanou, Y. *J. Am. Chem. Soc.* **2000**, *122*, 5929-5939.
7. Lacroix-Desmazes, P.; Lutz, J.-F.; Florence Chauvin; Severac, R.; Boutevin, B. *Macromolecules* **2001**, *34*, 8866-8871.
8. Bertin, D.; Gignes, D.; Marque, S. R. A.; Tordo, P. *Macromolecules* **2005**, *38*, 2638-2650.
9. Zytowski, T.; Knühl, B.; Fischer, H. *Helv. Chim. Acta* **2000**, *83*, 658-675.
10. Barner-Kowollik, C.; Günzler, F.; Junkers, T. *Macromolecules* **2008**, *41*, 8971-8973.
11. Chauvin, F.; Alb, A. M.; Bertin, D.; Tordo, P.; Reed, W. F. *Macromol. Chem. Phys.* **2002**, *203*, (14), 2029-2041.
12. Rantow, F. S.; Soroush, M.; Grady, M. C.; Kalfas, G. A. *Polymer* **2006**, *47*, 1423-1435.
13. Nikitin, A. N.; Hutchinson, R. A.; Buback, M.; Hesse, P. *Macromolecules* **2007**, *40*, 8631-8641.
14. Junkers, T.; Barner-kowollik, C. *J. Polym. Sci., Part A: Polym. Chem.* **2008**, *46*, 7585-7605.
15. Nikitin, A. N.; Hutchinson, R. A. *Macromol. Theory Simul.* **2006**, *15*, 128-136.
16. Marque, S.; Mercier, C. L.; Tordo, P.; Fischer, H. *Macromolecules* **2000**, *33*, 4403-4410.
17. Ananchenko, G. S.; Souaille, M.; Fischer, H.; Mercier, C. L.; Tordo, P. *J. Polym. Sci., Part A: Polym. Chem.* **2002**, *40*, 3264-3283.

18. Guillaneuf, Y.; Gimes, D.; Marque, S. R. A.; Tordo, P.; Bertin, D. *Macromol. Chem. Phys.* **2006**, 207, 1278-1288.
19. Nicolas, J.; Dire, C.; Mueller, L.; Belleney, J.; Charleux, B.; Marque, S. R. A.; Bertin, D.; Magnet, S.; Couvreur, L. *Macromolecules* **2006**, 39, 8274-8282.
20. Nicolas, J.; Mueller, L.; Dire, C.; Matyjaszewski, K.; Charleux, B. *Macromolecules* **2009**, 42, 4470-4478.

Chapter V: Nitroxide mediated copolymerization of styrene and *n*-butyl acrylate

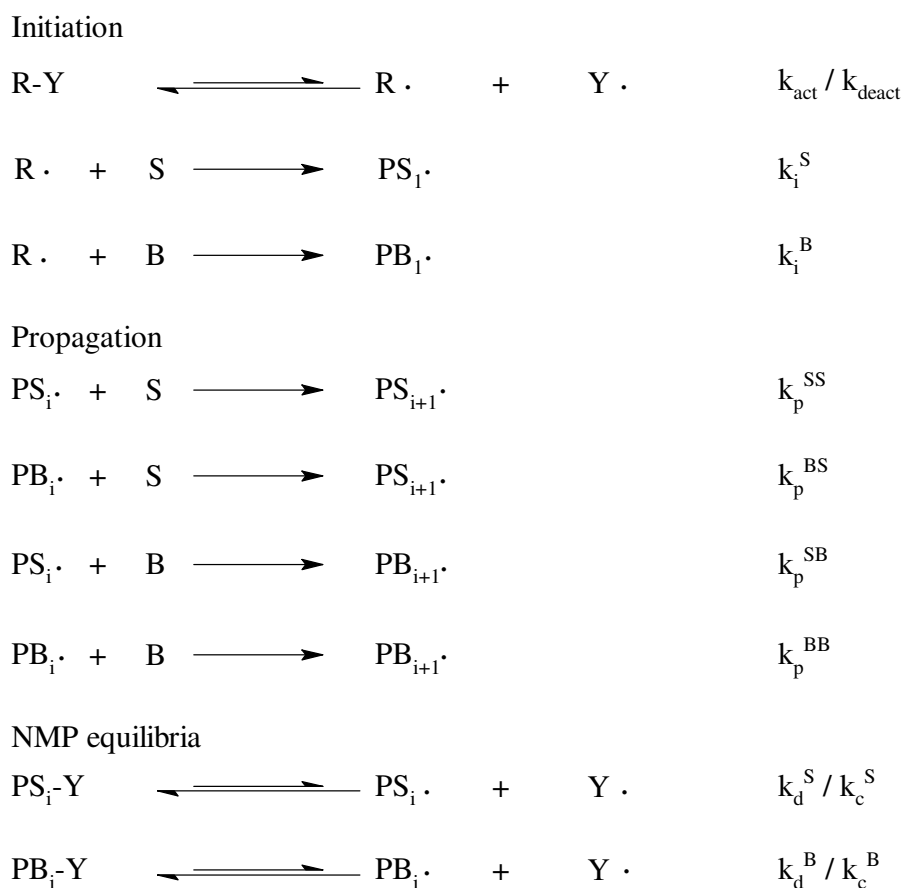
Synopsis

*This chapter deals with the copolymerization of styrene and *n*-butyl acrylate mediated by DEPN. High conversion data is used to determine the reactivity ratios of the styrene and *n*-butyl acrylate system. Simulations of the copolymerization system based on the implicit penultimate unit model were carried out using the Predici software package. Good agreement between simulated results and data extracted from both in situ ^1H and ^{31}P NMR experiments was observed. It has also been demonstrated that the NMP equilibrium constant obtained from *n*-butyl acrylate homopolymerization studies cannot be utilized for the description of a similar equilibrium in the copolymerization system.*

5.1 Introduction

5.1.1 Copolymerization models

Several models exist for describing free radical copolymerization processes.¹⁻⁶ In this chapter the terminal unit model (TUM) and the penultimate unit model (PUM) will be considered to describe the copolymerization of styrene (S) and *n*-butyl acrylate (B). The TUM is based on the assumption that the terminal unit of the active polymer chain is the only unit affecting the addition of the subsequent monomer. Scheme 5-1 illustrates the schematic representation of the TUM showing initiation, propagation and the NMP equilibria.



Scheme 5-1: Terminal unit model (TUM) reaction scheme for the copolymerization of styrene and *n*-butyl acrylate showing initiation, propagation and NMP equilibria reactions.

Copolymer composition and microstructure can be described well with TUM, but fails to adequately describe the overall propagation rate of the copolymerization. The TUM is defined by four characteristic coefficients which are two respective homopropagation rate coefficients (Equations (3-1) and (3-2)) and two reactivity ratios (Equation (5-1)).

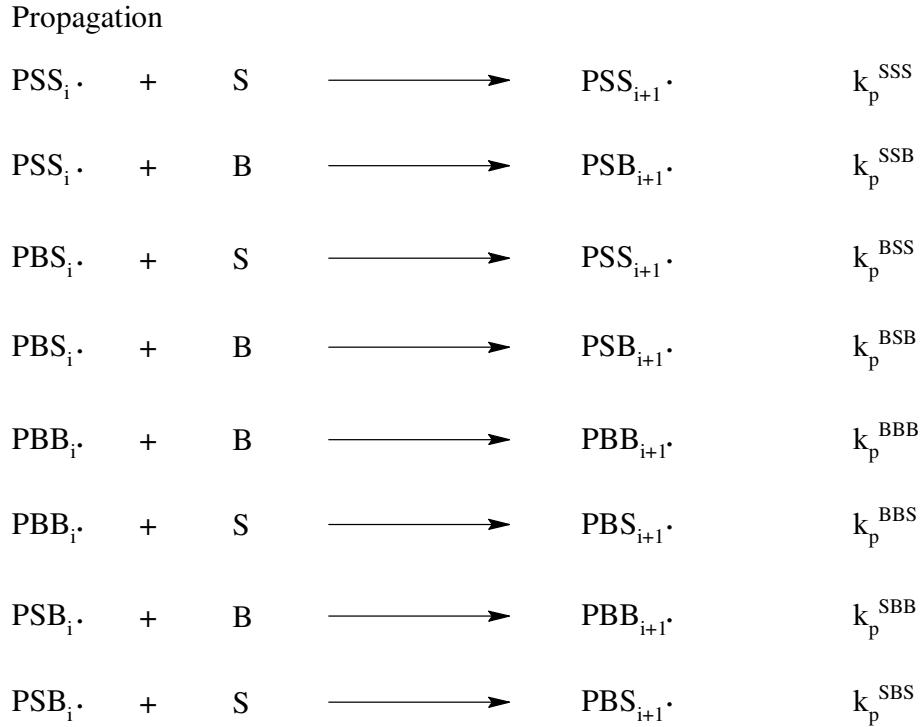
$$r_s = \frac{k_p^{SS}}{k_p^{SB}} \qquad r_B = \frac{k_p^{BB}}{k_p^{BS}} \qquad (5-1)$$

where k_p^{ii} retain their meaning and k_p^{ij} represents the respective cross-propagation rate coefficients where i and j are S or B and $i \neq j$. The average propagation rate coefficient for styrene and *n*-butyl acrylate copolymerization as defined by the TUM is expressed by Equation 5-2.

$$\langle k_p \rangle = \frac{r_s f_s^2 + 2f_s f_B + r_B f_B^2}{[r_s f_s / k_{SS}] + [r_B f_B / k_{BB}]} \qquad (5-2)$$

where f_s and f_B represent the mole fraction in the feed of styrene and *n*-butyl acrylate, respectively. Due to the inadequacy of the TUM in describing the overall propagation rate coefficient of copolymerizations, other copolymerization models were proposed.⁶ In this chapter the PUM will be considered due to its relative simplicity in addressing the description of the overall propagation rate coefficient. In PUM, it is assumed that both the penultimate and the ultimate units have an effect on the addition of the monomer to the active polymer chain.

Scheme 5-2 illustrates the propagation steps in the PUM of styrene and *n*-butyl acrylate. The expressions for the rate coefficients characteristic of PUM can then be expressed by Equations (5-3) to (5-5).



Scheme 5-2: Penultimate unit model (PUM) propagation scheme for the copolymerization of styrene and *n*-butyl acrylate.

$$r_{SS} = \frac{k_p^{SSS}}{k_p^{SSB}} \qquad r_{BB} = \frac{k_p^{BBB}}{k_p^{BBS}} \qquad (5-3)$$

$$r_{BS} = \frac{k_p^{BSS}}{k_p^{BSB}} \qquad r_{SB} = \frac{k_p^{SBB}}{k_p^{SBS}} \qquad (5-4)$$

$$s_S = \frac{k_p^{BSS}}{k_p^{SSS}} \qquad s_B = \frac{k_p^{SBB}}{k_p^{BBB}} \qquad (5-5)$$

where r_{SS} , r_{SB} , r_{BS} and r_{BB} are the four monomer reactivity ratios and s_S and s_B are the radical reactivity ratios. The expression for the overall propagation rate coefficient according to the PUM together with the supporting expressions is illustrated by Equations (5-6) to (5-8).

$$\langle k_p \rangle = \frac{\bar{r}_S f_S^2 + 2f_S f_B + \bar{r}_B f_B^2}{\left[\bar{r}_S f_S / \bar{k}_{SS} \right] + \left[\bar{r}_B f_B / \bar{k}_{BB} \right]} \quad (5-6)$$

$$\bar{k}_{SS} = k_{SSS} \left(\frac{r_{SS} f_S + f_B}{r_{SS} f_S + f_B / s_S} \right) \quad \bar{k}_{BB} = k_{BBB} \left(\frac{r_{BB} f_B + f_S}{r_{BB} f_B + f_S / s_B} \right) \quad (5-7)$$

$$\bar{r}_S = r_{BS} \left(\frac{r_{SS} f_S + f_B}{r_{BS} f_S + f_B} \right) \quad \bar{r}_B = r_{SB} \left(\frac{r_{BB} f_B + f_S}{r_{SB} f_B + f_S} \right) \quad (5-8)$$

$$r_{ii} = r_{ji} = r_i \quad (5-9)$$

where i and j can either be styrene or n -butyl acrylate and $i \neq j$. If Equation (5-9) is assumed to hold, the PUM as described can be reduced to the form known as the implicit penultimate unit model (IPUM). This assumption leads to a similar description of the copolymer composition according to both the TUM and the IPUM. However, the description of the average propagation rate coefficient includes the radical reactivity ratios in addition to monomer reactivity ratios in the case of IPUM.

5.1.2 Reactivity ratios in the copolymerization of styrene and n -butyl acrylate

The styrene/ n -butyl acrylate copolymerization system has been well studied over the past two decades and several sets of reactivity ratio values have been reported. Davis et al.³ studied the styrene/methyl acrylate and styrene/ n -butyl acrylate copolymerization systems. The reported reactivity ratio values for the latter system were $r_s = 0.95$ and $r_b = 0.18$. Cuervo-Rodriguez et al.⁷ studied the bimolecular nitroxide mediated copolymerization of styrene and n -butyl acrylate and reported r_s and r_b values of 0.74 and 0.29, respectively. The ATRP copolymerization study of styrene and n -butyl acrylate by Chambard reported values of r_s and r_b as 0.89 and 0.17, respectively.⁸

5.1.2.1 Determination of the reactivity ratios

Estimation of reliable reactivity ratios is of particular importance in that they enable the prediction of copolymer composition and microstructure for any given feed composition. The knowledge of these values also enables the classification of different monomers according to their reactivity towards active polymer chains. Several methods have been used for the determination of reactivity ratios and these include the Mayo-Lewis method,⁹ the Tidwell-Mortimer method¹⁰ and the Mao-Huglin method.¹¹ These methods are applicable for the determination of reactivity ratios at low monomer conversion. For the determination of reactivity ratios at higher monomer conversion, applicable methods are the extended Kelen-Tudos method¹² and the Mao-Huglin method.¹¹ Under the terminal unit model, the expression for the instantaneous copolymer composition is given by Equation (5-10).

$$F_S = \frac{r_S f_S^2 + f_S f_B}{r_S f_S^2 + 2f_S f_B + r_B f_B^2} \quad (5-10)$$

where F_i and f_i represent the mole fraction of monomer i in the copolymer and in the feed compositions, respectively. Aguilar et al.¹³ reported the determination of reactivity ratios with the aid of *in situ* ^1H NMR. The consumption of the monomers was monitored by ^1H NMR and the resultant data fitted to the integrated form of the copolymerization equation for the terminal unit model (Equation (5-11)).

$$\frac{[S]}{[S]_0} = \left(\frac{[S]_0 [B]}{[B]_0 [S]} \right)^{r_S / (1-r_S)} \left(\frac{(r_B - 1)([B]/[S]) - r_S + 1}{(r_B - 1)([B]_0/[S]_0) - r_S + 1} \right)^{(r_B r_S - 1) / [(1-r_B)(1-r_S)]} \quad (5-11)$$

Where $[M]_0$ represents the initial concentration of the monomer and $[M]$ represents the concentration of the monomer at time t . Equation (5-11) can be simplified and rewritten in the form illustrated by Equation (5-12).

$$\gamma = \gamma_0 (\delta / \delta_0)^{b/(1-b)} \left(\frac{1-b+(a-1)\delta}{1-b+(a-1)\delta_0} \right)^{(ab-1)/[(1-a)(1-b)]} \quad (5-12)$$

where $[B]/[S] = \delta$, $[B]_0/[S]_0 = \delta_0$, $[S] = \gamma$, $[S]_0 = \gamma_0$, $r_B = a$ and $r_S = b$.

5.1.2.2 Effect of the NMP equilibrium on the observed reactivity ratios

In conventional free radical copolymerization of styrene and *n*-butyl acrylate, Equation (5-13) will govern the ratio of $[PS\cdot]$ to $[PB\cdot]$ radicals under the steady state assumption. Thus according to Equation (5-13) the cross-propagation rate constants and the reactivity ratios will influence the ratio of the two propagating transient radicals. In the case of nitroxide mediated copolymerization the concentration of the respective propagating transient radicals will in addition be dependent on the two NMP equilibria. Thus Equation (5-13) can be rewritten for a nitroxide mediated copolymerization system to the forms expressed by Equations (5-14) and (5-15). The inclusion of the NMP equilibria can alter the ratio of the propagating transient radicals, which is the premise for the determination of reactivity ratios.

$$k_p^{SB} [PS\cdot][B] = k_p^{BS} [PB\cdot][S] \quad (5-13)$$

$$k_p^{BS} [PB\cdot][S] - k_p^{SB} [PS\cdot][B] + k_d^S [PS-Y] - k_c^S [PS\cdot][Y] = 0 \quad (5-14)$$

$$k_p^{SB} [PS\cdot][B] - k_p^{BS} [PB\cdot][S] + k_d^B [PB-Y] - k_c^B [PB\cdot][Y] = 0 \quad (5-15)$$

By simulations of ATRP and conventional radical copolymerization of styrene and *n*-butyl acrylate, it has been demonstrated that the ratio of the respective transient radicals in a controlled system will differ greatly from those in a conventional system at the early stages of the copolymerization (approximately up to 10% overall monomer conversion).⁸ At early stages of the copolymerization (CRP) before the equilibrium is attained, $k_d^S [PS-Y] \neq k_c^S [PS\cdot][Y]$ and $k_d^B [PB-Y] \neq k_c^B [PB\cdot][Y]$, and only after equilibrium will Equations 5-14 and 5-15 reduce to 5-13. In conventional systems, the steady state is attained almost instantaneously from the onset

of the copolymerization, which is not the case with controlled/living radical polymerization systems. As a result, use of high conversion data in the determination of reactivity ratios is important for the case of controlled/living radical copolymerizations.

5.2 Experimental

5.2.1 Chemicals

The alkoxyamine MAMA-DEPN was synthesized as described in Chapter III (Section 3.3). Styrene and *n*-butyl acrylate (Plascon Research Centre, University of Stellenbosch) were washed with 10 % aqueous solution of sodium hydroxide and then washed with distilled deionised water and dried over anhydrous magnesium sulphate. The respective monomers were then distilled under reduced pressure and stored at low temperatures. Deuterated dimethyl sulphoxide (DMSO- d_6 , Cambridge Isotope Laboratories, 99%) and dimethyl formamide (DMF, Aldrich) were used as received.

5.2.2 Procedure for the *in situ* ^1H NMR copolymerization of styrene and *n*-butyl acrylate

Styrene and *n*-butyl acrylate copolymerizations were followed via *in situ* ^1H NMR at 120 °C at different monomer feed compositions in DMSO- d_6 . In a typical copolymerization reaction, MAMA-DEPN (30.1 mg), styrene (0.0722 g), *n*-butyl acrylate (0.1314 g), DMF (20 μL) and DMSO- d_6 (0.3113 g) were thoroughly mixed and introduced into a J-Young type NMR tube. The DMF served as an internal reference. The reaction mixture was degassed by three freeze-pump-thaw cycles and a nitrogen gas blanket was introduced. The instrumental setups were as previously explained in Chapter III. The copolymerization was allowed to run for 90 minutes.

5.2.3 Procedure for the *in situ* ^{31}P NMR copolymerization of styrene and *n*-butyl acrylate

The ^{31}P NMR spectra were acquired with a 4.75 μs (45°) pulse width and a 1.6 seconds acquisition time. For the *in situ* NMR kinetic experiments, samples were first inserted into the magnet at 25 °C and the magnet completely shimmed on the sample and the spectrum collected at 25 °C against phosphoric acid external reference. This was followed by removal of the sample from the magnet and the cavity of the magnet was heated to 120 °C and allowed to stabilize

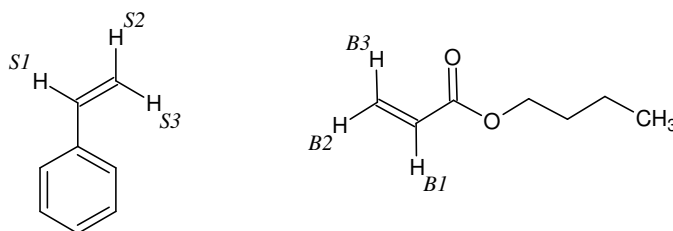
before introducing the sample again into the cavity of the magnet. Following the re-insertion of the sample, additional shimming was performed to acquire full optimum conditions and the first spectra were collected 3–5 minutes after re-insertion. The spectra were processed manually using ACD Labs 10.0 NMR processor[®].

Styrene and *n*-butyl acrylate copolymerizations were followed via *in situ* ³¹P NMR at 120 °C at different monomer feed compositions in DMSO-d₆. In a typical copolymerization reaction, MAMA-DEPN (30.3 mg), styrene (0.1191 g), *n*-butyl acrylate (0.1078 g) and DMSO-d₆ (0.3094 g) were thoroughly mixed and introduced into a J-Young type NMR tube. The reaction mixture was degassed by three freeze-pump-thaw cycles and a nitrogen gas blanket was introduced. The copolymerization was allowed to run for 90 minutes.

5.3 Results and discussion

5.3.1 Quantitative monitoring of monomer consumption via *in situ* ¹H NMR

Taking into consideration the structures of the monomers as illustrated in Scheme 5-3, the concentration profiles of the monomers can be followed from the peaks of the vinyl protons of the respective monomers from the *in situ* ¹H NMR spectra, Figure 5-1.



Scheme 5-3: Chemical structures of styrene and *n*-butyl acrylate indicating the vinylic protons that were monitored for concentration profiles.

Integration of the respective peaks against the internal reference provided a route for the determination of the concentration profiles of the species of interest. In Figure 5-1, the peak at $\delta \sim 7.95$ ppm corresponds to the single proton of the internal reference (DMF). The peaks used to monitor the concentration of styrene and *n*-butyl acrylate with time are labelled B1, B2, S2 and S3 corresponding to the protons labelled in Scheme 5-3. A typical profile illustrating the consumption of the respective monomers in a copolymerization reaction is shown in Figure 5-2.

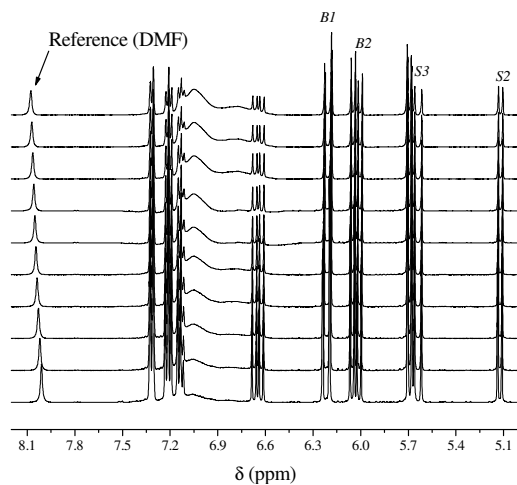


Figure 5-1: *In situ* ^1H NMR spectrum array for the copolymerization of styrene and *n*-butyl acrylate in DMSO-d_6 at $120\text{ }^\circ\text{C}$.

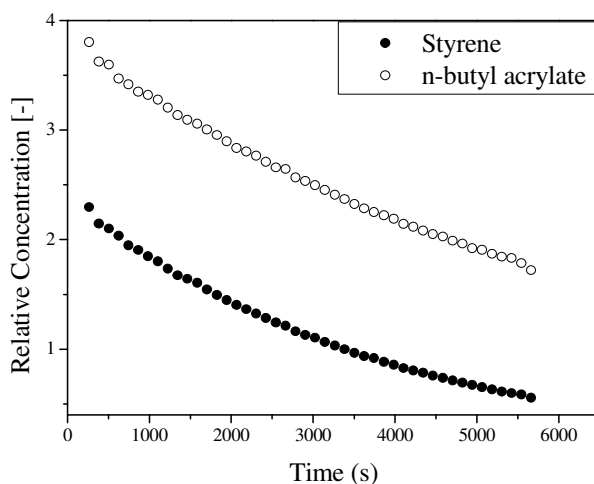


Figure 5-2: The concentration profiles of styrene and *n*-butyl acrylate relative to the DMF internal reference for the copolymerization conducted in DMSO-d_6 at $120\text{ }^\circ\text{C}$ ($f_S^0 = 0.4$).

5.3.2 Assessment of the reactivity ratios

The determination of the reactivity ratios according to the TUM for the copolymerization of styrene and *n*-butyl acrylate mediated by nitroxide was carried out using the method reported by Aguilar et al.¹³ The experimental data extracted from the *in situ* ^1H NMR experiments were fitted to Equation (5-12) using the non-linear least square fitting procedure.

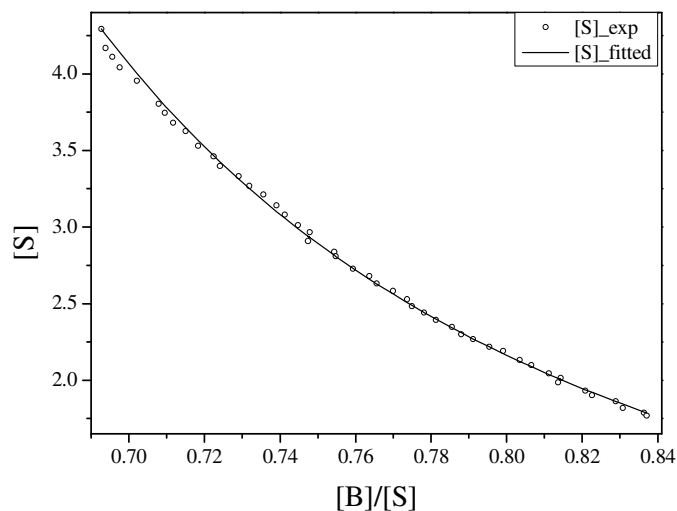


Figure 5-3: Relative concentration of styrene [S] versus the ratio [B] / [S] from the *in situ* ^1H NMR analysis of the copolymerization of styrene and *n*-butyl acrylate with initial feed composition of $f_S^0 = 0.6$ ($r_S = 0.74, r_B = 0.23$).

Based on the residual sum of squares between the experimental and the fitted data (as illustrated by Figure 5-3), the reactivity ratios for styrene and *n*-butyl acrylate were obtained as 0.74 and 0.23, respectively. In addition to the previously mentioned values of reactivity ratios in Section 5.1.2, r_S and r_B have also been obtained as 0.747 and 0.151, respectively under conventional free radical polymerization.¹⁴ For the copolymers prepared by ATRP, r_S and r_B were reported to fall within the ranges 0.68 – 0.82 and 0.22 – 0.26, respectively.¹⁵ This latter set of data is in good agreement with the reactivity ratios reported by Chambard.⁸ The general trend that can be deduced from the reactivity ratios of styrene and *n*-butyl acrylate is that $r_S > r_B$ and $r_S, r_B < 1$. This trend also holds for the copolymerization of styrene and other acrylate type monomers. For the styrene and *t*-butyl acrylate (*t*-B) copolymerization system, the reported reactivity ratios are $r_S = 0.4 - 0.49$ and $r_{i-B} = 0.09 - 0.12$, whereas in the case of styrene and *i*-butyl acrylate (*i*-B) the reactivity ratios are $r_S = 0.73$ and $r_{i-B} = 0.17$; $r_S = 0.72$ and $r_{i-B} = 0.18$.¹⁴

5.3.3 Instantaneous comonomer and copolymer composition

In the case of styrene and *n*-butyl acrylate copolymerization, both the reactivity ratios are observed to be less than unity. For any copolymerization system where both the reactivity ratios

are less than unity, there exists a comonomer feed composition at which both monomers are consumed at a similar rate. This particular feed composition is referred to as the azeotrope (or azeotropic composition), defined by Equation (5-16). At the azeotropic feed composition, the instantaneous comonomer and copolymer composition remain constant over the entire conversion range and $f_i = F_i$.

$$f_i^0 = \frac{1 - r_i}{2 - r_i - r_j} \quad (5-16)$$

Figure 5-4 illustrates the concept of the azeotropic composition by comparing the evolution of the instantaneous comonomer composition with overall conversion. A significant deviation in the instantaneous comonomer composition from the initial feed composition is observed with increased difference between the initial feed composition and the azeotropic feed composition.

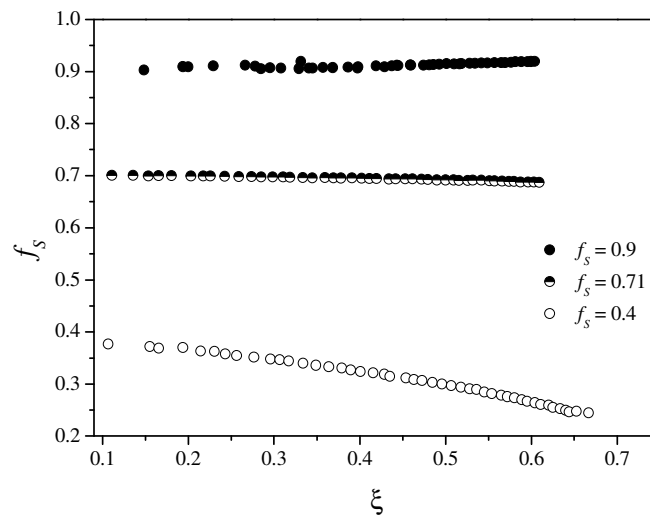


Figure 5-4: The effect of overall conversion on the instantaneous comonomer composition at different initial feed composition.

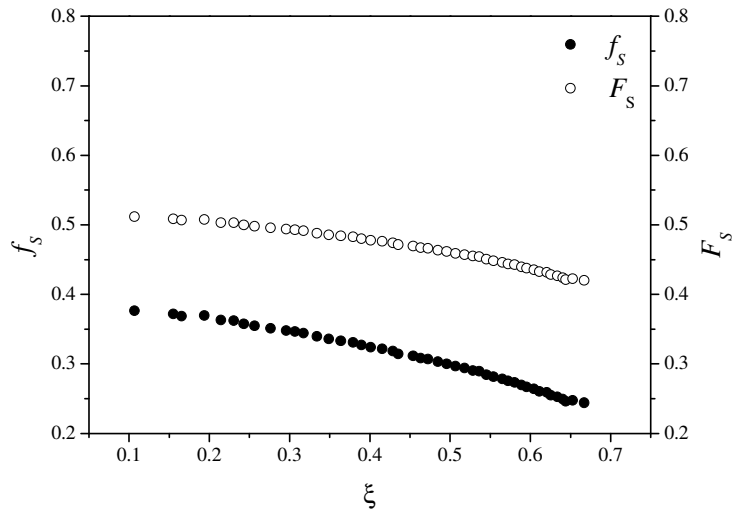


Figure 5-5: The effect of feed composition on both the instantaneous comonomer composition and the instantaneous copolymer composition for $f_s^0 = 0.4 \ll f_{azeotrope}$.

Figure 5-5 illustrates the difference between the evolution of the instantaneous comonomer composition and instantaneous copolymer composition for styrene, as a function of conversion at $f_s^0 = 0.4$.

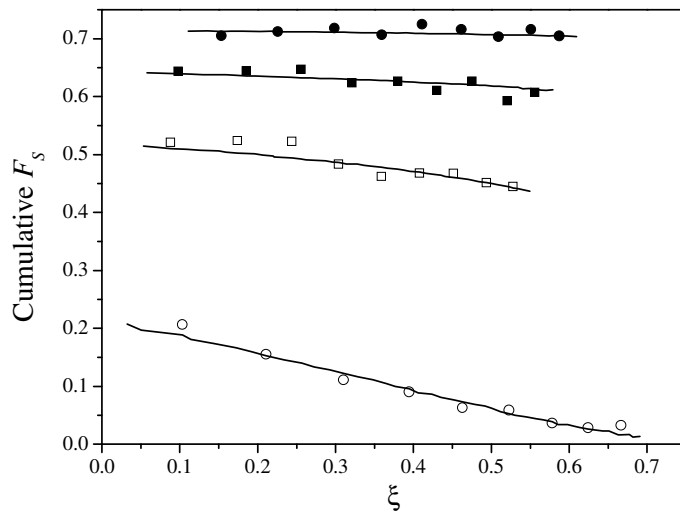


Figure 5-6: Evolution of the cumulative fraction of styrene in the copolymer as a function of overall monomer conversion for $f_s^0 = 0.1$ (\circ), $f_s^0 = 0.4$ (\square), $f_s^0 = 0.6$ (\blacksquare) and $f_s^0 = 0.71$ (\bullet) with the solid lines representing the respective calculated cumulative fractions of styrene using $r_s = 0.74$ and $r_B = 0.23$.

In Figure 5-6, the experimental and calculated cumulative copolymer composition with respect to styrene, are plotted as a function of overall monomer conversion at different initial feed compositions. The predicted cumulative copolymer compositions were calculated using the reactivity ratios determined in Section 5.3.2.

From the copolymerization reactions at different initial feed compositions (0.1 to 0.9), a copolymer composition curve (Figure 5-7) can be constructed. The cumulative copolymer compositions with respect to styrene were calculated from the respective monomer concentrations as follows. For a specific initial feed composition, the concentration of styrene and *n*-butyl acrylate corresponding to times t_1 and t_5 were used to calculate the first data point of the cumulative copolymer composition. The subsequent values were then calculated from the time pairs of $t_6 - t_{10}$, $t_{11} - t_{15}$ and so on, to cover the entire polymerization time. The procedure was repeated for the entire initial feed composition range studied. A good agreement between the experimental copolymer composition curve and the predicted curve using the reactivity ratios determined in Section 5.3.2 is observed.

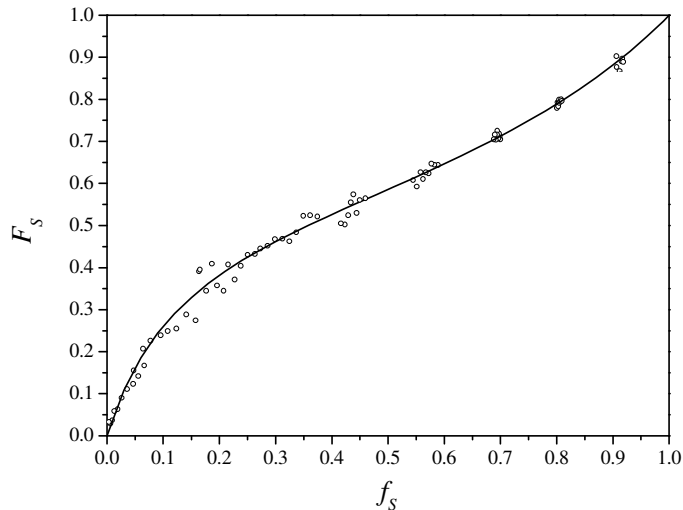


Figure 5-7: The copolymer composition curve (\circ) for the copolymerization of styrene and *n*-butyl acrylate with the solid line indicating the theoretical copolymer composition calculated according to Equation 5-10 using $r_S = 0.74$ and $r_B = 0.23$.

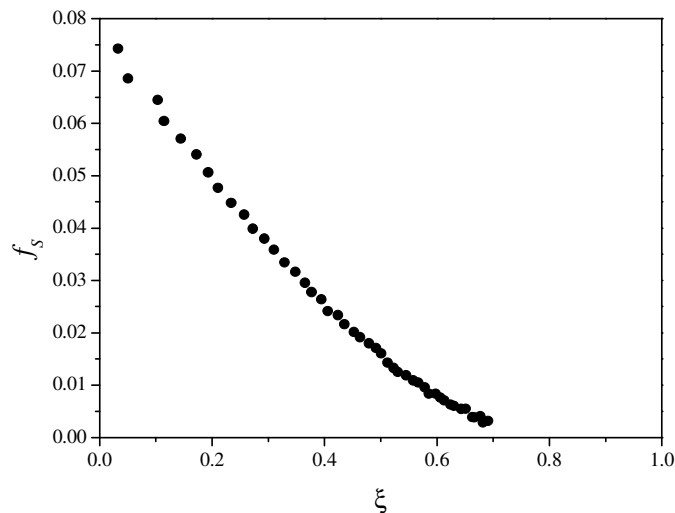


Figure 5-8: The evolution of instantaneous comonomer composition with overall conversion for $f_s^0 = 0.1$.

The extent (total conversion) to which the copolymerization reaction is allowed to run is important depending on the required microstructure of the polymer. In the case of $f_s^0 = 0.1$, Figure 5-8 illustrates that the copolymerization will occur to the overall conversion of slightly above 70%, beyond which a block of *n*-butyl acrylate homopolymer will form.

5.3.4 Conversion index plots

As mentioned earlier in the chapter, the styrene/*n*-butyl acrylate copolymerization system satisfies the conditions r_s and $r_B < 1$, indicating that the system possesses an azeotrope. An indication of the relative rates of consumption of the monomers below and above the azeotropic feed composition is observed in the conversion index plots (Figures 5-9 and 5-10).

Figures 5-9 and 5-10 illustrate the rate of consumption of styrene and *n*-butyl acrylate at initial feed composition slightly below and above the azeotropic feed composition. Below the azeotropic feed composition (relative to styrene), the rate of consumption of styrene will exceed that of *n*-butyl acrylate (Figure 5-9). However, above the azeotropic feed composition the opposite is true, where *n*-butyl acrylate is consumed faster (Figure 5-10). The relative rate of monomer consumption as a function of feed composition is illustrated in Figure 5-11. According

to Figure 5-11, the rate of consumption of styrene will gradually increase with the decreasing fraction of styrene in the feed which is in line with the expected behaviour.

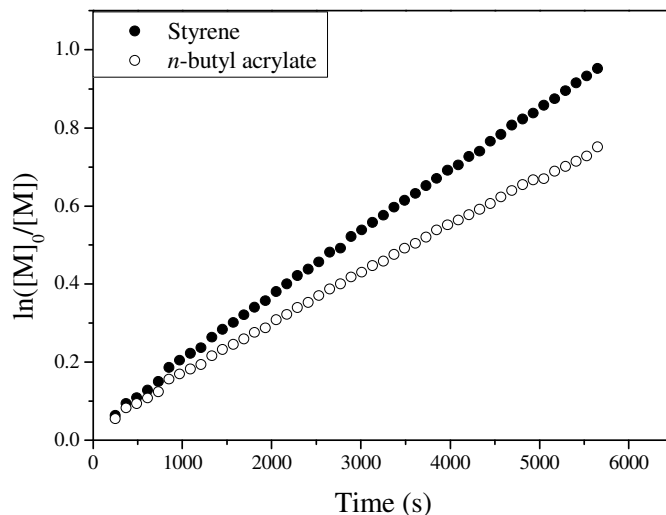


Figure 5-9: Conversion index plot for the copolymerization of styrene and *n*-butyl acrylate at 120°C in DMSO-d₆ with 0.6 mole fraction styrene in the initial feed composition, using MAMA-DEPN as a unimolecular initiator.

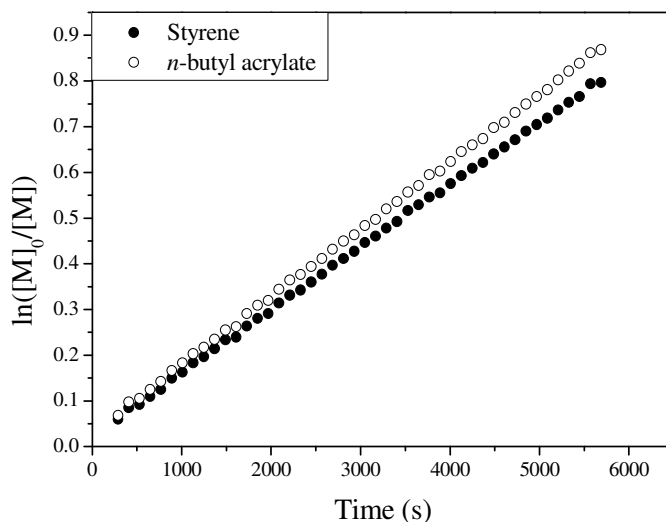


Figure 5-10: Conversion index plot for the copolymerization of styrene and *n*-butyl acrylate at 120°C in DMSO-d₆ with 0.8 mole fraction styrene in the initial feed composition, using MAMA-DEPN as a unimolecular initiator.

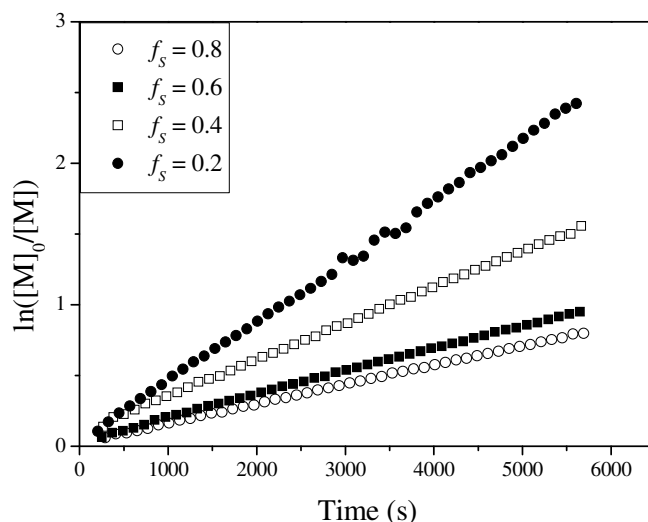


Figure 5-11: Conversion index plots for the fractional conversion of styrene at different initial feed compositions for the styrene/*n*-butyl acrylate copolymerization at 120°C using MAMA-DEPN in DMSO- d_6 .

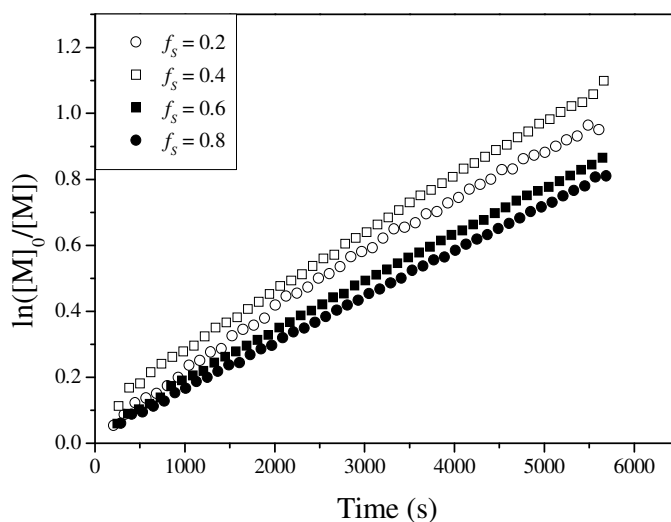


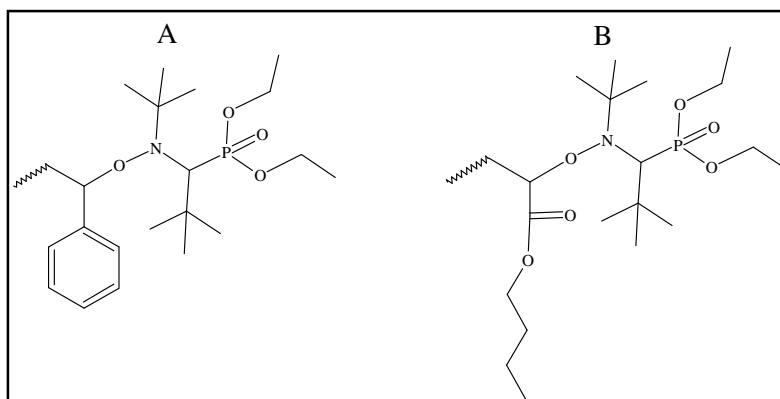
Figure 5-12: The overall conversion index plot for the copolymerization of styrene and *n*-butyl acrylate at 120°C using MAMA-DEPN in DMSO- d_6 at different initial feed compositions.

An additional interesting trend to consider is the overall rate of consumption of both monomers as a function of feed composition. Figure 5-12 illustrates the overall conversion index for the styrene/*n*-butyl acrylate copolymerization at four different initial feed compositions. For the selected initial feed compositions, the highest overall rate of consumption of the monomers is observed for the feed composition corresponding to $f_s^0 = 0.4$. When the fraction of styrene was

varied within the ranges $0.1 < f_s^0 < 0.3$ and $0.5 < f_s^0 < 0.8$, the overall rate of consumption of both monomers were lower than that observed for $f_s^0 = 0.4$.

5.3.5 Monitoring the terminal unit

The presence of a phosphorus atom in the structure of the nitroxide used in this study allowed for use of *in situ* ^{31}P NMR to further probe the mechanistic features of styrene/*n*-butyl acrylate copolymerization. Preliminary homopolymerization reactions of styrene and *n*-butyl acrylate monitored via *in situ* ^{31}P NMR were carried out, following the chemical shift of the phosphorus of the nitroxide chain end moiety (Scheme 5-4). In the dormant state of the growing chains, the signal due to phosphorus in which styrene is the terminal unit of the dormant chain can be resolved from that in which *n*-butyl acrylate is the terminal unit of the dormant chain.



Scheme 5-4: Structures of dormant chains with styrene (A) and *n*-butyl acrylate (B) as the terminal unit.

In the copolymerization reactions, the resulting phosphorus peaks can be used to distinguish dormant chains with either styrene or *n*-butyl acrylate as the terminal unit of a dormant polymer chain. Figure 5-13 shows a typical ^{31}P NMR spectrum acquired during the copolymerization of styrene and *n*-butyl acrylate, with the two distinct regions of peaks visible. The region labelled “S” is due to the styrene terminal unit and the “S+B” region is due to a combination of both styrene and *n*-butyl acrylate terminal units. From the preliminary *in situ* ^{31}P NMR homopolymerization of both styrene and *n*-butyl acrylate (Figure 5-15), the regions of peaks in Figure 5-13 could be assigned.

For the *in situ* ^{31}P NMR homopolymerization of styrene, two regions of peaks were observed and their ratio remained constant throughout the entire polymerization time. With the knowledge of this ratio, the overlapping region in Figure 5-13 could be resolved into its two respective components, being the dormant chains with styrene and *n*-butyl acrylate as the terminal unit.

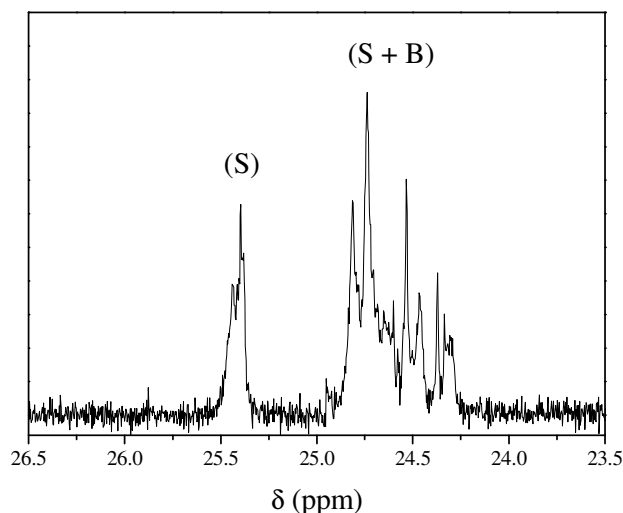


Figure 5-13: *In situ* ^{31}P NMR spectrum acquired 256 s into the copolymerization of styrene and *n*-butyl acrylate in DMSO-d_6 at $120\text{ }^\circ\text{C}$ with the alkoxyamine MAMA-DEPN, at initial feed composition corresponding to $f_s^0 = 0.3$.

To assess the effect of the initial feed composition on the ^{31}P NMR spectrum, *in situ* ^{31}P NMR copolymerizations were conducted at different initial feed compositions. Kelemen et al. reported a significant variation in the ^{15}N NMR spectra as a function of initial feed composition.¹⁶ Figure 5-14 shows the ^{31}P NMR spectra as a function of initial feed composition.

In Figure 5-14, the ^{31}P NMR spectra are shown for three different initial feed compositions. The signal at 25.5 ppm due to styrene being the terminal unit shifts up-field with the fraction of styrene decreasing in the initial feed composition. When considering the signal due to the styrene terminal at 25.5 ppm, there is a change in the shape of the peak. The change in chemical shift in the signal can be explained by considering the penultimate unit effects. At higher fractions of styrene in the feed, the contribution to the signal at 25.5 ppm is mainly due to the adduct $\text{PSS}_i\text{-DEPN}$. As the fraction of styrene in the feed is lowered, there is an increase in adduct of

type $\text{PBS}_i\text{-DEPN}$, resulting in the shift of the signal. The possibility of an effect of the antepenultimate unit also exists, although it cannot be distinguished from that of the penultimate unit effect from this data.

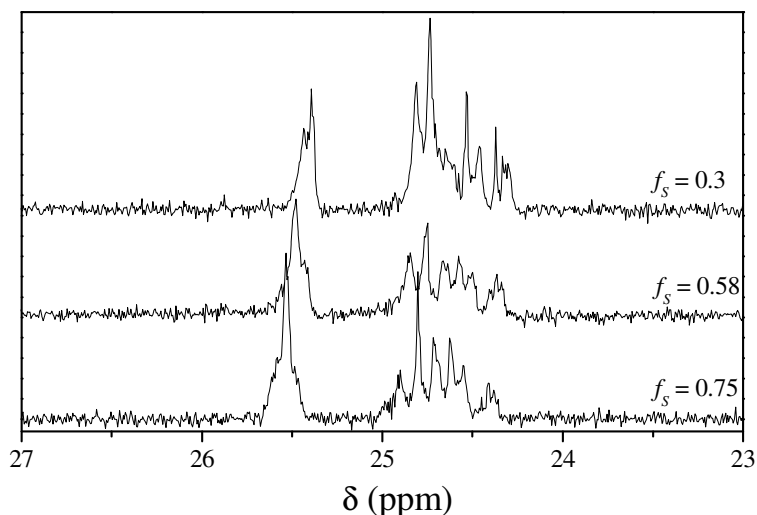


Figure 5-14: ^{31}P NMR spectra of the styrene/*n*-butyl acrylate copolymerization system at three initial feed compositions indicating signals due to dormant chains with styrene and *n*-butyl acrylate as terminal units.

The respective signal intensities in Figure 5-14 vary with the initial feed composition as would be expected. Although subtle, there seems to be a change in the shape of the peaks in the ^{31}P NMR spectra observed with varying initial feed composition. This observation can be related to the significant change reported in the ^{15}N NMR spectra of the styrene/methyl acrylate system as a function of initial feed composition.

The ^{31}P NMR spectra for the homopolymerizations of styrene and *n*-butyl acrylate are shown in Figure 5-15. The overlapping regions of the signals due to styrene and *n*-butyl acrylate can be clearly observed. However, a complex multiplicity of the signals observed in the case of both styrene and *n*-butyl acrylate terminal unit is observed.

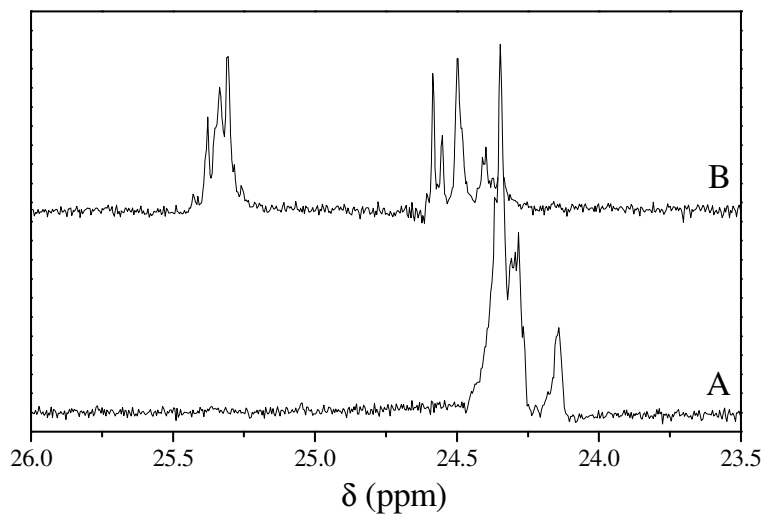


Figure 5-15: ^{31}P NMR spectra of the styrene (B) and *n*-butyl acrylate (A) homopolymerization indicating the regions in which signals due to dormant chains with styrene and *n*-butyl acrylate terminal units are observed.

Figure 5-16 illustrates the evolution of the fraction of dormant chains with styrene and *n*-butyl acrylate as the terminal unit in a copolymerization reaction where $f_s^0 = 0.3$. At the early stages of the reaction, slightly more than 50 % of dormant chains have styrene at the terminal unit. At about 15% overall monomer conversion, the system has approximately equal number of dormant chains with styrene and *n*-butyl acrylate as the terminal unit. Beyond the 15% conversion, the fraction of dormant chains with *n*-butyl acrylate as the terminal unit gradually increases to a total of about 70%.

At monomer feed compositions below the azeotrope (with respect to styrene), the rate of consumption of styrene is faster compared to that of *n*-butyl acrylate. The result is a decrease and increase in the instantaneous feed compositions of styrene and *n*-butyl acrylate, respectively. As a result, at monomer feed compositions below the azeotrope (with respect to styrene), the fraction of dormant chains with styrene terminal unit will show a gradual decrease with polymerization time. Figure 5-17 illustrates the evolution of the fraction of dormant chains with *n*-butyl acrylate as the terminal unit at two different feed compositions below the azeotropic feed composition of styrene. In both feed compositions a gradual increase in the fraction of dormant

chains with *n*-butyl acrylate as the terminal unit is observed, in line with the fact that below the azeotropic feed composition such a phenomenon is expected.

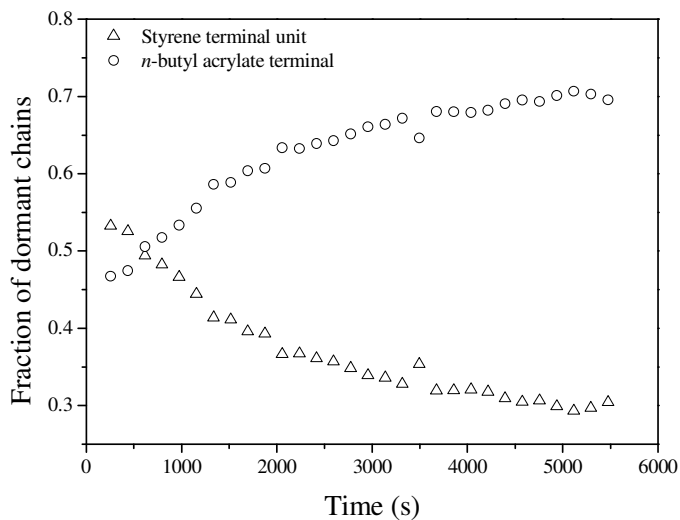


Figure 5-16: The evolution of the fraction of dormant chains with styrene and *n*-butyl acrylate as the terminal unit for $f_s^0 = 0.3$.

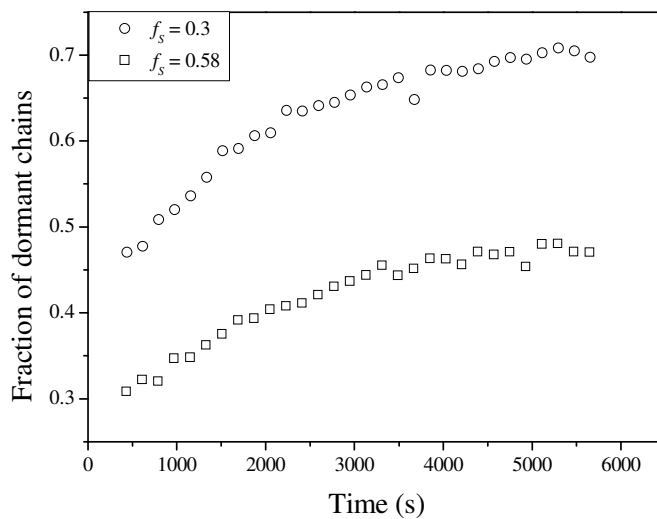


Figure 5-17: The evolution of the fraction of dormant chains with *n*-butyl acrylate as the terminal unit for $f_s^0 = 0.3$ and $f_s^0 = 0.58$.

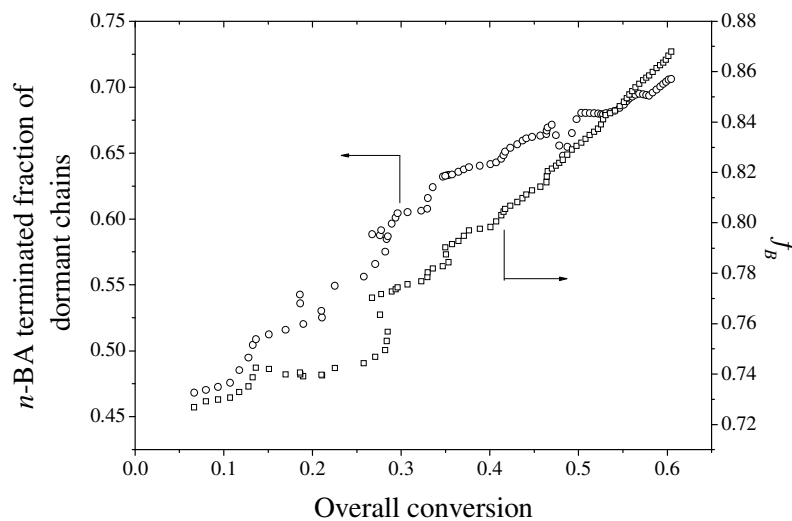


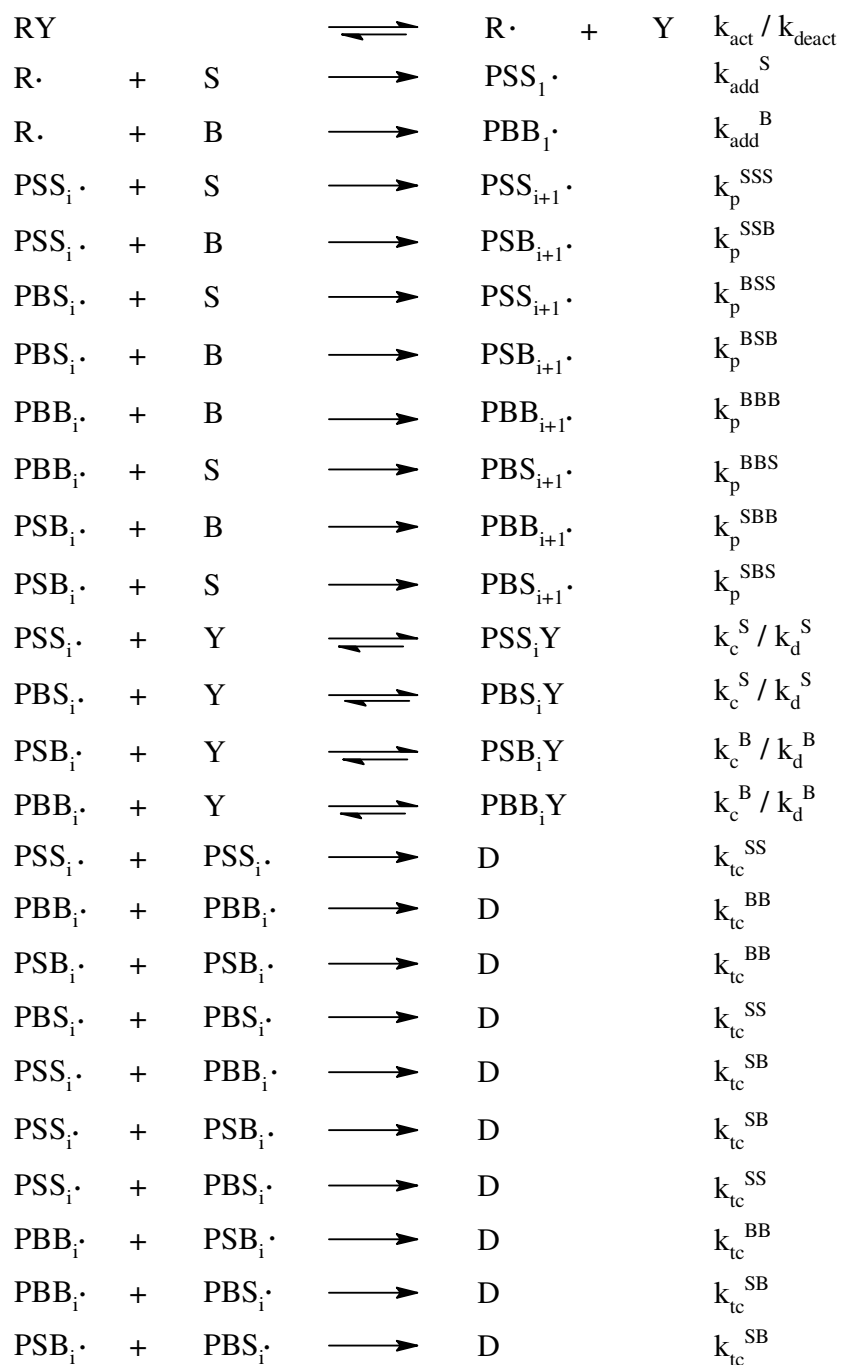
Figure 5-18: The evolution of the fraction of dormant chains with *n*-butyl acrylate as the terminal unit as a function of both overall monomer conversion and instantaneous feed composition for the copolymerization of styrene and *n*-butyl acrylate with $f_s^0 = 0.3$.

Two *in situ* NMR copolymerization experiments were conducted with both samples prepared as identically as possible. One copolymerization was followed via *in situ* ^1H NMR and the other via *in situ* ^{31}P NMR. From the former technique conversion data was attained that could be correlated with the terminal unit data from the latter technique. The results are summarized in Figure 5-18. In Figure 5-17, the increase with time of polymer chains with *n*-butyl acrylate as the terminal unit occurs faster at the early stages of the polymerization with feed composition further from the azeotropic composition. A linear fit to the linear parts of the plots in Figure 5-17 (first~ 2000 s) indicates a higher rate of accumulation of chains with *n*-butyl acrylate as the terminal unit for $f_s^0 = 0.3$.

From Figure 5-18, the fraction of dormant chains with *n*-butyl acrylate as the terminal unit is illustrated as a function of overall monomer conversion and instantaneous feed composition of styrene. With increasing overall monomer conversion, the instantaneous feed composition of styrene gradually decreases for copolymerizations conducted with initial feed composition below the azeotropic feed composition. The result is a gradual increase in dormant chains with *n*-butyl acrylate as the terminal unit.

Due to the overlap of peaks in the *in situ* ^{31}P NMR monitored copolymerizations, a separate independent method was required to validate the data. Simulations of styrene/*n*-butyl acrylate copolymerizations were carried out with the Predici software package for comparison with the experimental data. The implicit penultimate unit model (IPUM) was considered in the copolymerization process.

The terminal unit model (TUM) has been found inadequate in the description of the average propagation rate coefficient, and for the purpose of the rate description of copolymerization processes, higher copolymerization models like the PUM are employed. Before validation of the *in situ* ^{31}P NMR results on tracking the terminal unit of dormant chains, the copolymerization model was tested against experimental data in the feed composition range $0.2 \leq f_s^0 \leq 0.8$. The full copolymerization model description is illustrated by Scheme 5-5, with the applicable rate coefficients in Table 5-1.



Scheme 5-5: The implicit penultimate unit model (IPUM) for the copolymerization of styrene and *n*-butyl acrylate implemented into the Predici software package.

Table 5-1: Rate parameters used in the simulation of the nitroxide mediated copolymerization of styrene and *n*-butyl acrylate as depicted in Scheme 5-5

Coefficient	A	E (kJ/mol)	Value (120 °C)	Refs
k_{act}	$2.4 \times 10^{14} \text{ s}^{-1}$	112.3	0.289 s^{-1}	17
k_{deact}			$5.0 \times 10^6 \text{ L mol}^{-1} \text{ s}^{-1}$	18
k_{add}^S	$6.7 \times 10^6 \text{ L mol}^{-1} \text{ s}^{-1}$	16.5		18, 19
k_{add}^B	$4.0 \times 10^6 \text{ L mol}^{-1} \text{ s}^{-1}$	19.8		18, 19
k_p^{SS}	$4.27 \times 10^7 \text{ L mol}^{-1} \text{ s}^{-1}$	32.5		20
k_p^{BB}	$2.31 \times 10^7 \text{ L mol}^{-1} \text{ s}^{-1}$	18.1		21
r_S			0.74	This
r_B			0.23	This
s_S			0.48	8
s_B			0.06	8
k_c^S			$2.6 \times 10^5 \text{ L mol}^{-1} \text{ s}^{-1}$	18
k_d^S			$7.5 \times 10^{-3} \text{ L mol}^{-1} \text{ s}^{-1}$	18
k_c^B			$2.8 \times 10^7 \text{ L mol}^{-1} \text{ s}^{-1}$	18, 22
k_d^B			$1.55 \times 10^{-3} \text{ L mol}^{-1} \text{ s}^{-1}$	18
k_{tc}^{SS}			$1.8 \times 10^8 \text{ L mol}^{-1} \text{ s}^{-1}$	18
k_{tc}^{BB}			$7.34 \times 10^7 \text{ L mol}^{-1} \text{ s}^{-1}$	18
k_{tc}^{SB}			$1.0 \times 10^8 \text{ L mol}^{-1} \text{ s}^{-1}$	Estimate

Figures 5-19 and 5-20 illustrate simulated and experimental evolution of styrene and *n*-butyl acrylate concentrations with time. No agreement between the experimental data and the model is observed. The first possible explanation involves consideration of penultimate unit effects. This approach will not be addressed in this work because of lack of supporting data from the chosen technique. The second possible explanation that will be discussed further involves assessing the validity of the use of k_c^B and k_d^B determined from homopolymerizations in copolymerizations. These rate coefficients are determined from a homopolymerization of *n*-butyl acrylate and

utilized in the description of a copolymerization involving *n*-butyl acrylate. However, care should be exercised in their use in copolymerization reactions as it was demonstrated in Chapter IV that the equilibrium described in the case of nitroxide mediated polymerization of *n*-butyl acrylate involves both secondary and tertiary mid-chain radicals. In the case where *n*-butyl acrylate is a comonomer in a polymerization system, the contribution of the reversible deactivation of the tertiary mid-chain radical to the equilibrium constant is non-existent.

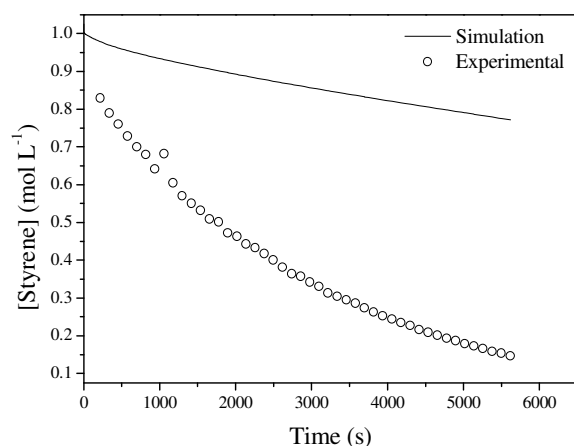


Figure 5-19: Theoretical vs. experimental evolution of styrene concentration with time for $f_s^0 = 0.3$. k_c^B and k_d^B values used in the simulation are in Table 5-1.

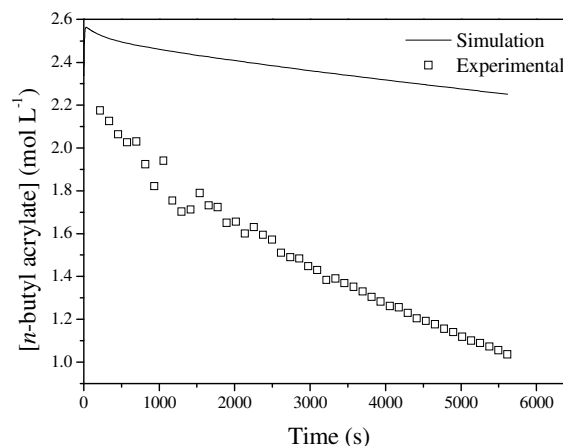


Figure 5-20: Theoretical vs. experimental evolution of *n*-butyl acrylate concentration with time for $f_s^0 = 0.3$. k_c^B and k_d^B values used in the simulation are in Table 5-1.

Parameter estimation (PE) studies with the Predici software package were then carried out to determine the optimum values of k_c^B and k_d^B for which the model would fit the experimental data in the feed composition range studied. The optimum values for the rate coefficients returned from the PE study were $k_c^B = 9.99 \times 10^5 \text{ L mol}^{-1} \text{ s}^{-1}$ and $k_d^B = 9.66 \times 10^{-4} \text{ s}^{-1}$. These optimum values were then adapted into the model to replace the values indicated in Table 5-1, for further modelling studies of the copolymerization process. Figures 5-21 – 5-24 illustrate the evolution of both styrene and *n*-butyl acrylate concentration with time, for two feed compositions.

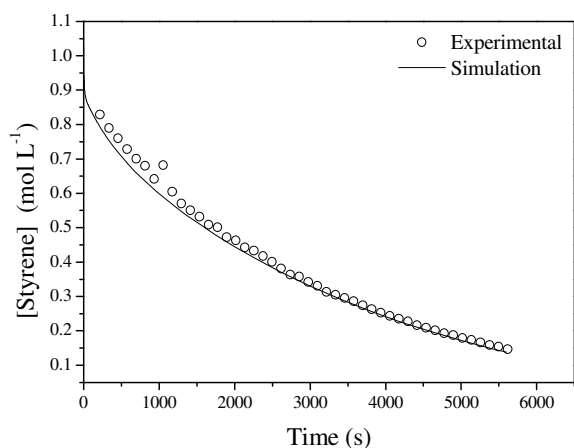


Figure 5-21: Theoretical vs. experimental evolution of styrene concentration with time for $f_s^0 = 0.3$. k_c^B and k_d^B values used are $9.99 \times 10^5 \text{ L mol}^{-1} \text{ s}^{-1}$ and $9.66 \times 10^{-4} \text{ s}^{-1}$, respectively.

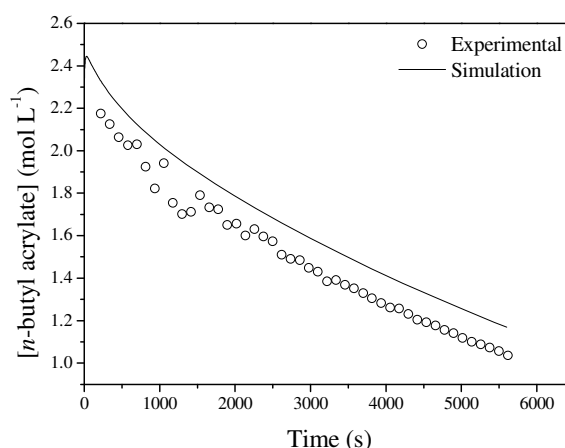


Figure 5-22: Theoretical vs. experimental evolution of *n*-butyl acrylate concentration with time for $f_s^0 = 0.3$. k_c^B and k_d^B values used are $9.99 \times 10^5 \text{ L mol}^{-1} \text{ s}^{-1}$ and $9.66 \times 10^{-4} \text{ s}^{-1}$, respectively.

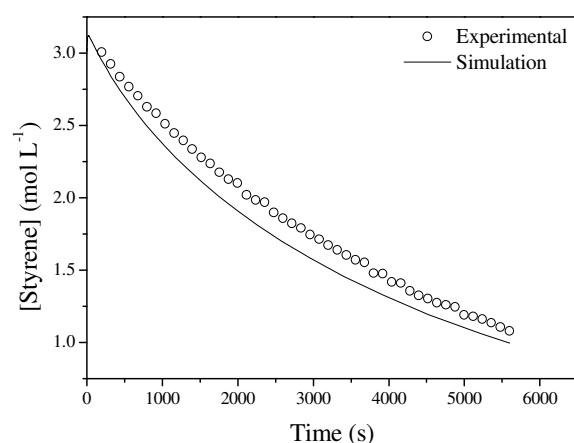


Figure 5-23: Theoretical vs. experimental evolution of styrene concentration with time for $f_s^0 = 0.8$. k_c^B and k_d^B values used are $9.99 \times 10^5 \text{ L mol}^{-1} \text{ s}^{-1}$ and $9.66 \times 10^{-4} \text{ s}^{-1}$, respectively.

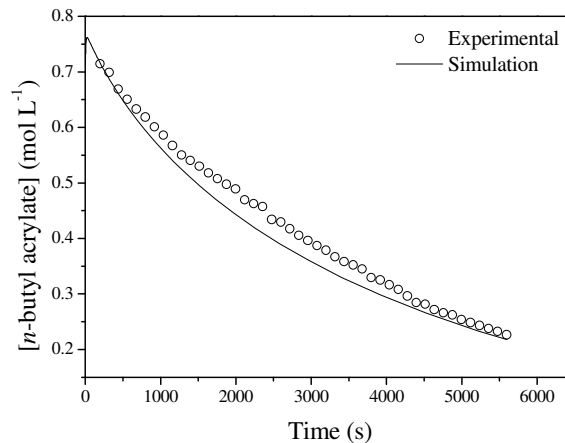


Figure 5-24: Theoretical vs. experimental evolution of *n*-butyl acrylate concentration with time for $f_s^0 = 0.8$. k_c^B and k_d^B values used are $9.99 \times 10^5 \text{ L mol}^{-1} \text{ s}^{-1}$ and $9.66 \times 10^{-4} \text{ s}^{-1}$, respectively.

An improved correlation between experimental and simulated data was observed in the feed composition range studied when the values of k_c^B and k_d^B determined from the PE study were used. Figures 5-21 and 5-22 illustrate the agreement between the model and experiments below the azeotropic feed composition of the styrene/*n*-butyl acrylate system, while Figures 5-23 and 5-24 show the agreement above the azeotropic feed composition.

To further probe how representative the proposed model is of the real copolymerization system, simulations were carried out to study the terminal unit of dormant chains. Figures 5-25 and 5-26 illustrate the evolution of the fraction of dormant chains which possesses *n*-butyl acrylate as the terminal unit. Even though the ^{31}P NMR spectra were marked by overlap of peaks from styrene and *n*-butyl acrylate terminated dormant chains, the method used to separate both signals resulted in data that is comparable with the simulation data from the proposed model. A reasonable quantitative agreement is observed between model data and experimental data. However, a fairly poor qualitative agreement between the model and experimental data is observed, with the greatest deviation in profile shape at short reaction times. This deviation can be ascribed to the uncertainties embedded in the approximated rate coefficients of first monomer addition (k_{add}^S and k_{add}^B). The actual values of the rate coefficients of addition of styrene and *n*-butyl acrylate to the 2-carboxyprop-2-yl radical are not known. But these rate coefficients are believed to be close to those of the addition of similar monomers to the 2-(alkoxy)carboxyprop-2-yl radical utilized in the model.¹⁸ The mode of initialization, governed by the rate coefficients of addition of the respective monomers, will determine the fraction of each respective dormant species, before the steady-state conditions are attained. This will occur until such a point that the radical ratio in the copolymerization system is governed by the reactivity ratios.

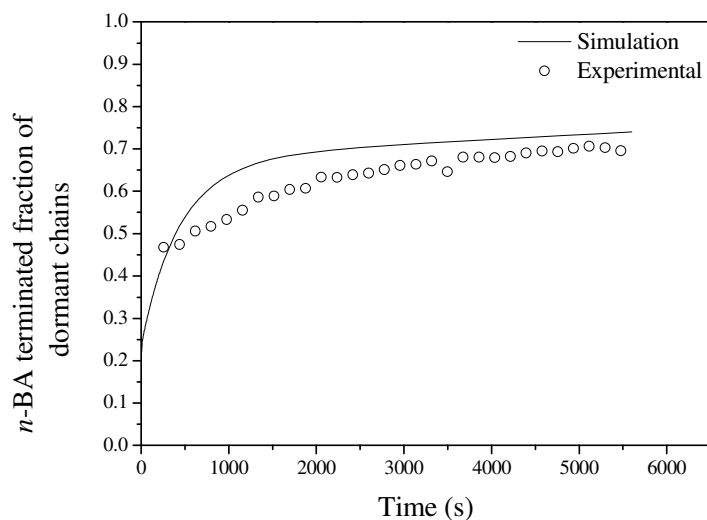


Figure 5-25: Experimental and simulated fraction of dormant chains with *n*-butyl acrylate as the terminal unit in the copolymerization of styrene and *n*-butyl acrylate with $f_s^0 = 0.29$.

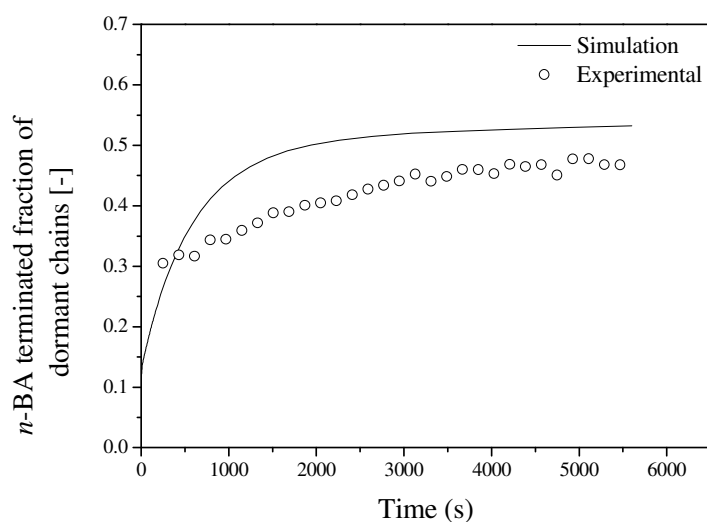


Figure 5-26: Experimental and simulated fraction of dormant chains with *n*-butyl acrylate as the terminal unit in the copolymerization of styrene and *n*-butyl acrylate with $f_s^0 = 0.58$.

Thus by comparison of model data and *in situ* ^{31}P NMR data, it can be observed that valuable quantitative results can be extracted from the *in situ* ^{31}P NMR experiments with careful analysis of the data.

Further improvements of the model are however required, to improve on both the qualitative and quantitative description of the copolymerization system with respect to the terminal unit of the dormant chains.

5.4 Conclusion

In situ ^1H and ^{31}P NMR monitored copolymerizations of styrene and *n*-butyl acrylate were successfully carried out. From the *in situ* ^1H NMR copolymerization data, the reactivity ratios of styrene and *n*-butyl acrylate were determined by fitting the high conversion data to the integrated form of the copolymerization equation. The copolymer composition curve was constructed from the *in situ* ^1H NMR data and was found to be in good agreement with a curve predicted from the reactivity ratios determined in this study. The overall rate of monomer consumption varied with initial feed composition, with the highest rate observed for $f_s^o = 0.4$. The terminal units of dormant polymer chains were profiled as a function of polymerization time via *in situ* ^{31}P NMR. Simulations carried out using the Predici software package, using the implicit penultimate unit model of the copolymerization of styrene and *n*-butyl acrylate mediated by DEPN are reported. The values of the rate coefficients describing the equilibrium involving the *n*-butyl acrylate terminal unit (k_c^B and k_d^B) were determined by fitting (via the parameter estimation tool of the Predici software package) the model to data extracted from *in situ* ^1H NMR experiments. The obtained values of k_c^B and k_d^B resulted in good agreement between the model and experimental data in the initial feed composition range studied. The resulting model also yielded good agreement between simulations and terminal unit data extracted from *in situ* ^{31}P NMR experiments.

References

1. Burke, A. L.; Duever, T. A.; Penlidis, A. *Chem. Eng. Sci.* **1995**, 50, (10), 1619 - 1634.
2. Coote, M. L.; Davis, T. P. *Macromolecules* **1999**, 32, 3626 - 3636.
3. Davis, T. P.; O'Driscoll, K. F. *Polym. Int.* **1991**, 24, 65-70.
4. Heuts, J. P. A.; Gilbert, R. G.; Maxwell, I. A. *Macromolecules* **1997**, 30, 726 - 736.
5. Moad, G.; Solomon, D. H.; Spurling, T. H.; Stone, R. A. *Macromolecules* **1989**, 22, 1145-1147.
6. Zetterlund, P. B.; Tagashira, S.; Izumi, K.; Nagano, Y.; Azukizawa, M.; Yamazoe, H.; Kumagai, M.; Yamada, B. *Macromolecules* **2002**, 35, 8209 - 8215.
7. Cuervo-Rodriguez, R.; Bordege', V.; Ferná'ndez-Monreal, M. C.; Ferná'ndez-Garci'a, M.; Madruga, E. L. *J. Polym. Sci., Part A: Polym. Chem.* **2004**, 42, 4168-4176.
8. Chambard, G. Control of Monomer Sequence Distribution; Strategic Approach based on Novel Insights in Atom Transfer Radical polymerization. PhD, Technische Universiteit Eindhoven, Eindhoven, 2000.
9. Mayo, F. R.; Lewis, F. M. *J. Am. Chem. Soc.* **1944**, 66, 1594.
10. Tidwell, P. W.; Mortimer, G. A. *J. Polym. Sci., Part A: Gen. Pap.* **1965**, 3, (1), 369 - 387.
11. Mao, R.; Huglin, M. B. *Polymer* **1993**, 34, (8), 1709-1715.
12. Kelen, T.; Tüdös, F.; Turcsányi, B.; Kennedy, J. P. *J. Polym. Sci.: Polym. Chem. Ed.* **1977**, 15, (12), 3047 - 3074.
13. Aguilar, M. R.; Gallardo, A.; Fernández, M. d. M.; Román, J. S. *Macromolecules* **2002**, 35, (6), 2036-2041.
14. Lessard, B. t.; Graffe, A.; Maric', M. *Macromolecules* **2007**, 40, 9284-9292.
15. Arehart, S. V.; Matyjaszewski, K. *Macromolecules* **1999**, 32, 2221-2231.
16. Kelemen, P.; Klumperman, B. *Macromolecules* **2004**, 37, 9338-9344.
17. Bertin, D.; Gigmes, D.; Marque, S. R. A.; Tordo, P. *Macromolecules* **2005**, 38, 2638-2650.
18. Chauvin, F.; Dufils, P.-E.; Gigmes, D.; Guillaneuf, Y.; Marque, S. R. A.; Tordo, P.; Bertin, D. *Macromolecules* **2006**, 39, 5238-5250.
19. Zytowski, T.; Knühl, B.; Fischer, H. *Helv. Chim. Acta* **2000**, 83, 658-675.
20. Beuermann, S.; Buback, M. *Progr. Polym. Sci.* **2002**, 27, (2), 191-254.

21. Barner-Kowollik, C.; Günzler, F.; Junkers, T. *Macromolecules* **2008**, 41, 8971-8973.
22. Chauvin, F.; Alb, A. M.; Bertin, D.; Tordo, P.; Reed, W. F. *Macromol. Chem. Phys.* **2002**, 203, (14), 2029-2041.

Chapter VI: Epilogue

This study has reported some important kinetic and mechanistic aspects in the styrene and *n*-butyl acrylate polymerization mediated by persistent radical species. A complete understanding of the respective systems leads to the theoretical explanation of observed phenomena if all major processes are taken into account. Some data derived from homopolymerization reactions cannot always be directly utilized in description of copolymerization reactions.

6.1 Homopolymerization of *n*-butyl acrylate

When MAMA-DEPN was used as a unimolecular initiator for the nitroxide mediated polymerization of *n*-butyl acrylate, the rate of polymerization was observed to be independent of the initial concentration of the initiator. In the case of high temperature styrene polymerization, the independence of rate of polymerization towards initial concentration of the initiator has been explained in terms of the pronounced thermal initiation of the styrene monomer. However, the kinetics and mechanistic features vary greatly between styrene and *n*-butyl acrylate, with the rate coefficient of thermal initiation of styrene far greater than that of *n*-butyl acrylate. One important question we investigated in this work was whether the tertiary mid-chain radicals reacted reversibly with the nitroxide. Through ¹H NMR studies of the poly(*n*-butyl acrylate) prepared from the alkoxyamine MAMA-DEPN, evidence of adducts of the mid-chain radical with the nitroxide DEPN were observed. As a result, this proved indirectly the existence of a reaction between the mid-chain and the nitroxide, which would be reversible in nature. The implication of the existence of this particular reaction is that the equilibrium constant reported in literature for the *n*-butyl acrylate/DEPN system is in actual fact a composite value within which the description of two equilibrium processes are embedded. The values for the rate coefficients describing the equilibrium involving the mid-chain radical proposed in this study should be treated as preliminary. Although the model for the polymerization of *n*-butyl acrylate has been made as comprehensive as presently possible, many reactions still have to be included in the model to bring the model as close to the real system as possible. Such reactions include:

- Intermolecular chain transfer to polymer
- Chain transfer to monomer
- Chain transfer to solvent
- The incorporation of the macromer (species bearing the 1,1-disubstituted alkene end group) resulting from β -fragmentation
- The use of chain length dependent rate coefficients

Practically the inclusion of some of the processes in the model is very difficult, and depends on the theoretical approach used to model the polymerization. For instance, Farcet et al.¹ has reported on poly(*n*-butyl acrylate) chains bearing multiple nitroxides, meaning that a single chain can possess several sites along the backbone on which the reversible deactivation-activation processes occur. The analytical description of such a process in the kinetic model of the polymerization is next to impossible. The fraction of such chains might be small in overall terms, but the inclusion of such a process might be very important in explaining subtle mismatches between experimental and model data.

The effects of the inclusion of the equilibrium involving the mid-chain radicals on the kinetics of *n*-butyl acrylate polymerization were investigated theoretically using the Predici software package. The rate of polymerization was lower for the system with only an equilibrium involving the secondary propagating radicals, and higher rates were observed if both equilibria were included in the kinetic model. The lower rate of polymerization in the former can be explained in terms of the loss of radical due to self termination of mid-chain radicals and their cross-coupling termination with secondary propagating radicals. The product of the β -fragmentation process, the chains bearing the 1,1-disubstituted alkene end group, showed a linear dependence on time. Based on this linear dependence, in the solution polymerization of *n*-butyl acrylate (fairly dilute) the incorporation of the 1,1-alkene species can be regarded negligible. The major conclusions drawn from the homopolymerization of *n*-butyl acrylate are that thermal auto-initiation and the equilibrium involving the mid-chain radical are crucial in explaining the kinetic features of *n*-butyl acrylate polymerization.

6.2 Copolymerization of styrene and *n*-butyl acrylate

In situ NMR has been demonstrated as a powerful technique in probing the kinetic and mechanistic features in controlled living radical copolymerization. From the data extracted from *in situ* ^1H NMR, the reactivity ratios for the styrene/*n*-butyl acrylate copolymerization system mediated by DEPN were reported. This technique is relatively simple and provides quick access to the determination of reactivity ratios. The reactivity ratios determined were in good agreement with literature reports for the same comonomer system under different polymerization conditions. The copolymer composition curve derived from the ^1H NMR data within the initial feed composition range studied was in good agreement with the predicted curve. With the inherent sensitivity of ^{31}P NMR, the terminal unit of dormant chains could be tracked with polymerization time as a function of initial feed composition. The use of a technique like *in situ* ^{31}P NMR, adds value to the already existing methods of understanding kinetic and mechanistic features of copolymerization systems. As demonstrated, the penultimate unit effects in the styrene/*n*-butyl acrylate copolymerization system could be detected. This technique of *in situ* ^{31}P NMR applied to polymerization systems is limited to nitroxide mediated systems, and only with phosphorus bearing nitroxides.

6.3 Simulation of the homopolymerization and copolymerization via Predici

Simulation of both homo- and copolymerization processes were carried out with the Predici software package (version 6.72.3). The rate coefficients of deactivation and activation in homo- (k_c^t and k_d^t) and copolymerization (k_c^B and k_d^B) were estimated with the parameter estimation tool of the Predici software package. The parameter estimation was carried out with reduced directions with automatic detection of number of essential directions. The simulations were carried out in the moment mode in Predici. For *n*-butyl acrylate homopolymerization, it was demonstrated that the equilibrium constant reported in literature must actually be resolved into its two respective components to get a model that can best fit experimental data. With the polymerization model of *n*-butyl acrylate mediated by DEPN, the effect of the inclusion of the equilibrium involving the mid-chain radical on the polymerization kinetics was studied. The co-existence of secondary propagating and tertiary mid-chain radicals could not be linked with the observed phenomenon of rate independence towards initiator concentration. As in the case of

styrene, the polymerization model revealed that thermal auto-initiation in *n*-butyl acrylate polymerization was the factor responsible for the observed phenomenon of rate independence. In the investigations into thermal auto-initiation of *n*-butyl acrylate, good agreement was observed between experimental and simulation data for initiator free polymerization of *n*-butyl acrylate in the presence of free DEPN. The rate coefficient of thermal auto-initiation determined in this study is in very good agreement with previously reported values. *In situ* ¹H NMR can thus provide a facile route for probing and quantifying thermal auto-initiation in other systems with proper experimental design.

For the simulation of the copolymerization of styrene and *n*-butyl acrylate assuming the implicit penultimate model, the use of rate coefficients of deactivation (k_c^B) and activation (k_d^B) reactions obtained from *n*-butyl acrylate homopolymerizations results in a massive discrepancy between the simulation and experimental data. Unlike in the case of styrene, side reactions present in *n*-butyl acrylate affect the determined value of the equilibrium constant. However, these side reactions are absent in copolymerization reactions, and hence the reversible deactivation of chains with *n*-butyl acrylate as the terminal unit and DEPN cannot be adequately described by the rate coefficients obtained from homopolymerization reactions. Through simulations, optimal values for the rate coefficients of deactivation and activation involving the *n*-butyl acrylate terminal radical and DEPN are reported in this work.

6.4 Recommendations

For the homopolymerization of *n*-butyl acrylate, investigation into the mechanistic features of thermal auto-initiation is necessary. Unlike in the case of styrene, very little is known about how thermal initiation occurs in *n*-butyl acrylate. The knowledge of this process will aid in ultimately constructing a polymerization model that is representative of the real system. Electron spin resonance (ESR) spectroscopy studies of *n*-butyl acrylate polymerization mediated by DEPN can provide valuable information by comparison with ESR data from conventional *n*-butyl acrylate polymerization. Construction of an extensive model for nitroxide-mediated *n*-butyl acrylate polymerization should be undertaken. This should be done while taking into account all major and side reactions to allow for better estimates of the values k_c^t and k_d^t . In the case where the

parameter estimation tool of Predici is used to determine the estimates, three or more sets of experimental data should be used in the fitting procedure.

Further investigation of the splitting pattern observed in the ^{31}P NMR spectrum of DEPNO-capped polystyrene should be undertaken.

References

1. Farcet, C.; Belleney, J.; Charleux, B.; Pirri, R. *Macromolecules* **2002**, 35, 4912-4918.

Acknowledgements

This section of the dissertation is dedicated to individuals who were instrumental, in one way or the other, in my research and personal life in Stellenbosch.

First and foremost I would like to thank God for the blessing that have been bestowed on me to this point in my life. I would like to sincerely express my gratitude to my supervisor Prof Bert Klumperman, for his guidance and assistance over the past four years, and for the contributions he made in this work, and mostly for his patience. I would like to thank Dr M. P. Tonge for the assistance at the beginning of this project.

I would like to thank Prof. Ron Sanderson for giving me the opportunity study Polymer Science at the University of Stellenbosch and for his guidance and advices during my honours programme in 2006. I would like to thank the Department of Chemistry and Polymer Science (University of Stellenbosch), the University of Stellenbosch and the NRF SARChI for funding, without which the last five years at the University of Stellenbosch would have been impossible.

I would like to thank Jean Mckenzie, Elsa Malherbe, Heidi Assumption and Jaco Brand for the assistance and endless valuable discussions about *in situ* NMR experiments. Special thanks to Elsa Malherbe for the efforts that helped make this study what it is. Dr G. Anortt is thanked for assistance with microwave reactions. Dr W. Weber is thanked for the assistance at the beginning of this study. Dr Michael Wulkow is thanked with assistance with the parameter estimations studies with the Predici software package. Thanks to Dr Gwen Pound for the assistance, guidance and time invested in endless invaluable discussions to make study what it turned out to be.

Special thanks to Dr E.T.A. van den Dungen, for the invaluable input he made in this work, the endless discussion in all disciplines of polymer science and for being a great mentor. Thank you for the time you invested reading and correcting this work.

To Erinda, Aneli, Margie, Deon, Jim, Calvin and Harnie, I thank you dearly for the assistance in all matters you contributed in, and to the smooth everyday running of the Polymer Science Institute.

The free radical research group, past and present members, Eric, Khotso, Reuben, Osama, Ahson, Welmarie, Walid, Neli, Hamilton, Paul, William, Jaco, Ahmed, Celeste, Lizel, Sandile, Barry, Nathalie, Wisdom, Reda, Niels, Njabu and Zaskia, I highly appreciate all the valuable discussions and the assistance I received over the past four years. To Reuben Pfukwa, I thank you for the time you spent listening to my theories, speculations and all I had to say to make sense of things at times, I highly appreciate it. Your contribution to this work is highly appreciated.

I would like to thank Dr. B. M. Taele, for the opportunity he gave me in September of 2005 to attend the WAMIII Conference at Stellenbosch University, which inspired me to join SU.

I would like to extend my gratitude to Prof B. Klumperman (SU), Prof P. E. Mallon (SU) and Prof J. M. Saiter (Université de Rouen) for the opportunity to attend the POLYCHAR 17 conference in Rouen, France.

I would like thank my family for their support during my time in Stellenbosch. To my mother, I thank you for the support over the years, and for believing in me. To Lesala, I am glad I have you as a brother, thanks for everything “tau”.

To Haydn, thanks for being a great friend, making Stellenbosch a great place it was, and most of all for the support you showed and the free advices throughout my time in Stellenbosch.

To Phiri and Khotso, your advices and support went a long way in making all this possible today, I am grateful for everything. To Aimee, Storm, Zengeni, Sean Maliehe, I am grateful for everything.

To friends and acquaintances I made along the way, Bas “Mr anionic” van Ravensteijn, Axel, Joris Salari, Sandile Mkwanzazi, Nagi Greesh, this journey would not have been the same without you, the good times we had made things worthwhile.

To my gym friend Al and his wife, I thank you for all the advices, and for hosting me at your home.

Lastly, I would like to thank all staff and colleagues at the Department of Chemistry and Polymer Science, Stellenbosch University.